VOLUME 46, NUMBER 4, DECEMBER 2023

HADRONIC JOURNAL Volume 46, Number 4, December 2023

HADRONIC JOURNAL

Founded in 1978 by Prof. R. M. Santilli at Harvard University. Some of the past Editors include Professors S. L. Adler, A. 0. Barut, L. C. Biedenharn, N. N. Bogoliubov, M. Froissart, J.Lohmus, S. Okubo, Nobel Laureate Ilya Prigogine, M. L. Tomber, J. P.Vigier, J. Wess, Nobel Laureate Chen Ning Yang.

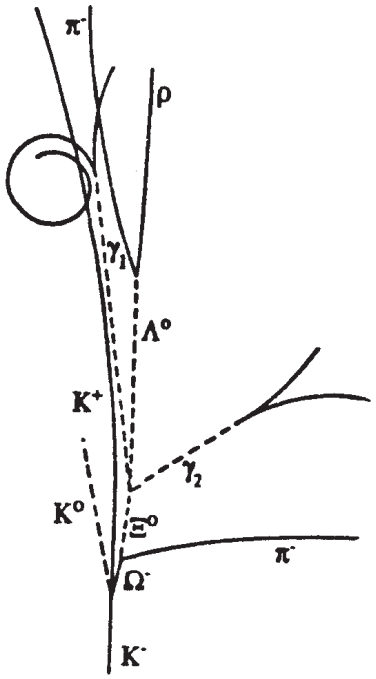

HADRONIC PRESS, INC.

HADRONIC JOURNAL

Established in 1978 by Prof. R. M. Santilli at Harvard University Hadronic Journal and Algebras, Groups and Geometries have been regularly published since 1978 without publication charges and are among the few remaining independent refereed journals.

This Journal publishes advances research papers and Ph. D. theses in any field of mathematics without publication charges.

For subscription, format and any other information please visit the website
http://www.hadronicpress.com

HADRONIC PRESS INC.
35246 U. S. 19 North Suite 215
Palm Harbor, FL 34684, U.S.A.
http://www.hadronicpress.com
Email: info@hadronicpress.com
Phone: +1-727-946-0427

HADRONIC JOURNAL

ISSN: 0162-5519

Established in 1978 by Prof. R. M. Santilli at Harvard University Hadronic Journal and Algebras, Groups and Geometries have been regularly published since 1978 without publication charges and are among the few remaining independent refereed journals.

This Journal publishes advances research papers and Ph. D. theses in any field of mathematics without publication charges.

For subscription, format and any other information please visit the website http://www.hadronicpress.com

HADRONIC PRESS INC.
35246 U. S. 19 North Suite 215
Palm Harbor, FL 34684, U.S.A.
http://www.hadronicpress.com
Email: info@hadronicpress.com
Phone: +1-727-946-0427

HADRONIC JOURNAL Volume 46, Number 4, December 2023

HADRONIC PRESS, INC.

HADRONIC JOURNAL

VOLUME 46, NUMBER 4, DECEMBER 2023

HADRONIC JOURNAL 46, 359 - 457 (2023)
DOI 10.29083/HJ.46.04.2023/SC359

SOLID-STATE MANIFESTATION OF QUANTUM CHROMODYNAMICS

V. G. Plekhanov
Fonoriton Sci. Lab.
Garon LtD, Tallinn
11413, Estonia
vgplekhanov@proton.me

Received September 28, 2023
Revised October 15, 2023

Abstract

This brief review is devoted to the results of non-accelerator study of strong nuclear long-range interaction in the mass isotope effect by the modern method of low-temperature optical spectroscopy of condensed matter. This became possible after the discovery that the addition of one neutron causes global changes in the macroscopic characteristics of a solid. The observation of an isotopic shift (0.103 eV) of the zero-phonon line of free excitons in the luminescence spectra of LiH (without strong interaction in the hydrogen nucleus) and LiD (with strong interaction in the deuterium nucleus) crystals was the first and direct evidence of the long-range interaction of the Yukawa potential. Indeed, in both crystals, the lithium ions, the proton and the electron are the same and, therefore, the gravitational, electromagnetic and weak interactions are the same, and the addition of a neutron, according to Yukawa, a strong interaction appears, the influence of which manifests itself in the isotopic shift. These experimental results demonstrate the neutron-electron binding energy (0.106 eV) which is in excellent agreement with the theoretical Breit estimate of 0.1067 eV. Another bright effect of the new physics is associated with the isotopic creation of mass by massless fermions (leptons) in graphene.

Keywords: strong interaction, quarks, gluons, excitons, phonons, QED, QCD

Introduction.

The traditional direction of the search for new physics and the origin of mass beyond the bound of the Standard Model (SM) in high energy physics is associated with the development of more powerful accelerator [1]. A low - energy approach, for example, in the problem of the origin of mass, was followed by author of the work [2]. The present brief review supplements work [1] with low - energy physics and at the same time is not only logical continuation of paper [2] but also its experimental proof [3]. In this connection, we must emphasize that outstanding works on hadron mechanics [4] deserve separate and fundamental study.

The history of physics shows that whenever experimental techniques advance to an extent that matter, as then known, newer and more powerful studies subsequently show that ≪elementary particles≫ have a structure themselves (see, e.g. [3 - 6]). Indeed this structure may be quite complex, so that the elegant ideas of elementarity must be abandoned. The modern concept of the atom emerged at the beginning of the 20th century, in particular as result of Rutherford's experiments [5, 6]. An atom is composed of a dense nucleus surrounded by an electron cloud (Fig. 1).

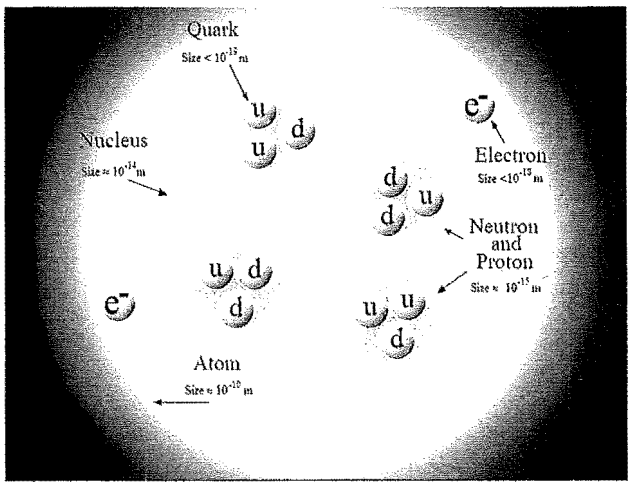

Fig. 1. Structure within the atom. (after http://.lbl.gov/abs/wallchart/).

After the discovery of the neutron in 1932 by Chadwick, there was no longer doubt that the building blocks of nuclei are protons and neutrons [7, 8] (collectively called nucleons).

The electron, neutron and proton were latter joined by fourth particle, the neutrino, which was postulated in 1930 by Pauli [6 in order to reconcile the description of β^- decay with the fundamental laws of conservation of energy , momentum and angular momentum. Thus, by the mid - thirties of the 20th century , these four particles could describe all the then known phenomena of atomic and nuclear physics. Today, these particles are still considered to be the main constituents of matter. In the fifties and sixties was showed that protons and neutrons are merely representative of a large family of particles called hadrons [9, 10]. More than 100 hadrons have thus far been detected. these hadrons, like atoms, can be classified in groups with similar properties. it was therefore assumed that they cannot be understood as fundamental constituents of matter. In the late sixties, the quark model (Fig. 1) established order in the hadronic zoo [11, 12].

Together with our changing conception of elementary particles, our understanding of the basic forces of nature and so of the fundamental interaction between elementary particles has evolved. As is well - known subatomic physics combines nuclear and particle physics. The two fields have many concepts and features in common. The exploration of subatomic physics started in 1896 with Becquerel's discovery of radioactivity; since then it has been a constant source of surprises, unexpected phenomena, and fresh insights into the law of Nature. In years that followed, the phenomenon was extensively investigated, notably by the husband and wife team of Pierre and Marie Curie and by Ernest Rutherford and his collaborators, and it was established that there were three distinct types of radiation involved. These were named (by Rutherford) α -, β -, and γ - rays. We know now that α -rays are bound states of two protons and two neutrons (the nuclei of helium atoms), β - rays are electrons and γ - rays are high energy photons. The energies of the α -, β -, and γ - particles are of the order of 0.1 MeV up to 10 MeV, whereas energies of the orbital electrons are of the order of electron volts. Also, α - particles were found to be barely able to penetrate a piece of paper, whereas β - particles could penetrate a few millimeters of aluminium, and the γ - rays could penetrate several centimeters of lead.

At about the same time as Becquerel's discovery, J.J. Tomson in 1897 was first to definitely establish the nature of free electrons. the view of the atom at that time was that it consist of two components, with positive and negative electric charges, the latter now being the electrons. In his experiments on α scattering by gold, Rutherford showed that α - particles encountered a very small positively charged central nucleus. To explain the results of these experiments Rutherford formulated a planetary model, where the atom was likened to a planetary system, with the electrons (the "planets") occupying discrete orbits about a central positively charged nucleus ("Sun").

Because photons of a definite energy would be emitted when electrons moved from one orbit to another, this model could explain the discrete nature of observed electromagnetic spectra when excited atoms decayed. In the simplest case of hydrogen, the nucleus is a single proton with electric charge +e, where - e is the magnitude of charge on the orbited a single electron. Heavier atoms were considered to have nuclei consisting of several protons. Examples are carbon and nitrogen, with masses of 12.0 and 14.0. However, it could not explain why chlorine has a mass of 35.5 in these units. At about the same time, the concept of isotopism was conceived by Soddy. Isotopes are atoms whose nuclei have different

masses, but the same charge. The explanation of isotopes was done by Chadwick. He had discovered the neutron and in so doing had produced almost final ingredient for understanding nuclei. Iwanenko and Heisenberg formulated a modern model, according to which all nuclei consist of a positively charged proton and a neutral neutron [7, 8].

By the early 1930s, the 19th century view of atoms as indivisible elementary particles had been replaced and a larger group of physically smaller entities now enjoyed this status; electrons, protons and neutrons. To these we should add two electrically neutral particles: the photon (γ) and the neutrino (ν). The photon was postulated by Planck in 1900 to explain black - body radiation, where the classical description of electromagnetic radiation led to results incompatible with experiments. the neutrino was postulated by Fermi in 1930 to explain the apparent non - conservation of energy observed in the decay products of some unstable nuclei where β - rays are emitted, the so - called β - decay [3].

Particle physics is the study of the fundamental constituents of matter and their interactions. However, which particles are regarded as fundamental has changed with time as physicists' knowledge has improved. The best theory of elementary particles we have at present is called, rather prosaically [14], the Standard Model (SM). The SM attempts to explain all the phenomena of particle physics in terms of the properties and interactions of a small number of particles of three distinct types: two spin - 1/2 families of fermions called leptons and quarks, and one family of spin -1 bosons - called gauge bosons - which act as 'force carriers' in the theory. In addition at least one spin-0 particle, called Higgs boson, is postulated to explain the origin of mass within the theory, since without it all the particles in the SM are predicted to have zero mass. All the particles of the SM are assumed to be elementary; they are treated as point particles, without internal structure or excited states.

Modern physics distinguishes three fundamental properties of atomic nuclei: mass , spin (and related magnetic moment), volume (surrounding field strength), which are the source of isotope effect. The stable elementary particles (electrons, protons and neutrons) have intrinsic properties. Some of these properties such as mass and electrical charge are the same for macroscopic objects. Some are purely quantum mechanical and have no macroscopic analog. Spin is an intrinsic angular momentum associated with elementary particles. The spin angular moment of an electron, measure along any particular direction, can only take on the values $\hbar/2$ or $-\hbar/2$. The nuclear magnetic moment associates with nuclear spin and produces the magnetic interaction with its environment.

Among the prime premises of quantum physics is the principle of indistinguishability of elementary particles. All electrons are by definition 'the same' and hence, after two (or more) electrons interact, it is possible to say 'who is who'. The same applies to other elementary particles and even identical atoms (e.g., two ^{70}Ge atoms are indistinguishable). Not so for isotopes. Due to their mass difference, various isotopes of the same chemical element (e.g., ^{70}Ge and ^{76}Ge) are classical distinguishable particles. Within the framework of statistical thermodynamics, this classical distinguishability of isotopes renders isotopic mixtures a prime illustrative tool for a discussion of the Gibbs paradox. The latter refers to the (alleged) discontinuity of entropy upon the mixture of two slightly different species.

Our present knowledge of physical phenomena suggests that there four types of forces between physical bodies (see, e.g. [10, 13]):

1) gravitational; 2) electromagnetic; 3) strong; 4) weak (Table 1).

Both the gravitational and the electromagnetic forces vary in strength as the inverse square of the distance and so able to influence the state of an object even at very large distances. Gravitational is important for the existence of stars, galaxes, and planetary systems as well as for our daily life, it is of no significance in subatomic physics, being far too weak to noticeably influence the interaction between elementary particles [14]. Electromagnetism is the force that acts between electrically charged particles (atoms, molecules, condensed matter). When nuclear physics developed, two new short - ranged forces joined the ranks. These are the nuclear force, which acts between nucleons (proton, neutron, etc.) and the weak force, which manifests itself in nuclear β- decay (see, e.g. [10]). The nuclear force is a result of the strong force binding quarks to form protons and neutrons. Due to experimental results of this paper connected to the manifestation of the strong interaction, we should briefly analyze the structure of subatomic particles and the strong interaction. We should underlined, that subatomic physics lacks so coherent theoretical formulation that would permit us to analyze and interpret all phenomena in a fundamental way: atomic physics has such a formulation in quantum electrodynamics, which permits calculations of some observable quantities to more than six figures. Subatomic physics deals with all entities smaller than the atom.

Table 1. The four fundamental forces.

Interaction	FQ	Mass	Range (m)	RS	Spin	TC-S (m^2)	TTS(s)
Str	Gluon	0	10^{-15}	1	1	10^{-30}	10^{-23}
We	W , Z	81, 93 GeV/c2	10^{-18}	10^{-5}	1, 1	10^{-44}	10^{-8}
Elec	Photon	0	∞	1/137	1	10^{-33}	10^{-20}
Gra	Graviton	0	∞	10^{-38}	2	-	-

Here - FQ field quant, RS relative strength, TC - S Typical cross - section, TTS - Typical time scale.

Particles are identical if they cannot be distinguished one from another by any intrinsic property, such as mass, charge, or spin [9]. There are does not exist, in act and in principle, any experimental procedure which can identify any one of the particles. In classical mechanics, even though all particles in the system may have the same intrinsic properties, each may be identified, at least in principle, by its precise trajectory as governed by Newton's laws of motion. This identification is not possible in quantum theory because each particle does not possess a trajectory; instead, the wave function gives the probability density for finding the particle at each point in space. When a particle is found to be in some small region, there is no way of determining either theoretically or experimentally which particle it is. Thus all electrons are identical and therefore indistinguishable, as are all protons, all neutrons, all hydrogen atoms with ^1H nuclei, all hydrogen atoms with ^2H nuclei,

all helium atoms with ^{4}He nuclei, all helium atoms with ^{3}He nuclei etc.

Symmetry and its mathematical framework - group theory - play an increasingly important role in physics. Both classical and quantum system usually display great complexity, but the analysis of their symmetry properties often gives rise to simplifications and new Insights which can lead to a deeper understanding. In addition, symmetries themselves can point the way toward formulation of a correct physical theory by providing constraints and guidelines in an otherwise intractable situation. Taking into account the symmetry, the proton and neutron are seen as different state of a single basic nucleon. These states bare differentiated by an internal property that have two values , +1/2 and -1/2, in analogy with the spin of a particle as the electron. This new property is called isotopic spin, or isospin for short, and the nuclear binding force is said to exhibit isospin symmetry [12, 13]. Thus, isospin symmetry is an important symmetry in particle physics, although it occurs only in the action of the nuclear binding force - or, in modern terminology, the strong force. Nuclear supersymmetry is a composite particle phenomenon, linking the properties of bosonic and fermionic systems, framed in the context of the Interacting Boson Model of nuclear structure [15, 17]. In modern physics, particles are classified into two groups based on their properties. There are known as fermions and bosons. In the Standard Model (SM) [12, 14] fermions are the fundamental particles of matter. Bosons on the other hand, are considered to be the force carriers. Nuclei having an odd number of nucleons are composite fermions whereas nuclei having an even number of nucleons are composite bosons.

Properties of fermions and bosons are very different especially at temperatures close to the absolute zero. Fermions are half - integer spin particles and described by the Fermi - Dirac statistics. Fermions obey the Pauli Exclusion Principle. So, two identical fermions do not occupy the same quantum state simultaneously. Basically, fermions can be classified into two groups: elementary and composite fermions. Elementary fermions are leptons (electron, electron neutrino, muon, muon neutrino, tau, and tau neutrino and quarks (up, down, top, bottom, strange and charm) (see, Table 2). Hadrons (neutrons, protons) containing an odd number of quarks, and nuclei made of an odd number of nucleons (for example ^{13}C nuclei contain six protons and seven neutrons) are considered to be composite fermions. Elementary fermions are the fundamental building blocks of matter and antimatter [10, 16].

Table 2. Quarks and leptons

	Family			Electric charge (e)
	1	2	3	
Leptons	e^-	μ^-	τ^-	- 1
	ν_e	ν_μ	ν_t	0
Quarks	u	c	t	2/3
	d	s	b	- 1/3

Bosons are identical particles having zero or integer spins. As fermions, bosons can be categorized into two groups: elementary and composite bosons. Unlike fermions, bosons do not obey the Pauli Exclusion Principle. In other words, any number bosons can occupy the same quantum state. Behaviors of bosons are described by the Bose - Einstein statistics. The SM [9] only consists of five elementary bosons (Fig. 2). They are namely the Higgs boson, gluon, Z and $W^{\pm}$ bosons [17]. The Higgs boson have zero electric charge and zero spin is the only scalar boson [16].

The discovery of the neutron by Chadwick in 1932 may be viewed as the birth of the strong interaction: it indicated that the nuclei consists of protons and neutrons and hence the presence of a force that holds them together, strong enough to counteract the electromagnetic repulsion. In 1935, Yukawa [18] pointed out that the nuclear force could be generated by the exchange of a hypothetical spinless particle, provided its mass intermediate between the masses of proton and electron - a meson. Yukawa predicted the pion [9, 10]. The strong forces does not act on leptons (electrons, positrons, muons and neutrinos), but only on protons and neutrons (more generally, on baryons and mesons - this is the reason for the collective name hadrons). It holds protons and neutrons together to form nuclei, and is insignificant at distances greater than 10^{-15} m [10]. Its macroscopic manifestations are restricted up to now to radioactivity and the release of nuclear energy.

The Table 1 given for the strength and range of the forces come from a comparison of the effects they produce on two protons. In some respect these resemble an ordinary Newtonian force between the protons, varying with the distance between them as if the force was derived from a potential function:

$$V(r) = \frac{ke^{-r/R}}{r^n} \qquad (1)$$

for some n. This Is an inverse - power force which is diminished by an exponential factor at distances larger than a certain distance R, the range of the force. The strength of the force is measured by the constant k. The unit of strength is $hc/2\pi$ where h is Planck's constant and c the speed of light. Since the protons and neutrons which make up the nucleus are themselves considered to be made up of quarks are considered to be held together by the color force [11, 12], the strong force between nucleons may be considered to be a residual color force (see, also ([10, 14). In the SM, therefore the base exchange is the gluon which mediates the forces between quarks.

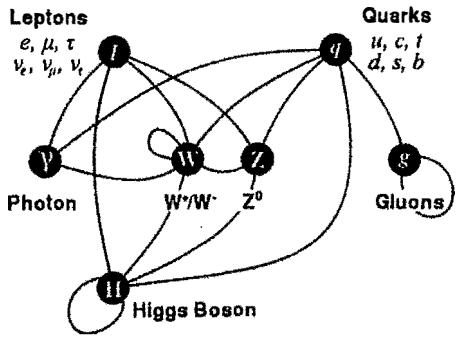

Fig. 2. Summary of interactions between particles described by the Standard Model.

The modern quantummechanical view of the three fundamental forces (all except gravity) is that particles of matter (fermions neutrons, protons, electrons) do not directly interact with each other, but rather carry a charge, and exchange virtual particles (gauge bosons photons, gluons, gravitons) which are the interaction carriers or force mediators. As can be see from Table 1, photons are the mediators of the interaction of electric charges (protons, electrons, positrons); and gluons are the mediators of the interaction of color charges (quarks). In our days, the accepted view is that all matter is made of quarks and leptons (see Table 2). As can be see, of the three pairs of quarks and leptons, one pair of each - the quark u and d and the leptons e and e (velectrons neutino) - are necessary to make up the every day world, and a world which contained only these would seem to be quite possible.

The facts, summarized in the modern nuclear and subatomic physics (see, e.g. [9, 10]) allow to draw several conclusions in regard to nuclear forces, most notably that the binding energy of a nucleus is proportional to the number of nucleons and that the density of nuclear matter is approximately constant. This lead to conclude that nuclear forces have a "saturation property". It seems from the last conclusion it is enough to change the number of neutrons in nucleus to change strength of nuclear force. But the last one constitutes the main ideas of the isotope effect [13].

2. Energy bands of electron in a solid.

2.1. Introduction.

Any solid consists, i.e. is so collection of nuclei and electrons. In crystalline solids, the

atom's nuclei are located at the nodes of the crystal lattice which has a spatial periodicity. The stationary state of all particles is described by the Schrödinger equation (see, for example [19])

$$\hat{H}\Psi = E\Psi, \quad (2)$$

where $\hat{H}$ **is the Hamiltonian of the entire set of particles, i.e. Hamiltonian of a solid,** Ψ is own wave function, E is the energy of solid body. Let $\vec{r}_1, \vec{r}_2, \ldots$ be the radius-vectors of electrons and $\vec{R}_1, \vec{R}_2, \ldots$ be the radius - vectors of nuclei. Denote by M_k the mass of the nucleus of an k - atom and m the mass of the electron.

The Hamiltonian of the system of particles is described by the following expression:

$$\hat{H} = \hat{K} + U \quad (3)$$

where $\hat{K}$ is the operator of the kinetic energy of this system, U is its potential energy. The kinetic energy operator for the solid state under consideration will be

$$\hat{K} = \left(\sum_i \frac{\hbar^2}{2m}\Delta_i + \sum_k \frac{\hbar^2}{2M_k}\Delta_k\right). \quad (4)$$

Here $\Delta_i = \frac{\partial^2}{\partial x_i^2} + \frac{\partial^2}{\partial y_i^2} + \frac{\partial^2}{\partial z_i^2}$ is the Laplace operator for i - particle. First term in (4) is the operator of the kinetic energy of electrons and the second one of nuclei. The potential energy of a set of particles that make up solid is the sum of the energies of the pairwise interaction of electrons with electrons, nuclei with nuclei and electron with nuclei.

$$U = \frac{1}{2}\sum_i \sum_{j \neq i} \frac{e^2}{4\pi\varepsilon\varepsilon_0 |\vec{r}_i - \vec{r}_j|} + \frac{1}{2}\sum_k \sum_{L=k} \frac{Z_k Z_L e^2}{4\pi\varepsilon\varepsilon_0 |\vec{R}_k - \vec{R}_L|} - \frac{1}{2}\sum_i \sum_k \frac{Z_k e^2}{4\pi\varepsilon\varepsilon_0 |\vec{r}_i - \vec{R}_k|}. \quad (5)$$

The first two terms in (5) express the energy of the Coulomb repulsion of electrons and nuclei, respectively, and the third term is the energy of attracted of electrons to nuclei. Substituting (4) and (5) into Schrödinger equation of our system, we get:

$$\left[-\left(\sum_i \frac{\hbar^2}{2m}\Delta_i + \sum_k \frac{\hbar^2}{2M_k}\Delta_k\right) + \frac{1}{2}\sum_i \sum_{j \neq i} \frac{e^2}{4\pi\varepsilon\varepsilon_0 |\vec{r}_i - \vec{r}_j|} + \frac{1}{2}\sum_k \sum_{L=k} \frac{Z_k Z_L e^2}{4\pi\varepsilon\varepsilon_0 |\vec{R}_k - \vec{R}_L|} - \frac{1}{2}\sum_i \sum_k \frac{Z_k e^2}{4\pi\varepsilon\varepsilon_0 |\vec{r}_i - \vec{R}_k|} \right] = E\Psi. \quad (6)$$

The wave function in equation (6) depends on the coordinates of all particles, i.e.

$$\Psi = \Psi(\vec{r}_1, \vec{r}_2, \vec{r}_3, \ldots\ldots \vec{r}_n, \vec{r}_1, \vec{R}_1, \vec{R}_2, \ldots\ldots, \vec{R}_N). \qquad (7)$$

If this wave function is constrained by its physical meaning (finiteness, unambiguity, continuity), then the Schrödinger equation (6) will have a solution not at any energy values E, but only at some. These values E, which is solution to equation (6) determine the energies (energy spectrum) of the solid. However, due to the vast number of independent variables, equation (6) cannot currently be solved in general form. To find an approximate solution, they resort to a number of simplifying assumptions.

Given the large difference in the masses of nuclei and electrons ($M_k \gg m$) and therefore the nature of movement these particles is significantly different. This approximation is called the adiabatic or Born - Oppengeimer [20] approximation. Indeed, if the nuclei rest, then the kinetic energy of the nuclei turns to zero. The potential energy of interaction of nuclei becomes some constant, i.e.

$$\frac{1}{2}\sum_k \sum_{L=k} \frac{Z_k Z_L e^2}{4\pi\varepsilon\varepsilon_0 |\vec{R}_k - \vec{R}_L|} = \text{const.} \qquad (8)$$

By choosing the starting point, we can turn it to zero. Taking this into account, the Schrödinger equation accepts the form:

$$\left[-\left(\sum_i \frac{\hbar^2}{2m}\Delta_i + \frac{1}{2}\sum_i \sum_{j\neq i} \frac{e^2}{4\pi\varepsilon\varepsilon_0 |\vec{r}_i - \vec{r}_j|} - \frac{1}{2}\sum_i \sum_k \frac{Z_k e^2}{4\pi\varepsilon\varepsilon_0 |\vec{r}_i - \vec{R}_k|}\right)\right]\Psi_e = E_e \Psi_e. \qquad (9)$$

Here the energy of electrons E_e and their wave function Ψ_e depend on resting nuclei $\vec{R}_{0k}$ only parametrically. The following approximation is called valence approximation

Despite significant simplifications, the Schrödinger equation (9) cannot be solved. The following approximation is called valence approximation. It is believed here that all electrons of the inner shells of an atom form a resting atomic residue together with nucleus, and, therefore, the Schrödinger equation is written only for valence electrons. As part of the adiabatic approximation and valence approximation, the wave function of the system remains dependent on the coordinates of a valence electrons. Since the latter interact with each other, the variables in the Schrödinger equation (9) are not separated . Therefore, a single - electron approximation is used to solve the problem, for which the Hartree - Fock method is used. The main ideas of this method is to replace the potential energy of

electrons $\frac{1}{2}\sum_i\sum_{j\neq i}\frac{e^2}{4\pi\varepsilon\varepsilon_0|\vec{r}_i-\vec{r}_j|}$ in equation (9) , the potential energy of the form $\sum_i \tilde{U}_i(\vec{r}_i)$, which is the interaction energy of the i - electron with some effective field in which each electron moves independently. This effective field characterizes the effect of all other electrons on the i - electron. Indirectly, it also depends on the movement of the i - electron affects the movement of all other electrons. Assuming that such a field is found, rewrite the Schrödinger equation (9) as

$$\left\{\sum_i\left[-\frac{\hbar^2}{2m}\Delta_i+\tilde{U}_i(\vec{r}_i)+U_i(\vec{r}_i)\right]\right\}\Psi_e=E_e\Psi_e. \qquad (10)$$

Here the $U_i(\vec{r}_i)$ denotes the potential energy of the i - electron in the field of all nuclei. Under the sign of the sum (10) is the Hamiltonian i - electron

$$\hat{H}_i=-\frac{\hbar^2}{2m}\Delta_i+\tilde{U}_i(\vec{r}_i)+U_i\vec{r}_i. \qquad (11)$$

So the Schrödinger equation can be rewriten like this:

$$\hat{H}\Psi_e=(\sum_i\hat{H}_i)\Psi_e=E_e\Psi_e \qquad (12)$$

Since now Hamiltonian does not contain the energy of interaction of electrons and is the Hamiltonian sum of individual electrons, the solutions to equation (12) is the product of single - electron functions

$$\Psi_e(\vec{r}_1,\vec{r}_2,\ldots.)=\psi_1(\vec{r}_1)\psi_2(\vec{r}_2)\ldots.=\Pi\psi_i(\vec{r}_i). \qquad (13)$$

And each function $\psi_i(\vec{r}_i)$ satisfies the one-electron Schrödinger equation

$$\hat{H}_i\psi_i=E_i\psi_i, \qquad (14)$$

in which the interaction of the i - electron with the rest is described by the potential $\tilde{U}_{ii}(\vec{r}_i)$

Thus, the introduction of an effective field allows to reduce the multi - electron equation to a single - electron system. At the same time, the energy of systems

$$E_e=\sum_i E_i. \qquad (15)$$

Although the wave function (13) is a solution to the Schrödinger equation for a crystal, it does not satisfy The Pauli principle [21]. According to Pauli's principle, one quantum state cannot contain more than two electrons with different spin orientations. The complete wave function of the system satisfying this condition must be antisymmetric, i.e. when rearranging coordinates and projecting the spin, it must change the sign. Our function (13) does not satisfy this condition. As a rule, an antisymmetric function is written in the form of a Slater determinant (for more details see, for example [21]). The antisymmetric properties of such a function derive from the properties of the Slater determinant. Since atom are located in space strictly periodically in the crystal, the full potential $V(\vec{r}) = \tilde{U}_i(\vec{r}\ ) + U(\vec{r})$ must have a three - dimensional periodicity. Although the exact species $V(\vec{r})$ is unknown, it is important to know that this potential is a periodic function whose period coincides with the period of the crystal lattice of the object under study. This periodicity leads to the formation of a band energy structure (Fig. 3). An electron from the valence band (see Fig. 3) is excited into the conduction band.

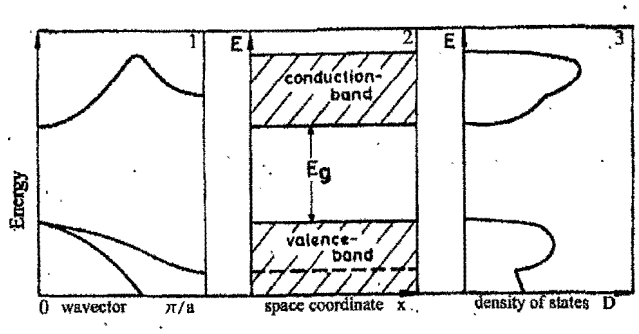

Fig. 3. Various possibilities to present the band - structure of homogeneous, undoped insulator (semiconductor). 1 - the dispersion relation, i.e. the energy E as a function of the wave vector $\vec{k}$, 2 - the energy regions of allowed and forbidden states as function of a space coordinate x and , 3 - the density of states (all curves are schematic ones).

The dependence of the energy of an electron on its quasi - pulse (the curvature of isoenergy surfaces in $\vec{k}$ - space) is connected by another fundamentally important characteristic of the electron, which is called its effective mass. According its definition [19] we have:

$$m^* = \hbar^2 \left(\frac{d^2E}{d\vec{k}^2} \right)^{-1} \qquad (16)$$

The effective mass reflects the influence of the lattice potential on the motion of the electron in the crystal under the action of an external force. In the case where the electron is in the vicinity of the minimum energy, i.e. the vicinity of the bottom of the conduction band $\frac{d^2E}{d\vec{k}^2} > 0$ and $m^* = \text{constant} > 0$, i.e. the electrons behave as negatively charged particles with a positive mass. In the vicinity of the maximum energy, i.e. in the vicinity of the vertex of the valence band $\frac{d^2E}{d\vec{k}^2} < 0$ and $m^* = \text{constant} < 0$ and, therefore in the vicinity of the vertex of the valence band , such a charge carrier behaves as a particle with a positive charge and a positive effective mass and is called a hole. As will be shown below by way of specific examples, the effective electron mass in different crystal varies from 1 to hundreths of the free electron mass.

2.2. Excitons.

The properties of the electron and the hole are both described by the band structure within the one - electron approximation. in this section we shall go beyond this approximation and consider the effects of electron - electron interaction on the absorption spectra. To simplify the calculation we shall make the following assumptions. We shall include only the Coulombic part of the electron - electron interaction neglecting both exchange and correlation terms. Furthermore, the interaction between the excited electron in conduction band (see, Fig. 3) and those left behind in the now almost filled valence band will be replaced by an electron - hole interaction. Attraction between the electron and the hole causes their to be correlated and the resultant electron - hole pair is known as an exciton.

It has been more than eight decades since the introduction of quasiparticle exciton by Frenkel [22] and the extreme fertility of this idea has been demonstrated most powerfully. According to Frenkel the exciton is an electron excitation of one of the atoms (ions) of the crystal lattice, because of the translation symmetry, moves through the crystal in an electrically neutral formation. Since Frenkel the concept of an exciton has been developed in the papers of Peierls [23] and Slater and Schokley [24]. Problems concerning light absorption by solid state have been considered somewhat differently Wannier [24] and Mott [25]. According to the Wannier - Mott results the exciton is the state of an electron and hole bonded by the Coulomb force. The electron and hole in exciton state are spatially separated and their charges are screened. In the Frenkel papers the excitations localized on the lattice site were described thus, after the Wannier - Mott papers, the excitons became divided into the excitons on the Frenkel (small radius) excitons (for details see [55]) and the Wannier - Mott (large radius) excitons ([65]). However, a description of the basic difference between these two models is absent [27 - 29]. The experimental discovery (see e.g. Gross [30]) of

the Wannier - Mott exciton (see Fig.4) on the hydrogen-like absorption spectrum in the semiconducting crystals was the basis of a new subject - exciton physics (see also Agekyan [31]; Permogorov [32]). The influence of external perturbation (electrical and magnetic fields, uniaxial and hydrostatic deformation) on the optical spectra of the Wannier - Mott excitons (see e.g., Gross [30]) and their energetic characteristics has been demonstrated repeatedly. These investigations permitted high-accuracy measurements not only the exciton binding energy but also of their translational mass, values of effective masses of the electron and hole, their g - factors etc. Moreover, the detailed account of the photon - exciton interaction has led to the concept of polaritons [33]. From the time of the experimental discovery of the Wannier - Mott exciton the problem concerning the interaction of excitons and the crystal lattice has persisted for more than four decades (Haken [34]; Haug and Koch [35]).

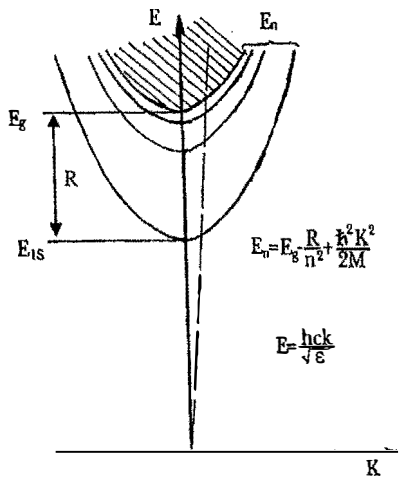

Fig. 4. Discrete and continuos (hatched area) Wannier - Mott exciton energy spectrum taking into account its kinetic energy. The broken line connects to the dispersion o light in the medium. R - is the exciton binding energy, n = 1, 2, 3, ...

Below we briefly consider quantitatively the effect of Coulomb attraction on the motion of electrons and holes (see, also [36]) in the vicinity of an M_0 critical point of a direct bandgap semiconductor in three dimensions. Further we shall assume the conduction band to be spherical with energy

$$E_e\left(\vec{k_e}\right) = E_g + \frac{\hbar^2 k_e^2}{2m_e}, \qquad (17)$$

where E_g is the band gap, and the corresponding hole energy to be given by

$$E_h\left(\vec{k_h}\right) = E_g + \frac{\hbar^2 k_h^2}{2m_h} . \sum \qquad (18)$$

Let the Bloch function and the hole be represented by $\Psi_{\vec{k_e}}\left(\vec{r_e}\right)$ and $\Psi_{\vec{k_h}}\left(\vec{r_h}\right)$, respectively. As usually we assume that the Coulomb interaction between electron and hole is weak due to screening by the valence electrons so that the effective mass approximation is valid. We can write the exciton wavefunction Ψ as linear combination of the electron and hole wave functions:

$$\Psi = \sum_{\vec{k_e},\vec{k_h}} C\left(\vec{k_e}, \vec{k_h}\right)\Psi_{\vec{k_e}}\left(\vec{r_e}\right)\Psi_{\vec{k_h}}\left(\vec{r_h}\right). \qquad (19)$$

Similar of the donor electron (see, e.g. [37, 38]), the electron and hole in an exciton are localized relative to their center of mass, so it is more convenient to express their wavefunctions in terms of Wannier functions rather than Bloch functions. In terms of the Wannier functions $a_{\vec{R_e}}\left(\vec{r_e}\right)$ and $a_{\vec{R_h}}\left(\vec{r_h}\right)$ for electron and hole, respectively, the exciton wavefunction can be written as

$$\Psi\left(\vec{r_e}, \vec{r_h}\right) = N^{-1/2} \sum_{\vec{R_e}, \vec{R_h}} \Phi\left(\vec{R_e}, \vec{R_h}\right) a_{\vec{R_e}}\left(\vec{r_e}\right) a_{\vec{R_h}}\left(\vec{r_h}\right) , \qquad (20)$$

where $\Phi\left(\vec{R_e}, \vec{R_h}\right)$ is the exciton envelope wavefunction. The wave equation for $\Phi\left(\vec{R_e}, \vec{R_h}\right)$ is

$$\left[- \left(\frac{\hbar^2}{2m_e}\right)\nabla^2_{\vec{R_e}} - \left(\frac{\hbar^2}{2m_h}\right)\nabla^2_{\vec{R_h}} - \frac{e^2}{\varepsilon_0 |\vec{R_e} - \vec{R_h}|} \right]\Phi\left(\vec{R_e}, \vec{R_h}\right) = E\Phi\left(\vec{R_e}, \vec{R_h}\right) , \qquad (21)$$

where ε_0 is the zero - frequency dielectric constant of material (insulators or semiconductors). Equation (21) can be solved in the same way as in the case of the hydrogen atom [39].

One expresses $\vec{R_e}$ and $\vec{R_h}$ in terms of two new coordinates: a center of mass coordinate $\vec{R}$ and a relative coordinate $\vec{r}$ defined by

$$\vec{R} = \frac{\vec{R_e}m_e + \vec{R_h}m_h}{m_e + m_h} \text{ and } \vec{r} = \vec{R_e} - \vec{R_h}. \qquad (22)$$

The equation of motion for the center of mass is now decoupled from that for the relative motion because the Coulomb interaction term does not involve $\vec{R}$ (see, also [36, 38]). The two resultant equations are

$$\left(-\frac{\hbar^2}{2M}\right)\nabla^2_{\vec{R}}\Psi\left(\vec{R}\right) = E_R\Psi\left(\vec{R}\right), \qquad (23)$$

$$\left(-\frac{\hbar^2}{2\mu}\nabla^2_{\vec{r}} - \frac{e^2}{\varepsilon_0 r}\right)\phi\left(\vec{r}\right) = E_R\phi\left(\vec{r}\right), \qquad (24)$$

where μ, the reduced mass of the exciton, is defined by

$$\frac{1}{\mu} = \frac{1}{m_e} + \frac{1}{m_h}. \qquad (25)$$

The total energy of the exciton E is simply the sum of E_R and E_r. The solution of (23) and (24) can be obtained readely. Equation (23) describes a free particle whose eigenfunction and energy are given by

$$\Psi_K\left(\vec{R}\right) = N^{-1/2}\exp\left(i\vec{K}\cdot\vec{R}\right) \text{ and } E_R = \frac{\hbar^2K^2}{2M}. \qquad (26)$$

E_R represents the kinetic energy of the center of mass motion [36].

Equation (25) is similar to the equation describing the motion of the donor electron [38]. As in the hydrogen atom, its wavefunctions and energies can be described by three quantum numbers: a principal quantum number n, the angular momentum quantum number *l* and the magnetic quantum number m. The wavefunction ϕ can be expressed in polar coordinates (r, θ, φ) as

$$\phi_{nlm}(\vec{r}) = R_{nl}(\vec{r})Y_{lm}(\theta, \varphi), \qquad (27)$$

where $R_{nl}(\vec{r})$ and $Y_{lm}(\theta, \varphi)$ are, respectively, the associated Laguerre polynomials and the spherical harmonic functions. These functions are tabulated in many quantum mechanics textbooks and therefore will not reproduce here (see, e.g. [40]). For isotropic effective masses E_r depends on n only and is given by

$$E_r(n) = E_r(\infty) - \frac{R^*}{n^2}, \qquad (28)$$

where $E_r(\infty)$ is the minimum energy of the continuum states (see, Fig. 4), i.e. the energy gap E_g and R^* is the Rydberg constant for the exciton defined as [36]

$$R^* = \frac{\mu e^4}{2\hbar^2\varepsilon_0^2} = 13.6 \cdot \left(\frac{\mu}{m\varepsilon_0^2}\right) \text{eV}. \qquad (29)$$

Combining the above result for the relative motion and the center of mass motion of the exciton, we obtain the following envelope functions and energies for the excitons:

$$\Phi_{nlm}(\vec{R}, \vec{r}) = (1/\sqrt{N})\exp(i\vec{K} \cdot \vec{R})R_{nl}(\vec{r})Y_{lm}(\theta, \varphi), \quad (30)$$

$$E_{nlm} = E_g + \frac{\hbar^2K^2}{2M} - \frac{R^*}{n^2}. \qquad (31)$$

The energy spectrum of a Wannier - Mott excitons is shown in greater detail in Fig. 4. The above model of excltons based on electrons and holes with spherically symmetric parabolic dispersion is useful for understanding exciton effects on optical spectra. However, it is not accurate enough for quantitative interpretation of experimental spectra in diamond and zinc - blende - type semiconductors. Of the various attempts to calculate excltonic effects based on realistic band structures, we shall mention the paper [41] (see, also [42]).

A) LiH

LiH crystal is of NaCl structure type. The simple electronic structure of Li^+ and H^- ions,

having $1s^2$ configuration, gives LiH a special place among the binary crystals and in many aspects allows it to serve as an ideal model for ionic compounds. The spectrum of one - electron states of crystal is determined by the solution of Schrodinger equation for the 'extra' particle (hole or electron) moving in the averaged field created by all the remaining electrons and nuclei (see, also [43]):

$$\left[-\frac{\hbar^2}{2m}\Delta + V(\vec{r})\right]\Psi_{\vec{k}}(\vec{r}) = E_n\left(\vec{k}\right)\Psi_{\vec{k}}(\vec{r}), \qquad (32)$$

where the notation is conventional, and $V(\vec{r})$ is the periodic potential. The existing calculation techniques differ in the method of constructing the electron potential $V(\vec{r})$, the approximation of the wave function $\Psi_{\vec{k}}(\vec{r})$, the ways of ensuring self - consistency, the reliance on empirical parameters, etc. In particular, two factors are especially important in case of ionic crystals: (1) the inclusion of exchange interaction, and (2) the inclusion of polarization of the electron and ion subsystems of crystal by the extra particle [44].

The one-electron potential of any many-electron system is nonlocal because of the exchange interaction between the electrons. It is very difficult to take this interaction into account. Because of this, the exact potential in the band theory is often replaced by the local potential of the form $V_{exchange}(\vec{r}) \propto \alpha[\rho(\vec{r})]^{1/3}$, where $\rho(\vec{r})$ is the charge density function, and the constant α is selected in the range from 1 (Slater potential [45]) to 2/3 (Cohn-Sham potential) [43]

Two effects are associated with the local exchange. First, the results of calculation depend strongly on the numerical value of α, and second, this approximation always underestimates the values of E_g and E_v (the width of the valence band). It is the low values of E_v obtained by many authors in the approximation of local exchange that are responsible for the wrong conclusion concerning the inapplicability of band theory to ionic dielectrics. These problems reflect the fundamental drawback of the one-electron approximation which does not take into account the reciprocal effect of the selected electron (hole) on the rest of the system. This effect consists in the polarization of the crystal by the particle, and is generally made up of two parts: the electron polarization (inertialess), and the lattice polarization (inertial). In the common optical phenomena, related to absorption or scattering of photons, the lattice polarization is not important, because the frequency of optical transitions is much higher than the average frequencies of phonons. The electron polarization is different. The extra particle (electron, hole) is regarded by this theory as the slowest particle in the system - in other words, all the remaining electrons adiabatically follow it. Hence it follows that the inertlaless polarization definitely must be included in the calculation of energy spectrum. An important feature of ionic crystals is that the polarization energy E_p is of the same order of magnitude as the bandwidth. Such a correction obviously cannot be regarded as small. In the extreme case of particle at rest, the polarization energy can be calculated by methods of classical electrostatics (the Mott - Littleton method [19]), or by the newer and more accurate technique proposed by Fowler [46]. The value of E_p for AHC found by this method is 2-3 eV for each of the quasi-particles ($E_p > 0$ for electrons,

and $E_p < 0$ for holes). This implies that the inclusion of electron polarization will reduce the magnitude of E_g by 4-5 eV [43]. By assumption, the electron bands are displaced rigidly, without changing the dispersion law $E(\vec{k})$.

The simple electron structure of lithium hydride (combined with the negligibly small spin-orbital interaction) is very helpful for calculating the band structure: all electron shells can easily be taken into account in the construction of the electron potential. The first calculations of band structure of lithium hydride were carried out as early as 1936 by Ewing and Seitz [47] using the Wigner-Seitz cell method. This method consists essentially in the following. The straight lattice is divided into polyhedra in such a way that the latter fill the entire space; inside each polyhedron is an atom forming the basis of the lattice (Wigner-Seitz cells). The potential inside each cell is assumed to be spherically symmetrical and coinciding with the potential of free ion. This approximation works well for ions with closed shells. The radial Schrodinger equation in the coordinate function $R_l(\vec{r})$ is solved within each selected cell, the energy being regarded as a parameter. Then the Bloch function is constructed in the form of expansion

$$\Psi_{\vec{k}}(\vec{r}) = \sum_{l=0}^{\infty} \sum_{m=-l}^{l} C_{lm}\left(\vec{k}\right) Y_{lm}(\theta, \varphi) R_l(\vec{r}, E), \qquad (33)$$

where $\vec{r}$, θ, φ are the spherical coordinates (with respect to the center of the cell); Y_{lm} are spherical functions. The coefficients $C_{lm}(\vec{k})$ and the energy $E(\vec{k})$ are found from conditions of periodicity and continuity on the boundaries of the cell. if $\vec{r}_1$ and $\vec{r}_2$ are the coordinates of two points on the surface of Wigner-Seitz cell, linked by the translation vector $\vec{R}_l$, then the boundary conditions are

$$\Psi_{\vec{k}}(\vec{r}_2) = \exp\left(i\vec{k}\vec{R}_l\right)\Psi_{\vec{k}}(\vec{r}_1), \qquad (34)$$

and

$$\nabla_n \Psi_{\vec{k}}(\vec{r}_2) = \exp\left(-i\vec{k}\vec{R}_l\right)\nabla_n \Psi_{\vec{k}}(\vec{r}_1), \qquad (35)$$

where ∇_n is the gradient normal to the surface of the cell. We see that the method of cells only differs from the problem of free atom in the boundary conditions. Owing to the complex shape of the cell, however, the construction of boundary conditions is a very complicated task, and this method is rarely used nowadays.

The method of plane associated waves (PAW) was used for calculating the band structure and the equation of state for LiH was used in Perrot [48]. According to this method, the crystal potential is assumed to be spherically symmetrical within a sphere of radius $\vec{r}_s$ described around each atom, and constant between the spheres (the so-called cellular muffin-tin (MT) potential). inside each sphere, like in the Wigner-Seitz method, the solutions of Schrodinger equation have the form of spherical harmonics; outside the

spheres they become plane waves. Accordingly, the basis functions have the form

$$\Psi_{\vec{k}}(\vec{r}) = \exp\left(i\vec{k}\vec{r}\right)\theta\left(\vec{r} - \vec{r}_s\right) + \sum a_{lm} Y_{lm}\left(\theta, \varphi\right) R_l\left(E, \vec{r}\right)\theta\left(\vec{r}_s - \vec{r}\right), \quad (36)$$

where $\theta(x) = 1$ at $x \geq 0$, and $\theta(x) = 0$ at $x < 0$. The coefficients a_{lm} can be easily found from condition of sewing on the boundary of the sphere. This is an important advantage of the PAW method over the method of cells. The calculations of Perrot [48] are self-consistent, and the local potential is used in the Cohn-Sham form. The correlation corrections were neglected. The method of Corrlngi-Cohn-Rostocker (CCR method), or the method of Green's functions, was used for calculating the band structure of LiH in Zavt et all. [49] (only concerned with the valence band) and in Kulikov [50]. Calculation of band structure of LiH in Grosso and Paravicini [51] was based on the wave function used in the method of orthogonalized plane waves (OPW) of the form

$$\Psi_{\vec{k}}(\vec{r}) = \exp\left(i\vec{k}\vec{r}\right) - \sum_c \left\langle \exp\left(i\vec{k}\vec{r}\right) \mid X_c \right\rangle X_c(\vec{r}), \quad (37)$$

where X_c are the atomic functions of state of the skeleton; $\left\langle \exp\left(i\vec{k}\vec{r}\right) \mid X_c \right\rangle$ is the integral of overlapping of plane wave with skeleton function (see also [52]). The method of linear combination of local basis functions was applied to the calculation of band structure of LiH in Kunz and Mickish [53]. This method is based on constructing the local orbitals for the occupied atom states, based on certain invariant properties of the Fock operator. The main feature of local orbitals is that they are much less extensive than the atom orbitals. Importantly, the correlation correction is taken into account in Kunz and Mickish [53]. Owing to the high polarizability of hydrogen molecules, the correlation effect in lithium hydride is exceptionally strong. Yet another calculation of band structure of LiH was carried out in Zavt et al. [49] using the so-called method of extended elementary cell. This approach is based on the semlempirical techniques of the theory of molecules, and is much similar to the cluster calculations. Let us add that the cluster is selected in such a way that the quasi-molecular wave function transforms in accordance with the group symmetry of certain wave vectors in the Brillouin zone. This methods only yields the energy values at the points of high symmetry. We ought to mention also Hama and Kawakaml [54], where, in connection with the study of high pressure effects on the transition NaCl - CsCl in lithium hydride, the band structure and the equation of state of the latter are analyzed in detail. The calculated band structures of LiH are compared in Fig. 5.

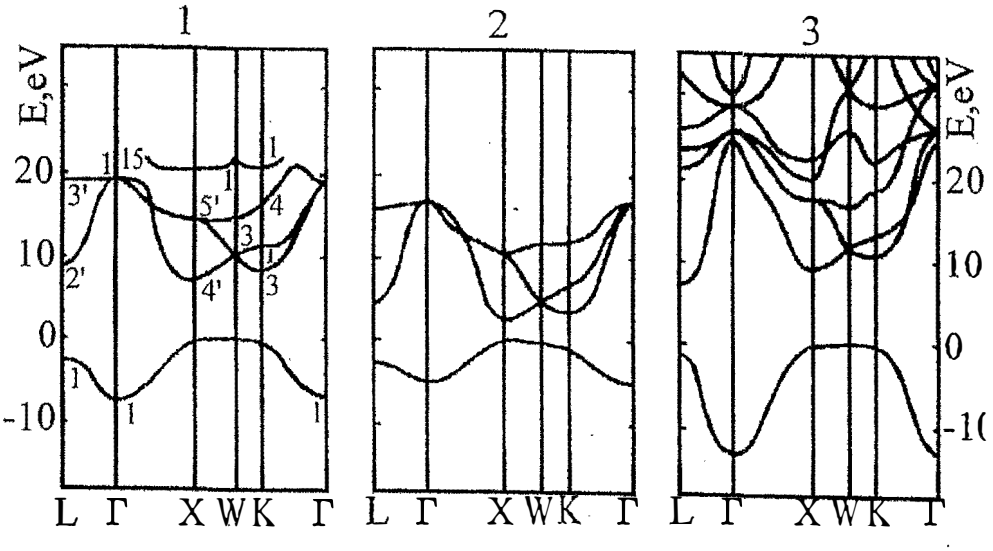

Fig. 5. band structure of LiH crysta als calculated: [53] - 1; [3] - 2; [52] - 3.

We see that the overall picture given by various methods is generally the same, despite the vast spread of the transition energy values (see Table 3).

Table 3. Calculated energy values of some direct optical transitions in LiH reduced to the experimental value of $E_g = 5.0$ eV.

Transition	1	2	3,4	5
$K_1 - K_3$	6.9	7.5	6.5	6.4
$W_1 - W_3$	8.0	7.9	7.3	7.4
$L_1 - L'_2$	9.2	9.6	9.0	9.1
$W_1 - W'_2$	12.6	14.9	12.2	
$X_1 - X'_5$	12.9	13.8	13.6	
$K_1 - K_4$	14.7	16.1	15.0	
$L_1 - L'_3$	19.7	20.9	20.7	
$\Gamma_1 - \Gamma_{15}$	24.5	25.3	33.3	

Looking at the structure of the valence band we see that it is very similar to the s - band in the method of strong bond (see also [37]). This is surprising, given the strong overlap of

the anion s - functions in lithium hydride. The wave functions in this band are almost entirely composed of the Is states of hydrogen ion. Different authors place the ceiling of the band either at point X or at point W of the Brillouin zone. Although in all cases the energies of the states X_1 and W_1 differ little ($\leq$ 0.3 eV), the question of the actual location of the top of the valence band may be important for the dynamics of the hole. Different calculations also disagree on the width of the valence band. For example, the width of the valence band in LiH without correlation is, according to Kunz and Micklsh [53], E_v = 14.5 eV, and the value of E_v is reduced to one half of this when correlation is taken into account. This shows how much the polarization of crystal by the hole affects the width of the valence band E_v. According to Perrot [29], the width of the valence band in LiH is 5.6 eV. The density of electron states in the valence band of LiH was measured in Betenekova et al. [55] and Ichikava et al. [56]. In Betenekova et al. the measurements were carried out with a magnetic spectrometer having the resolution of 1.5 eV, whereas the resolution of hemispherical analyzer used in Ichikawa et al. [56] was 1.1 eV. From experimental data, the width of the valence band is 6 eV according to Betenekova et al., and 6.3 eV according to Ichikawa et al. Observe the good agreement with the calculated value of E_v in this theory. Let us add also that the measured distribution of the electron density of states in the valence band of LiH exhibits asymmetry typical of s-bands (for more details see Betenekova et al. [55] and Ichikawa et al. [56]). The lower part of the conduction band is formed wholly by p-states and displays an absolute minimum at point X which corresponds to the singlet symmetry state X_4. The inversion of order of s and p - states in the spirit of LCAO method may be understood as the result of the s - nature of valence band. Mixing of s - states of the two bands leads to their hybridization and spreading, which changes the sequence of levels. If we compare the structure of the conduction band with the p - band of the method of strong bond (see, also [58]), we see that the general structure and the sequence of levels are the same except for some minor details (the location of L_3 level, and the behavior of $E(\vec{k})$ in the neighborhood of Γ_{15}). In other words, the lower part of the conduction band in lithium hydride is very close to the valence p - band of AHC. The direct optical gap In LiH according to all calculations is located at X point and corresponds to the allowed transition X_1-X_4. The indirect transition W_1-X_4 ought to have a similar energy. According to the above calculations, the energies of these transitions differ by 0.03-0.3 eV. The different values of E_g for LiH obtained by different authors are apparently due to the various methods used for taking into account the exchange and correlation corrections (see above). As follows from Table 3, the transitions at critical points in the low-energy region form two groups at 7 - 9 and 13 - 15 eV. Measurements of reflection spectra in the 4 - 25 eV range at 5 K (Kink et al. [57]) and 4 - 40 eV at 300 K throw new light on the results of calculations (see also review by Plekhanov [58]). The singularities occurring at 7.9 and 12.7 eV in reflection spectra are associated in the above papers with the interband transitions W_1 -W_4 and X_1 -X_5 respectively.

From the standpoint of dynamics of quasi-particles, an important consequence of such band structure is the high anisotropy of the tensor of effective mass of electrons and (especially) holes. The estimated mass of electron in the neighborhood of X_4 is, according to Kunz and Mickish [53], $(m_e)_x \simeq 0.3m_0$ in the direction X - Γ, and $(m_e)_y = (m_e)_z \simeq 0.8\ m_0$ in

the direction X - W. Similarly, the mass of hole in the neighborhood of X_1 is X - Γ in the direction $(m_e)_x \simeq 0.55\, m_0$ and about the same in the neighborhood of W_1. It is assumed that the transverse components of m_h are greater by several orders of magnitude (Zavt et al. [49]). Note also that, according to Baroni et al. [52], the estimated masses of carriers are: $m_{el} = 0{,}121$; $m_{et} = 0{,}938$; $m_{ht} = 0{,}150$; $m_{ht} = 4{,}304\, m_e$, where the subscripts 1 and t denote, respectively, the longitudinal (in the direction Γ - X) and the transverse (in the direction X - W) components. This high anisotropy of masses of electron and hole ought to have resulted in the high anisotropy of the reduced ($1/\mu = 1/m_e + 1/m_h$) and the translation ($M = m_e + m_h$) masses of exciton. This, however, is not the case. Moreover, the study of Plekhanov and Altukhov [59] reveals that with a good degree of confidence one may assume that in the energy range $E \leq 40$ meV the exciton band is isotropic and exhibits parabolic dispersion ($m_e = 0.04m$ and $m_h = 0.15m$). As was shown below, the studies of exciton - phonon luminescence of free excitons and resonance Raman scattering of light in LiH crystals [43] reveal that the kinetic energy of excitons in these crystals is greater than E_b by an order of magnitude exactly because of the very small masses of electron and hole. The last one may indicate that in the metallic phase of hydrogen at the high pressure [43] we can expect the Dirac character of the electronic excitations [60]. We should add that isotope substitution will be very useful method for renormalization of the band - gap energy in graphene - future semiconducting material [61].

B) Diamond

Carbon atom is built from 6 protons, A neutrons and 6 electrons, where A = 6 or 7, yield the stable isotopes ^{12}C and ^{13}C, respectively, and A =8 characterizes the radioactive isotope ^{14}C. The isotope ^{12}C, with nuclear spin I = 0, is the most common one in nature with 99% of all carbon atoms, whereas only ~ 1% are ^{13}C with nuclear spin I = 1/2. There only traces of ^{14}C (10^{-12} of all carbon atoms) which β - decays into nitrogen ^{14}N. Although ^{14}C only occurs rarely, it is important isotope used for historical dating (see, e.g. [62]).

Carbon, one of the most basic elements in nature, still gives a lot surprises. It is found in many different forms - allotropes - from zero dimensional fullerene, one dimensional carbon nanotubes, two dimensional graphene and graphite, to three dimensional diamond (Fig. 6) - and the properties of the various carbon allotropes can vary widely [63]. For instance, diamond is the hardest material, while graphite is one of the softest: diamond is transparent to the visible part of spectrum, while graphite is opaque; diamond is an electrical insulator, while graphite is a conductor. Very important is that all these different properties originate from the same carbon atoms, simply with different arrangements of the atomic structure.

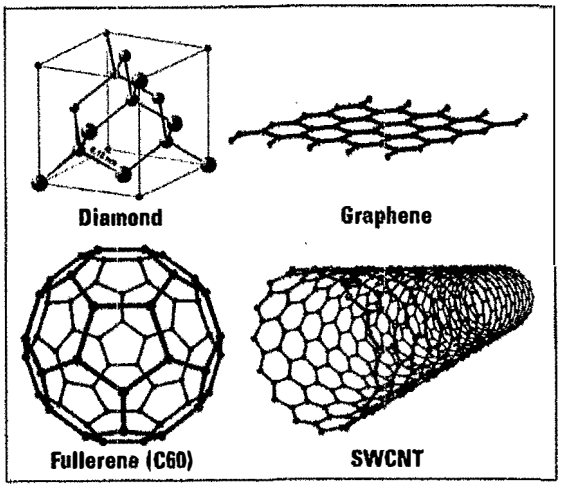

Fig. 6.Structure of some representative carbon allotropes.

The Diamond is one of the simplest and most important systems, especially in isotope effect of condensed matter. It has considerable mechanical strength; also it has high thermal conductivity and chemical stability even at several hundreds of degrees Celsius [64, 65]. Diamond has, perhaps, the simplest and most basic covalent band structure. Fig. 7 shows the electronic energy - band along several lines of high symmetry from the center (Γ) to the boundary of the first BZ as calculated with modified LCAO method in paper [66].

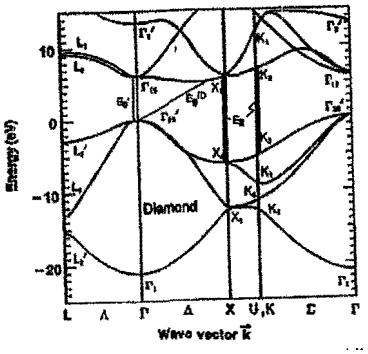

Fig.7. Electronic energy band structure of diamond along several lines of high symmetry from the center to the boundary of the first BZ as calculated with a modified LCAO method [66].

The electronic states are labeled using the notation for the single group of the diamond structure. The location of several interband transitions are included by the vertical arrows. The fundamental absorption edge of diamond corresponds to indirect transitions from highest valence band at the Γ point to the lowest conduction band in the Δ direction (X point) (i.e., $\Gamma_{25'} \rightarrow \Delta_1$ [X_1]). The theoretical indirect gap energy E_g^{ID} lays between 5.05 and 5.6 eV [67], that in reasonable agreement with the experimental data: $E_g^{ID} = 5.470 \pm 0.005$ eV [64, 65]. Like in Si, the lowest - lying conduction band at Γ point of BZ in diamond, Γ_{15} is p - like, however, as we can see, in Ge the s - like $\Gamma_{2'}$ band is the lowest conduction band. As mentioned in literature (see, e.g. [68] and references therein), one common characteristic of all published spectra in the UV region of diamond is the presence of two major peaks at ~7.02 - 7.4 eV and ~ 12.2 - 12.7 eV. The first peak may originate from $\Gamma_{25'} \rightarrow \Gamma_{15}$ transition (E_0') and the second one from $X_4 \rightarrow X_1$ and $\Sigma_2 \rightarrow \Sigma_3$ transitions (E_2) (the more detail see [65]).

The dependence of the band gap energy on isotopic composition has already been observed for insulators and lowest (indirect-direct) gap of different semiconductors ([69, 70]). It has been shown to result primarily from the effect of the average isotopic mass on the electron-phonon interaction (for details see below), with a smaller contribution from the change in lattice constant. This simplest approximation, in which crystals of mixed isotopic composition are treated as crystals of identical atoms having the average isotopic mass is referred to as virtual crystal approximation (VCA). Going beyond the VCA, in Isotoplcally mixed crystals one would also expect local fluctuations in the band gap energy from statistical fluctuations in local isotopic composition within some effectlve volume, such as that of an exciton.

C) Graphene.

Graphene is a single - atom - thick two - dimensional planar layer of carbon atoms in hexagonal honeycomb array composed of two superposed triangular sub - lattices. Graphene, a monolayer of sp^2 - bonded carbon atoms or one monolayer of graphite. It can be wrapped up into 0D fullerenes, rolled into 1D nanotubes or stacked 3D graphite. The band structure of graphene involves two nodal zero - gap points (K - points, see Fig. 8) in the first Brillouin zone at which the conduction and valence band touch. In the vicinity of these points, the low - energy electron/hole energy dispersion relation is proportional to momentum, rather than its square. This is analogous to the energy dispersion relation of massless relativistic electrons, so the electrons/holes of graphene are described as "Dirac fermions" having no mass. The relativistic - like description of electron waves on

honeycomb lattices has been known theoretically for many years, never failing to attract attention, and the experimental discovery of graphene now provides a way to probe quantum electrodynamics (QED) phenomena by measuring graphene's electronic properties (for details see [15] and references therein).

Graphene can be considered as the building block of many carbon allotropes. As was shown [15] (Fig. 3^c, chapter 5 in [15]) it is a two - dimensional crystal with hexagonal structure consisting of bipartite lattice of two triangular sublattices. We should remind that the fourth valence electron Is in the $2p_z$ orbital which is orthogonal to the graphene plane. A weak π bond is formed by the overlap of half - filled $2p_z$ orbitals with other $2p_z$ orbitals. The transport properties of graphene are determined by these delocalized π electrons [71]. Further we will present a very brief description of the band structure. As mentioned above, graphene is a honeycomb lattice of carbon atom (Fig. 6). It is a bipartite lattice with two sublattices A and B that are triangular Bravais lattice with two atoms per unit cell (A and B). Each A - or B - type atom is surrounded by three atoms of the opposite type. In a simple neighbor model graphene is a semimetal with zero - overlap between valence and conduction bands [15]. Considering only the xy plane, the unt vectors in real space, $\vec{a}_1$ and $\vec{a}_2$, and the reciprocal lattice vectors $\vec{b}_1$ and $\vec{b}_2$ are shown in (Fig. 3, chapter 5 in [15]. The real space lattice vectors are written as

$$\vec{a}_1 = \frac{a}{2}\left(\sqrt{3}, 1\right), \quad \vec{a}_2 = \frac{a}{2}\left(\sqrt{3}, -1\right), \tag{38}$$

where $a = |\vec{a}_1| = |\vec{a}_2| = 0.246$ nm is the lattice constant. The corresponding unit in the reciprocal lattice are

$$\vec{b}_1 = \frac{2\pi}{a}\left(\frac{1}{\sqrt{3}}, 1\right), \quad \vec{b}_2 = \frac{2\pi}{a}\left(\frac{1}{\sqrt{3}}, -1\right), \tag{39}$$

with a reciprocal space lattice constant $4\pi/\left(a\sqrt{3}\right)$. The first Brillouin zone is a hexagon (Fig. 3^a in chapter 5 in [15]), where the corners are called the K points (see below).

The energy dispersion of π electrons in graphene was first derived in 1947 by Wallace [72] within the tight - binding approximation. In this case, the wave function of graphene is a linear combination of Bloch function for sublattice A

$$\Phi_A = \frac{1}{\sqrt{N}} \sum_{\vec{R}_A} e^{i\vec{k}\vec{R}_A} \varphi(\vec{r} - \vec{R}_A), \tag{40}$$

and equilibrium function Φ_B for the B sublattice. Here N is the number of unit cells, $\vec{R}_A$ are the position of the atom A and $\varphi(\vec{r} - \vec{R_A})$ is the $2p_z$ orbital of the atom at $\vec{R}_A$. The sum runs over all unit cells, i.e. all possible lattice vectors. in the nearest neighbor approximation (every A site has three nearest B sites, and vice versa), the energy eigenvalues can be obtained in a closed form [72, 73]

$$\varepsilon(k_x, k_y) = \pm \gamma_0 \left[1 + 4\cos\frac{\sqrt{3}k_x a}{2}\cos\frac{k_y a}{2} + 4\cos^2\frac{k_y a}{2}\right]^{1/2}, \qquad (41)$$

where γ_0 is the transfer integral between the nearest neighbors. The energy dispersion of two - dimensional graphene according to this formula is plotted in Fig. 8 as a function of the wave vector $\vec{k}$.

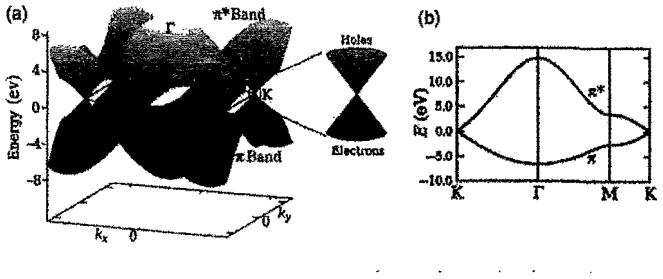

Fig. 8. Energy dispersion of graphene obtained within the tight - binding approximation. (a) Energy dispersion relation for graphene, drawn in the energy region of the Brillouin zone. Since in this approximation to ignore the coupling between the graphene sheets, the band depend only on k_x and k_y. The π band is completely filled and meets the totally empty π^* band at the K points. Near these points both bands have linear dispersion as described in the text. (b) The dispersion along the high - symmetry points ΓMK.

The upper half of the curves is called the π^* or the antlbonding band while the lower one is π or the bonding band. The two bands degenerate at the two K points given by the reciprocal space vectors $\vec{K} = (2\pi/a)(1/3, 1/\sqrt{3})$ and $\vec{K}' = (2\pi/a)(-1/3, 1/\sqrt{3})$ points where the dispersion vanishes (Fig. 9).

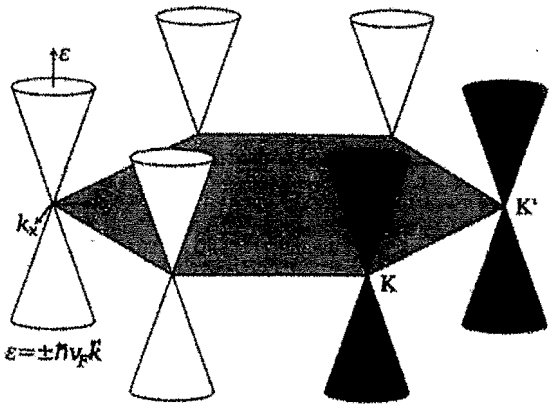

Fig. 9. Dirac cones at the K points.

Three σ –bonds join a C atom to its three neighbors. They are quite strong, leading to optical - phonon frequencies much higher than observed in diamond (see below). Such orbitals are even with respect to the planar symmetry. The σ bonds are strongly covalent bonds determining the energetic stability and the elastic properties of graphene. The remaining p_z orbital, pointing out of the graphene sheet is odd with respect to the planar symmetry and decoupled from the σ states. From the lateral interaction with neighboring p_z orbitals (called the ppπ interaction), localized π (bonding) and π^* (antibonding) orbitals are formed [73]. Graphite consists of a stack of many graphene layers. The unit cell in graphite can be primarily defined using two graphene layers translated from each other by a C-C distance ($a_{c\text{-}c}$ =1.42 Å). The three-dimensional structure of graphite is maintained by the weak interlayer van der Waals interaction between π bonds of adjacent layers, which generate a weak but finite out-of-plane delocalization [73]. The bonding and antibonding σ bands are actually strongly separated in energy > 12 eV at , and therefore their contribution to electronic properties is commonly disregarded, while the bonding and antibonding π states lie in the vicinity of the Fermi level (see, e.g. Fig. 2 in [74]) . The two remaining π bands completely describe the low energy electronic excitations in both graphene and graphite (see [73] and references therein). The bonding π and antibonding π^* orbitals produce valence and conduction bands which cross at the charge neutrality point (Fermi level of undoped graphene) at vertices of the hexagonal Brillouin zone. Carbon atoms in a

graphene plane are located at the vertices of a hexagonal lattice.

Basically, graphene has redefined the limits of what a material can do: it boasts record thermal conductivity and the highest current density at room temperature ever measured (a million times that of copper!); it is the strongest materlal known (a hundred times stronger than steel!) yet is highly mechanically flexible; it is the least permeable material known (not even helium atoms can pass through it!); the best transparent conductive film; the thinnest material known; and the list goes on [75]. In the vicinity of K - points of the Brillouin zone, the low - energy electron/hole dispersion relation is proportional to momentum, rather than its square. This is analogous to the energy dispersion relation of massless relativistic electrons, so the electrons/holes of graphene are described as Dirac fermions having no mass (see also Fig. 10). In a simple neighbor model graphene is a semimetal with zero - overlap between valence and conduction bands. In order to make graphene a real technology, a special issue must be solved: creating an energy gap at K - points in the Brillouin zone [63, 75, 76].

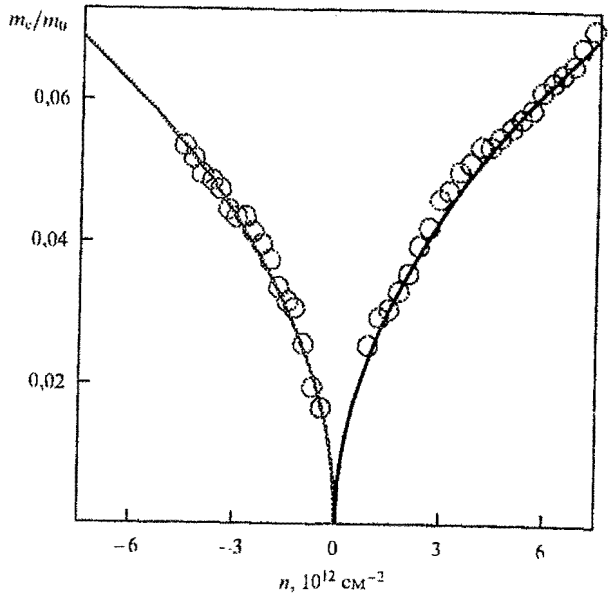

Fig. 10. Cyclotron mass m_c of electrons and holes as a function of their concentrations Symbols are experimental data, solid curves the best fit to theory (after [77]).

Further we describe how the tight - binding model discussed above yields the famous massless Dirac fermions which have made the study of monolayer graphene so enticing. As noted above, the Fermi energy corresponds to $\varepsilon = 0$ at the K points. The low - energy properties, corresponding to the electronic states near the Fermi energy, can be described by expanding the energy dispersion around the K points. Writing the graphene wave vector $\vec{q} = \vec{K} + \vec{k}$, such that $| \vec{k} | a \ll 1$, one can write a Taylor expansion of $\varepsilon_{\pm}(\vec{q})$ near $\vec{K}$ which yields

$$\varepsilon_{\pm}\left(\vec{k}\right) = \pm\frac{\sqrt{3}}{2}\gamma_0 ak \approx \pm v_F \hbar k, \qquad (42)$$

where $v_F = \sqrt{3}\gamma_0 a/2\hbar \approx 10^6\ ms^{-1}$ is the Fermi velocity. This velocity is independent of the carrier density [77] therefore the energy dispersion corresponds to two cones meeting at the K point (see Fig. 8^b) with linear dependence on the wave vector. The corresponding density of states is

$$\rho(\varepsilon) \propto | \varepsilon |, \qquad (42)$$

i.e. the density of states is linear and vanishes at zero energy. This is a direct consequence of the linear dispersion near K, in marked contrast to conventual two - dimensional electron gas, where the density of states is constant [78]. The unique band structure of graphene just described, brings about profound changes in the electronic properties of the system. In the continuum limit and in the effective - mass approximation, The Hamiltonian in the vicinity of the K point is [79]

$$H_k\left(\vec{k}\right) = \hbar v_F \begin{pmatrix} 0 & k_x - ik_y \\ k_x + ik_y & 0 \end{pmatrix} = \hbar v_F \vec{\sigma} \cdot \vec{k} = - H_{k'}^{T}\left(\vec{k}\right), \qquad (43)$$

where $\vec{\sigma} = (\sigma_x, \sigma_y)$ is a vector of Pauli matrices. The Hamiltonian therefore describes two - dimensional massless neitrinos with a linear dispersion, $\varepsilon_{\pm}\left(\vec{k}\right) = \pm v_F \hbar k$. The wave functions of these relativistic - like (Dirac) particles have a spinor structure. or the K and K' points, they are without normalization

$$\Psi_{s,\vec{k}}{}^{K} = e^{i\vec{k}\vec{r}} = \begin{pmatrix} s \\ e^{i\theta_{\vec{k}}} \end{pmatrix}; \quad \Psi_{s,\vec{k}}{}^{K'} = e^{i\vec{k}\vec{r}} \begin{pmatrix} e^{i\theta_{\vec{k}}} \\ s \end{pmatrix}, \tag{44}$$

where s = +1 for upper band (electrons) and - 1 for the lowest band (holes0, $\tan\theta_{\vec{k}} = k_y/k_x$. the upper and lower terms correspond to the quantum mechanical amplitudes or pseudospin) of finding the particle on one of the two sublattices A and B. In such approximation the Hamiltonian and wave functions for either valley can be written as the 2 x 2 matrix

$$H_{\xi}\left(\vec{k}\right) = \xi\hbar v_F \begin{pmatrix} 0 & k_x - ik_y \\ k_x + ik_y & 0 \end{pmatrix}; \quad \Psi_{s,\vec{k}}{}^{\xi} = e^{i\vec{k}\vec{r}} \begin{pmatrix} \xi s \\ e^{i\theta_{\vec{k}}} \end{pmatrix}. \tag{45}$$

Interestingly, in graphene, the pseudospln direction is associated with the momentum of the particles [80]. This means that the wave functions in the vicinity of the K and K' points (Dirac points, Fig. 10) are chiral, or helical fermions. One consequence of this is that any backscattering, i.e scattering particles from the wave vector $\vec{k}$ to $-\vec{k}$, is supressed (see, e.g. [86, 89]). Particles have opposite chirality in the K or K' valley or in the electron or hole bands. The energy bands in the vicinity of these Dirac points are two cones meeting at k = 0 (see also Fig. 6). The charge carrier in graphene are usually described as massless fermions [63, 79]. Experimental observation [77] of full Dirac cone dispersion have been measured in [81]. In such way the graphene provides unexpected connections between condensed matter physics and quantum field theory of the elementary particle physics.

Phonons denote the quantized normal mode vibrations that strongly affect many processes in condensed matter systems, including thermal, transport and elastic properties (see, e.g. [91]). Phonons provide a sensitive probe of the electronic structure through Raman techniques since the absence of a band gap in graphene makes all incident wavelengths resonant, so that the Raman spectrum contains information about both atomic structure and electronic properties. An understanding of the phonon dispersion of graphene is essential to interpret the Raman spectra of graphene. Since the unit cell of monolayer graphene contains two carbon atoms, A and B, there six phonon dispersion bands (see Fig. 8 in chapter 5 in [15]), in which three are acoustic branches (A) and the other three are optic (O) branches. For one acoustic branch (A) and one optic (O) phonon branch, the atomic vibrations are perpendicular to the graphene plan, and they correspond to the out - of - plane(o) phonon modes. For two acoustic and two optic phonon branches, the vibration are in - plan (i). Traditionally, the directions of the vibrations are considered with respect to the direction of the nearest carbon - carbon atoms and, therefore the phonon modes are classified as longitudinal (L) or transverse (T) according to vibrations parallel with or perpendicular to, respectively, the A - B carbon - carbon directions. Therefore, along the high symmetry ΓM and ΓK directions, the six phonon dispersion curves are assigned to LO,

iTO, oTO, LA, iTA, and oTA phonon modes.

3. Particles phenomenology.

3.1. Range of forces.

The inability to deserve the stable of the atom by classical electrodynamics led to the creation of quantum electrodynamics (QED).

A qualitative estimation of the radius of action of nuclear force can be made as follows. Since the nuclear forces do not depend on the electric charge and are of a purely quantum nature, the radius of action of the forces can only depend on mass of the carrier particles m_π and world constants $\hbar$ and c. Of these three quantities, only one constant of the dimension of length can be compiled - the Compton pion wave length

$$R \sim \frac{\hbar}{m_\pi c}, \qquad (46)$$

Where m_π is the pion mass If we assume that the pion travels at the speed of light ~ c, then in time τ it travels a path

$$R \sim c\tau \sim \frac{\hbar}{m_\pi c}. \qquad (47)$$

The obtained distance is the radius of action of nuclear forces.

Naturally, a complete quantum mechanical calculation of the radius of nuclear forces was made by Yukawa in 1935 [16].

The smallest entities of accessible strongly interacting matter in the world are hadrons, either baryons that are aggregates of three quarks or mesons that are made from quark - antiquark pairs. The most stable baryons, the protons and neutrons, are the major constituents of atomic nuclei, and the lightest meson is the pion. Understanding the structure of hadrons and how the properties of these particles arise from quantum chromodynamics(QCD) is a major interest of nuclear physics [83] (see, also [84]). This part of our review is devoted to pions and other strongly interacting bosons. For this reason we briefly describe the Yukawa approximation in task of strong interaction [85]. In 1935 Yukawa [18] tried to develop a theory of nuclear forces (see, e.g. [85]). The most important feature of these forces is that they have a small range. That is, nuclear forces decrease extremely rapidly when the interacting particles are more than about 10^{-15} m apart. The fundamental idea thus antedates the discovery of the pion by years. The role mesons in nuclear physics was not discovered experimentally; it was predicted through a brilliant theoretical

speculation. Below we shall introduce the Yukawa potential in its simplest form by analogy with the electromagnetic interaction.

According quantum electrodynamics (QED) the scalar potential A_0 produced by a charge distribution $q\rho(x')$ satisfies the wave equation [86]:

$$\nabla^2 A_0 - \frac{1}{c^2}\frac{\partial^2 A_0}{\partial t^2} = -4\pi q\rho, \qquad (48)$$

here q - electric charge and ρ is the nucleon probability density. If the charge distribution is time - independent, the wave equation reduces to the Poisson equation,

$$\nabla^2 A_0 = -4\pi q\rho. \qquad (49)$$

In QED the simplest situation arises if the electromagnetic field is produced by a point charge q, at rest at x'. The potential is then given by

$$A_0(x) = \frac{q}{|x - x'|} \qquad (50)$$

and the interaction is ordinary Coulomb energy [87]. In this case, we have the solution of the Poisson equation in the next form:

$$A_0(x) = \int d^3x' \frac{q\rho(x')}{|x - x'|}. \qquad (51)$$

For a point charge q located at the origin, A_0 reduces to the Coulomb potential

$$A_0(r) = \frac{q}{r}. \qquad (52)$$

The important step at the solution of the Poisson equation can be summarized in the relation $\nabla^2(\frac{1}{r}) = -4\pi\delta(x)$, where δ is the Dirac delta function.

Yukawa noticed that the electromagnetic interaction could provide a model but it did not fall off rapidly enough with distance. To force a more rapid decrease, he added a term $k^2\Phi$ to Eq. (49):

$$(\nabla^2 - k^2)\Phi(x) = 4\pi\frac{q}{(\hbar c)^{1/2}}\rho(x). \qquad (53)$$

The last equation is the Klein-Fock-Gordon equation [86]. The electromagnetic potential A_0 has been replaced by the field $\Phi(x)$, and the strength of the field is determined by the strong source $g\rho(x)$, where g determines the dimensionless strength, and ρ, as early, is probability density. The sign of the source term has been chosen opposite to the electromagnetic case. The solution of Eq. (53) that vanishes at infinity is

$$\Phi(x) = \frac{-q}{(\hbar c)^{1/2}} \int \frac{\exp(-k|x - x'|)}{|x - x'|} \rho(x')d^3x'. \qquad (54)$$

For a strong point source, placed at position $x' = 0$, this solution becomes the Yukawa potential [18],

$$\Phi(r) = \frac{-q}{(\hbar c)^{1/2}} \cdot \frac{\exp(-kr)}{r}. \qquad (55)$$

The constant k can be determined by considering Eq. (53) for the case ($\rho(x) = 0$) and comparing it to the corresponding quantized equation. For substitution

$$E \rightarrow i\hbar\frac{\partial}{\partial t}, \quad \vec{p} = -i\hbar\vec{\nabla}, \qquad (56)$$

changes the energy - momentum relation,

$$E^2 = (pc)^2 + (mc^2)^2, \qquad (57)$$

into Klein - Fock - Gordon equation

$$\left[\frac{1}{c^2}\frac{\partial}{\partial t} - \nabla^2 + \left(\frac{mc}{\hbar}\right)^2\right]\Phi(x) = 0. \qquad (58)$$

For a time - independent field and $\rho(x) = 0$, comparison of Eqs. (57) and (58) yields

$$k = \frac{mc}{\hbar}. \qquad (59)$$

The constant k in the Yukawa potential is just the inverse of the Compton wavelength of the field quantum (see Table 2). The mass of the field quantum determines the range of the potential. The simple form of the Yukawa theory thus provides a description of the strong potential produced by a point nucleon in terms of the mass of the field quantum. It explains the short range of the strong forces. Below we briefly describe the most important properties of the nuclear force, that is, the strong force between a proton and an neutron.

Table 4. Comparison between electromagnetic and Yukawa fields (after [88]).

	Electromagnetic field	Nuclear field
Static potential	$V = g/r$	$V = g(e^{-kr}/r)$
Eq. of propagation for potential	$\nabla^2 V - (\frac{1}{c^2})(\partial^2 V/\partial t^2) = 0$	$\nabla^2 V - k^2 V - (\frac{1}{c^2})(\partial^2 V/\partial t^2) = 0$
Relation between $\lambda = \hbar/p$ and ω	$\frac{1}{\lambda^2} + \frac{\omega^2}{c^2} = 0$	$\frac{1}{\lambda^2} + \frac{\omega^2}{c^2} - k^2 = 0$
Relation between $p = \frac{\hbar\omega}{c}$ and E	$\frac{p^2}{\hbar^2} + \frac{E^2}{\hbar^2 c^2} = 0$	$\frac{p^2}{\hbar^2} + \frac{E^2}{\hbar^2 c^2} - k^2 = 0$
or	$E = cp$	$(c^2p^2 + \hbar^2k^2c^2)^{1/2} = E$

1. **Attraction.** The force is predominantly attractive, otherwise stable nuclei could not exist.

2. **Range and strength.** The comparison of the binding energies of ^2H, ^3H and ^4He (see, e.g. [88]) indicates that the range of the nuclear force is of the order 1 fm. If the force is represented by a potential with such width, a depth about 50 MeV is found [89].

3. **Charge independence.** The strong force is charge independent. After correction for the electromagnetic interaction [87, 90, 91] the *pp*, *nn* and *np* forces between nucleons in the same states are identical.

4. **Saturation.** If every nucleon interact attractively with every other one, there would be A(A - 1)/2 distinct interacting pairs. The binding energy would be expected to be proportional to $A(A - 1) \approx A^2$, and all nuclei would have a diameter equal to the range of the nuclear force. Both prediction, binding energy proportional to A^2 and constant nuclear volume, disagree violently with experiment for $A > 4$. For most nuclei, the volume and the binding energy are proportional to the mass number [92]. Consequently, the nuclear force exhibits saturation: one particle attracts only a limited number others; additional nucleons are either not influenced or are repelled. A similar behavior occurs in chemical bonding and with van der Waals' forces (see, e.g. [30]). Saturation can be explained through exchange forced or through strongly repulsive forces at short distances (hard core) [88].

5. **Spin dependence.** The force between two nucleons depends on the orientation of the nucleon spins [93 - 97].

6. **Noncentral forces.** Nuclear forces contain a noncentral component (see, also

below).

To conclude this paragraph we should stress that the perturbation theory does not use for strong interaction. Furthermore, pions are not the only particles in the nucleon - nucleon force (Fig. 11).

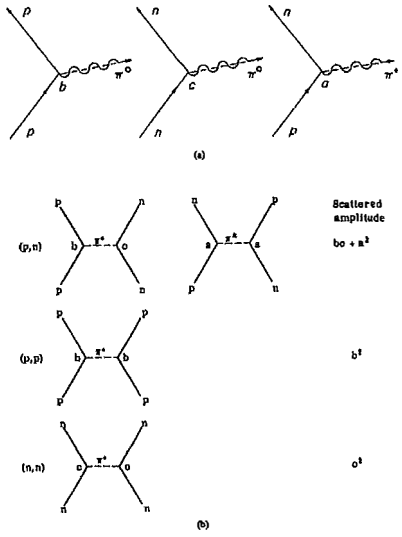

Fig. 11. The diagrams corresponding to the fundamental pion - nucleon interactions. Charge independence requires that the coupling constants a, b, c, be connected $a = (2b)^{1/2}$ and b = - c, b - The combining diagrams giving all cases of nucleon - nucleon scattering. The scattered amplitude for (p,n) is $bc + a^2$, for (p,p) it is b^2, for (n,n) it is c^2 (after [25]).

As is well - known [88, 89] in 1947, the Yukawa particle, the pion was finally discovered in nuclear emissions. After 1947, more mesons kept turning up, and at present the list is long (see, e.g. [89] and references therein).

As was noted above, once major problem in contemporary particle physics to explain why quarks and gluons are never seen as isolated particles. Usually, most particle physicists use "fields" and "particles" interchangeably, i.e. as denoting the same things. That is because the almost universal use of Feynman diagrams (see, e.g [98] and reference quoted therein) gives the false impression that particles (quanta) are always exchanged, even when they do not exist. The use of Feynman diagrams can be justified in weak nonlinear theories (weak coupling limit0 but breaks down for strongly coupled nonabelian theories. This is correct also for strongly couple abelian theories with sources. This is an

example of mistaking the approximation (perturbation theory) for the exact theory. We try below to show that color confinement is a direct result of the nonabelian, i.e. nonlinear, nature of the color interaction QCD. This make it in general impossible to describe the color field as collection of elementary quants (e.g. gluons). In quantum field theory [99] an elementary particle, i.e. quantum = a harmonic excitation of a fundamental field (see, e.g. [86] , is defined through the creation and annihilation operators, $a^\dagger$ and a, of the "second - quantized" theory. For instance, in QED, the entire electromagnetic field can be seen as a collection of superposed quanta, each with energy ω_k. the Hamiltonian of the electromagnetic field (omitting the zero - point energy) can be written

$$H = \sum_k N_k \omega_k \qquad (60)$$

where

$$N_k = a^\dagger a, \qquad (61)$$

is the "number operator", i.e. giving the number of quanta with a specific four - momentum k when operating on a free state,

$$N_k \; |....n_k.....\rangle = n_k \; |....n_k....\rangle. \qquad (62)$$

As all oscillators are independent,

$$|....n_k....\rangle = \prod_k |n_k\rangle, \qquad (63)$$

where n_k is a positive integer, the number of quanta with that particular momentum. The energy in the electromagnetic field is thus the eigenvalue of the Hamiltonian (64). The reasoning for fermion fields is the same, but then the number of quanta in any given state can be only 0 or 1 (Fermi statistics).

Now, assuming that QCD is the correct theory of quark interactions, a problem arises, as it is general impossible to writeof the color fields in terms of superimposed harmonic oscillators. It is not possible to represent the solution as a Fourier expansion and then interpret the Fourier coefficient [100] as creation/annihilation operators through "second quantization", as the color vector potentials A^b_μ (b $\in$ 1, ...,8) are governed by nonlinear evolution by nonlinear evolution equations,

$$D^{\mu}F_{\mu\nu} = j_{\nu}, \qquad (64)$$

and Fourier methods are inapplicable to nonlinear equations [100].
Without a quark current, $j_{\nu} \equiv g_s\bar{\psi}\gamma_{\nu}\psi = 0$, we get, in component for

$$(\delta_{ab}\partial^{\mu} + g_s f_{abc}A_c^{\mu})(\partial_{\mu}A_{\nu}^{b} - \partial_{\nu}A_{\mu}^{b} + g_s f_{bde}A_{\mu}^{d}A_{\nu}^{e}) = 0, \qquad (65)$$

where g_s is the color coupling constant (summation over repeated indices implied). When we have an abelian dynamical group, as in QED, all the structure constants f_{abc} are zero. Eq. (65) then reduces to a linear differential equation, and a general solution can be obtained the Fourier expansion

$$A_{\mu}^{QED} = \int d^3k \sum_{\lambda=0}^{3} [a_k(\lambda)\varepsilon_{\mu}(k, \lambda)e^{-ikx} + a_k^{\dagger}(\lambda)\varepsilon_{\mu}^{*}(k, \lambda)e^{ikx}], \qquad (66)$$

where ε_{μ} is the polarization factor.
However, for a theory based on a nonabelian group, like QCD, this can no longer be done, due to the nonlinear nature of Eq. (65) when $f_{abc}f_{bde} \neq 0$,

$$A_{\mu}^{bQCD} \neq \int d^3k \sum_{\lambda=0}^{3} [a_k^{b}(\lambda)\varepsilon_{\mu}(k, \lambda)e^{-ikx} + a_k^{bt}(\lambda)\varepsilon_{\mu}^{*}(k, \lambda)e^{ikx}]. \qquad (67)$$

Thus, the color fields can be represented by harmonic oscillators (gluons) only in the trivial, and physically empty, limit when the strong interaction coupling constants tends to zero, $g_s \rightarrow 0$ (or, within perturbation theory, equivalently when $Q^2 \rightarrow \infty$ because of asymptotic freedom. Hence, no elementary quanta of the color interaction, in the usual sense, can exist. This means that no gluon particles are possible, and that Eq. (60) does not hold for color fields. The fields are there, but their quanta, gluons (and quarks), are relevant only when probed at sufficiently (infinitely) short distances. we note that a quark field is the source of a color field, but this color is itself a source of a color fie;d. Hence, a quark field is never removed from other sources, is always interacting, and can never be considered to be freely propagating. This results in that the quark fields can never be represented by harmonic oscillator modes, unless $Q^2 \rightarrow \infty$, whereas physical particles, observable in nature, should exist as $Q^2 \rightarrow \infty$. this means that no quark field quanta (quarks) can ever exist. In QCD, the particles "giuons" and "quarks" are merely artifacts of

the approximation method used, i.e. the perturbative expansion in the interaction on a "background" of assumed free gluons and quarks. They are simply absent in the exact theory (in details see [101]).

Contemporary theory predicts that both quarks and gluon acquire running mass distribution in QCD, which are large at infrared momenta [15]. The current - quark of perturbative QCD evolves into constituent - quark as its momentum becomes smaller. The constituent - quark mass arises from a cloud of low - momentum gluons attaching themselves to the current quark. This is dynamically chiral symmetry breaking (DCSB) : an essentially nonperturbative effect that generates a quark mass from nothing, namely it occurs even in the chiral limit. DCSB namely the generation of mass from nothing, is a theoretically - established nonperturbative feature of QCD [14].

3.2.The quark - gluon interaction.

It is well - known that including the color property, a kind of quark charge, the Pauli principle may be asserting. As was shown above, the quantum number color can assume three values, which called red, blue and green. Accordingly, antiquark carry the anticolors anti - red, anti - blue, and anti - green. Now the three u - quarks (for example in $|\Delta^{++}\rangle = |u\uparrow u\uparrow u\uparrow\rangle$) may be distinguished [102]. Thus, a color wave function antisymmetric under particle interchange can be constructed, and we so have antisymmetry for the total wave function. We all know too that the interaction binding quarks into hadrons is called the strong interaction. Such a fundamental interactions always connected with a particle exchange. For the strong interaction, gluons are the exchange particles that couple to the color charge of quarks. This is analogous to the electromagnetic interaction in which photons are exchanged between electrically charged particles. The modern experimental findings (see, e.g. [103]) led to the development of a field theory called quantum chromodynamics - short QCD. As its name implies, QCD is modelled upon quantum electrodynamics - QED [104]. In both, the interaction is mediated by exchange of a massless field particle with $J^P = 1^-$ (a vector boson). Each gluon carries one unit of color and one of antlcolor. It should appear, then, that there should be nine species of gluons - $r\bar{r}$, $r\bar{b}$, $r\bar{g}$, $b\bar{r}$, $b\bar{b}$, $b\bar{g}$, $g\bar{r}$, $g\bar{b}$, $g\bar{g}$. Such nine - gluon theory is perfectly possible in principle, but it would describe a world very different from our own [105]. In terms of group theory of color SU(3) symmetry (on which QCD is based [14, 106]), the 3 x 3 color combinations form two multiplets of states: a 'coloroctet':

$$\left\{\begin{array}{ll} |1\rangle = (r\bar{b} + b\bar{r})/\sqrt{2} & |5\rangle = -i(r\bar{g} - g\bar{r})/\sqrt{2} \\ |2\rangle = -i(r\bar{b} - b\bar{r})/\sqrt{2} & |6\rangle = (b\bar{g} + g\bar{b})/\sqrt{2} \\ |3\rangle = (r\bar{r} - b\bar{b})/\sqrt{2} & |7\rangle = -i(b\bar{g} - g\bar{b})/\sqrt{2} \\ |4\rangle = (r\bar{g} + g\bar{r})/\sqrt{2} & |8\rangle = (r\bar{r} + b\bar{b} - 2g\bar{g})/\sqrt{6} \end{array}\right\} \quad (68)$$

and a 'color singlet'

$$|9\rangle = (r\bar{r} + b\bar{b} + g\bar{g})1/\sqrt{3}\,. \quad (69)$$

If the singlet gluon existed, it would be a common and conspicuous as photon. May be the ninth gluon is the photon. Confinement requires that all naturally occurring particles be color singlets, and this explain why the octet gluons never appear as free particles [107, 108]. But $|9\rangle$ is a color singlet, and if it exists as a mediator it should also occur as a free particle. Moreover, it could be exchanged between two color singlets (a proton and a neutron, say) giving rise to a long - range force strong coupling, whereas in fact up to present time we know that the strong force is of very short range. Therefore, there are evidently only eight kinds of gluons. We should add because gluons are massless, they mediate a force of infinite range (the same as electrodynamics). In this since the force between two quarks is actually long range. However, confinement, and the absence of a singlet gluon, conceals this from us. A singlet state (such as the neutron) can only emit and absorb a singlet (such as the pion), so individual gluons cannot be exchanged between a proton and neutron. That's why the force we observe is of short range. If the singlet gluon existed, it could be exchanged between singlets, and the strong force would have a component of infinite range.

By their exchange the eight gluons mediate the interaction between particles carrying color charge (quarks), i.e. not only quarks but also the gluons themselves. This is an important difference to the electromagnetic interaction, where the photon field quanta have no charge, and therefore cannot couple with each other. In analogy processes of QED (emission and absorption, pair production and annihilation); emission and absorption of gluons (Fig. 12^{a} take place in QCD, as do production and annihilation of quark - antlquark pairs (Fig. 12^{b}). In addition, however three or four gluons can couple to each other in QCD (Fig. 12^{c,d}).

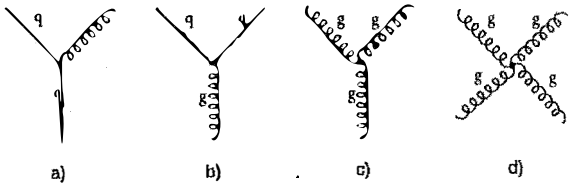

Fig. 12. The fundamental interaction diagrams of the strong interaction: emission of a gluon by a quark (a), splitting of a gluon into quark - antiquark pair (b), and 'self - coupling' of gluons (c, d).

Further we briefly consider some main properties of group SU(3). The set of unitary 3x3 matrices with det U = 1 form the group SU(3). The generators may be taken to be any (3^2 - 1 = 8) linearly independent traceless Hermitian 3x3 matrices (see e.g. [14]). Since it is possible to have only two of these traceless matrices diagonal, this is the maximum number of mutually commuting generators. This number is called the rank of the group [106], so that SU(3) has rank 2, and SU(2) has rank 1. According to the theory of groups, the fundamental representation of SU(3) is a triple. The three color charges of a quark R, G, and B form the fundamental representation of an SU(3) symmetry group. In this representation, the generators are 3x3 matrices, which is called by λ_i, where i = 1, 2 ....8. For λ_i, the convention is to adopt Gell-Mann matrices [109], which are defined as

$$\lambda_1 = \begin{pmatrix} 0 & 1 & 0 \\ 1 & 0 & 0 \\ 0 & 0 & 0 \end{pmatrix} \quad \lambda_2 = \begin{pmatrix} 0 & -i & 0 \\ i & 0 & 0 \\ 0 & 0 & 0 \end{pmatrix} \quad \lambda_3 = \begin{pmatrix} 1 & 0 & 0 \\ 0 & -1 & 0 \\ 0 & 0 & 0 \end{pmatrix} \quad \lambda_4 = \begin{pmatrix} 0 & 0 & 1 \\ 0 & 0 & 0 \\ 1 & 0 & 0 \end{pmatrix}$$

$$\lambda_5 = \begin{pmatrix} 0 & 0 & -i \\ 0 & 0 & 0 \\ i & 0 & 0 \end{pmatrix} \quad \lambda_6 = \begin{pmatrix} 0 & 0 & 0 \\ 0 & 0 & 1 \\ 0 & 1 & 0 \end{pmatrix} \quad \lambda_7 = \begin{pmatrix} 0 & 0 & 0 \\ 0 & 0 & -i \\ 0 & i & 0 \end{pmatrix} \quad \lambda_8 = \frac{1}{\sqrt{3}} \begin{pmatrix} 1 & 0 & 0 \\ 0 & 1 & 0 \\ 0 & 0 & -2 \end{pmatrix} \tag{70}$$

with simultaneous eigenvectors

$$R = \begin{pmatrix} 1 \\ 0 \\ 0 \end{pmatrix} \quad G = \begin{pmatrix} 0 \\ 1 \\ 0 \end{pmatrix} \quad B = \begin{pmatrix} 0 \\ 0 \\ 1 \end{pmatrix}. \tag{71}$$

The eight λ_i's satisfy the following commutations relations:

$$\left[\frac{\lambda_i}{2}, \frac{\lambda_j}{2}\right] = if_{ijk}\frac{\lambda_k}{2} \qquad (72^a)$$

$$\left[\frac{\lambda_i}{2}, \frac{\lambda_j}{2}\right] = \frac{1}{3}\delta_{ij} + id_{ijk}\frac{\lambda_k}{2}, \qquad (73^b)$$

where f_{ijk} is called the structure constant of SU(3) with $\{a, b\} = ab + ba$ and f_{ijk}, d_{ijk} are totally antisymmetric or symmetric with respect to i j k permutations and have the values listed in Table 5.

Table 5. Structure constant of SU(3).

$f_{123} = 1$

$f_{147} = f_{246} = f_{257} = f_{345} = f_{516} = f_{637} = \frac{1}{2}$

$f_{458} = f_{678} = \frac{\sqrt{3}}{2}$

$d_{118} = d_{228} = d_{338} = -d_{888} = \frac{1}{\sqrt{3}}$

$d_{146} = d_{157} = d_{256} = d_{344} = d_{355} = \frac{1}{2}$

$d_{247} = d_{366} = d_{377} = -\frac{1}{2}$

$d_{448} = d_{558} = d_{668} = d_{779} = -\frac{1}{2\sqrt{3}}$

Below we briefly consider the interaction of a quark and anti - quark, in QCD. We shall assume that they have different flavors, so the only diagram (in lowest order is one in Fig. 13)., representing for instance , $u + \bar{d} \rightarrow u + \bar{d}$. The amplitude of this process is given (see Fig. 13) by (see e.g. [110]

$$M = \frac{-g_s}{4}\frac{1}{q^2}[\bar{u}(3)\gamma^\mu u(1)][\bar{v}(2)\gamma_\mu v(4)](c_3^*\lambda^\alpha c_1)(c_2^*\lambda^\alpha c_4) \qquad (74)$$

Here summation over α implied. This is exactly what we have for electron - positron scattering in QED, except that we use g_s (of course), and we have in addition the 'color' factor

$$f = \tfrac{1}{4}(c_3^* \lambda^\alpha c_1)(c_2^* \lambda^\alpha c_4) \,. \qquad (75)$$

The potentlal describing the $q\bar{q}$ interaction is, therefore, the same as that acting in electrodynamics between two opposite charges, only with α replaced by $f\alpha_s$:

$$V_{q\bar{q}}(r) = -f\frac{(\alpha_s \hbar c)}{r}. \qquad (76)$$

Now, the color factor itself depends on the color state of the interacting quarks. From a quark and an antiquark we can make a color octet (68) and a color singlet (69) (all members of which yield the same f). A typical octet state (68) is $r\bar{b}$ (any of the others would do just as well) .Here the incoming quark is red, and outgoing quark must also be red and the antlquark antiblue. Thus

$$c_1 = c_3 = \begin{pmatrix} 1 \\ 0 \\ 0 \end{pmatrix}, \; c_2 = c_4 = \begin{pmatrix} 0 \\ 1 \\ 0 \end{pmatrix} \qquad (77)$$

$$\text{and hence } f = \tfrac{1}{4}[(100)\lambda^\alpha \begin{pmatrix} 1 \\ 0 \\ 0 \end{pmatrix}][(010)\lambda^\alpha \begin{pmatrix} 0 \\ 1 \\ 0 \end{pmatrix}] = \tfrac{1}{4}\lambda_{11}^\alpha \lambda_{22}^\alpha. \qquad (78)$$

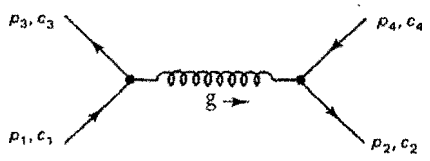

Fig. 13. The quark - antiquark interaction.

A glance at the λ martices (70) reveals that the only ones with entries in the 11 and 22

positions are λ_3 and λ_8. So we can write

$$f = \frac{1}{4}\left(\lambda_3^{(11)}\lambda_3^{(22)} + \lambda_8^{(11)}\lambda_8^{(22)}\right) = \frac{1}{4}[(1)(-1) + \left(1/\sqrt{3}\right)\left(1/\sqrt{3}\right)] = -\frac{1}{6}. \quad (79)$$

The color singlet state is (69) $[(r\bar{r} + b\bar{b} + g\bar{g})1/\sqrt{3}]$ If the incoming quarks are in the singlet state the color factor is a sum of three terms:

$$f = \frac{1}{4\sqrt{3}}\left\{\left[\left[c_3^*\lambda^\alpha\begin{pmatrix}1\\0\\0\end{pmatrix}\right](100)\lambda^\alpha c_4 + \left[c_3^*\lambda^\alpha\begin{pmatrix}0\\1\\0\end{pmatrix}\right](010)\lambda^\alpha c_4 + \left[c_3^*\lambda^\alpha\begin{pmatrix}0\\0\\1\end{pmatrix}\right](001)\lambda^\alpha c\right. \quad (80)$$

The outgoing quarks are necessary also in the singlet state, and we get nine terms in all, which can be written compactly as follows:

$$f = \frac{1}{4}\frac{1}{\sqrt{3}}\frac{1}{\sqrt{3}}(\lambda_{ij}\lambda_{ij}) = \frac{1}{12}\mathrm{Tr}(\lambda^\alpha\lambda^\alpha) \quad (81)$$

in last formula summation over i and j, from 1 to 3, implied in the second expression. Now

$$\mathrm{Tr}(\lambda^\alpha\lambda^\alpha) = 2\delta^{\alpha\beta}, \quad (82)$$

so, with the summation over α,

$$\mathrm{Tr}(\lambda^\alpha\lambda^\alpha) = 16 \quad (83)$$

Evidently, then, for the color singlet

$$f = \frac{4}{3} \quad (84)$$

Putting equations (80) and (85) into equation (77), we conclude that quark - antiquark

potentials are

$$V_{q\bar{q}}(r) = -\frac{4}{3}\frac{(\alpha_s\hbar c)}{r} \qquad (85)$$ (color singlet) and

$$V_{qq}(r) = \frac{1}{6}\frac{(\alpha_s\hbar c)}{r}. \qquad (86)$$ (color octet).

from the signs we see that the force is attractive in the color singlet but repulsive for the octet. This helps to explain why quark - antiquark binding (to form mesons) occurs in the singlet configuration but not in the octet (which would have produced colored mesons) (see, also [11]) .

3.3. Modern view of the origin of the nuclear force.

As is well - known the nuclear force is that force which binds together the nucleons in the nucleus. Historically, the nuclear force was called the Strong Nuclear Force and was considered to be one of the four forces, along with the gravitational force, the electromagnetic force and the weak nuclear force [111, 112]. Soon after the discovery of quarks, the force which holds the quarks together in a nucleon was called the Cromo (hadron) Dynamic Force. This chromo dynamic force, which is a sub - nucleon force, is considered to be much larger than the nuclear force. Later, the chromo dynamic force was redefined as the strong nuclear force, which is now considered to be a sub - nucleon force responsible for the behavior and interactions of sub - nucleon particles. The force which hold the nucleons together in a nucleus was renamed as the Nuclear Force. to add to this confusion even more, there is a model of the nuclear force, which is called the residual chromo dynamic force. Because of this model, it is presumed that the nuclear force is simply a subset of the strong nuclear force. Because of this assumption, it is still claimed that there are only four forces in nature: thestrong nuclear force, the electromagnetic force, the gravitational force, and the weak nuclear force. So The strong nuclear force has two parts, the chromo dynamic force which is sub - nucleon force, and the nuclear force, which is that force holding the nucleons together in a nucleus. In this part of our chapter we use the term nuclear force, which will be used to describe that force which holds together the nucleons in a nucleus. Our present view is that nuclear force may be divided into three parts, as illustrated schematically in Fig. 14. The long - range part ($r \rangle 2$ fm) is dominated by one - pion exchange. If exchanges of a single pion are important, there is no reason to exclude similar processes involving two or more pions and mesons heavier than pions. The range of interaction associated with these more massive bosons is shorter, and for this reason, the intermediate - range part of the nuclear force ($1\text{fm} \langle r \langle 2$ fm) comes mainly from exchanges of single heavier mesons and two pions. The hard core in the interaction ($r \lesssim 1$ fm) is made of heavy meson exchanges, multipion exchanges, as well as QCD effects

(the more detail see [3])

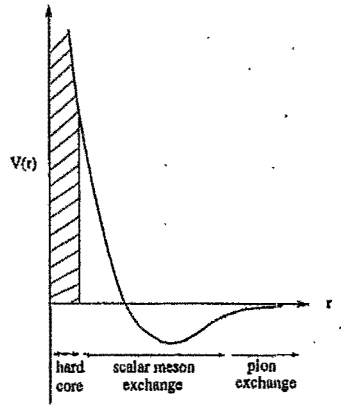

Fig. 14. Schematic diagram showing the different parts of a nucleon - nucleon potential as a function of distance r between two nucleon. The hard core radius is around o.4 fm and it takes energy › 1 GeV to bring two nucleons closer than (twice) this distance. The main part of the attractions lies at intermediate ranges, at radius ~ 1 fm, and is believed to be dominated by the exchange of scalar mesons. The long - range part, starting at around 2 fm, is due to the single - pion exchange.

Now we turn to the task of understanding the strength and the form of the nuclear force from the structure of the nucleons and the strong interaction of the quarks inside the nucleons. Naturally in the following discussion we will employ qualitative arguments. The structure of the nucleon will be approached via the nonrelativistic quark model where the nucleons are built out of three constituent quarks. The nuclear force is primarily transmitted by quark - antiquark pairs, which we can only introduce ad hoc through plausibility arguments. We should repeat that a consistent theory of the nuclear force, based upon the interaction of quarks and gluons, does not yet exist [10, 88, 92, 112].

We begin with the short distance repulsive part of the nuclear force (see Fig. 14) and try to construct analogies to better understood phenomena. We remember that atoms repel each other at short distances is a consequence of the Pauli principle. The electron clouds of both atoms occupy the lowest possible energy levels and if the clouds overlap then some electrons must be elevated into excited states using the kinetic energy of the colliding atoms. Hence we observe a repulsive force at short distances (see, also [78]). The quarks in a system of two nucleons also obey the Pauli principle, i.e. the 6 quark wave function must be totally antisymmetric. It is, however, possible to put as many as 12 quarks into the lowest $I = 0$ state without violating the Pauli principle, since the quarks come in three colors

and have two possible spin (↓, ↑) and isospin (u - quark, d - quark) directions. The spin - isospin part of the complete wave functions must be symmetric since the color part is antisymmetric and, for $l = 0$, the spatial part is symmetric. We thus see that the Pauli principle does not limit the occupation of the lowest quark energy levels in the spatial wave function, and so the fundamental reason for the repulsive core must be sought elsewhere. The real reason is the spin - spin interaction between the quarks [94, 95 113, 114]. The potential energy then increases if two nucleons overlap (see below Fig. 10) and all 6 quarks remain in the $l = 0$ state since the number of quark pairs with parallel spins is greater for separated nucleons. Of course the nucleon - nucleon system tries to minimize its 'chromomagnetic' energy of maximizing the number of antiparallel quark spin pairs. But this is incompatible with remaining in an $l = 0$ state since the spin - flavor part of the wave function must be completely symmetric. The colormagnetic energy can be reduced if at least two quarks are put into the $l = 1$ state. The necessary excitation energy is comparable to the decrease in the chromomagnetic energy, so the total energy will in any case increase if the nucleons strongly overlap. Hence the effective repulsion at short distances is in equal parts a consequence of an increase in the chromomagnetic and the excitation energies. If the nucleons approach each other very close ($r = 0$) one finds in a non - adiabatic approximation that there is an 8/9 probability of two of the quarks being in a p state (see, e.g. [115, 116]. This configuration express itself in the relative wave function of the nucleons through a node at 0.4 fm. This together with the chromomagnetic energy causes a strong, short range repulsion. The nuclear force may be described by a nucleon - nucleon potential which rises sharply at separation less than 0.8 nm [89, 92].

Further we turn to the attractive part of the nuclear force. Again we will pursue analogies from atomic physics. As we know the bonds between atoms are connected to a change in their internal structure and we expect something similar from the nucleons bound in the nucleus. Indeed a change in the quark structure of bound nucleons compared to that of their free brethren has been observed in deep inelastic scattering off nuclei (EMC effect [117, 118]). It is clear upon a moments reflection that the nuclear force is not going to be well described by an ionic bond [78]: the confining forces are so strong that it is not possible to lend a quark from one nucleon to another. A van der Waals force, where the atoms polarize each other and then stick to each other via the resulting dipole - dipole interaction can also not serve us as a paradigm (see, also [119, 120]). A van der Waals force transmitted by the exchange of two gluons (in analogy to two photon exchange in the atomic case) would be too weak to explain the nuclear force at distances where the nucleons overlap and confinement does not forbid qluon exchange. At greater separations gluons cannot exchanged because confinement. Although color neutral gluonic states (glueballs) could still be exchanged, none which are light enough have ever been experimentally observed (see however below experimental manifestation of the strong interaction in solids).

The only analogy left to us to explain the nuclear force is a covalent bond [78], such as that which is, e.g., responsible for holding the H_2 molecule together [121]. Here the electrons of the two H atoms are continually swapped around and can be ascribe to both atoms. The attractive part of the nuclear force is strongest at distances around 1 fm and indeed reminds us of the atomic covalent bond. To simplify what follows, let us assume that

the nucleon is made up of a two quark system (diquark*) and a quark (Fig. 15). Such description has proven to be very successful in describing many phenomena [16].

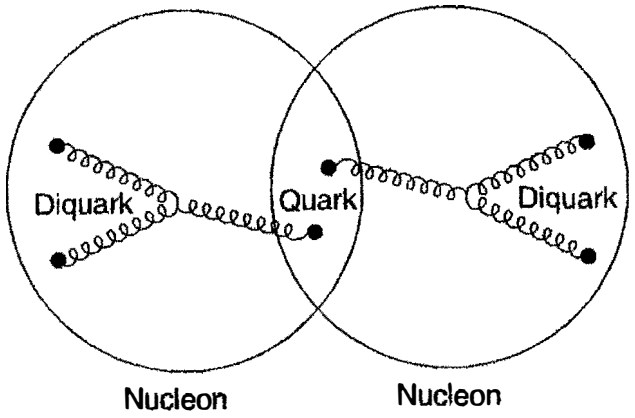

Fig. 15. Quark configurations in a covalent bond picture. At large separations, when the nucleons just overlap, we may understand them as each being diquark - quark systems.

The most energetically favorable configuration is that where a u - and d - quark combine to form a diquark with spin 0 and isospin 0. The alternative spin 1 and isospin 1 diquark is not favored. The covalent bond is then expressed by the exchange of the single quarks. Since the nuclear attraction is strongest at distances of the order of 1 fm [9, 85], we do not to worry about confinement effects. The covalent bond contribution to this force can be worked out analogously to the molecular case. However, the depth of the potential that is found in this way is only about one third of the experimental value [122, 9, 33]. In fact quark exchange is less effective to be exchanged the quarks must have the same color, and there is only a 1/3 probability of this. The contribution of direct quark exchange sinks still further if one takes the part of the nucleon wave function into account where the diquarks have spin 1 and isospin 1. Thus the covalent bond concept, if it is directly transferred from molecules to nuclei, does not give us a good quantitative description of what is going on in nuclei. It should be noted that this is not a consequence of confinement, but rather of direct quark exchange being suppressed as a result of the quarks having three different color charges.

---

*) See, also: S.-X. Qin, C.D. Roberts, S.M. Schmidt, Spectrum of light - and heavy -

baryons, Few - Body Systems **60**, 26 - 44 (2019); M.Y. Baranov, M.A. Bedola, W.K. Brooks et al., Diquark correlation in hadron physics: Origin, Impact and Evidence, ArXiv/ hep - ph/ 2008.07630 (2020).

One more the degree of freedom is an effective quark - quark exchange which may be produced by color neutral quark - antiquark pairs (see quarks). These pairs are continually being created from gluons and annihilated back into them again. This quark - antiquark exchange actually plays a larger role in the nucleon - nucleon interaction than does the simple swapping of two quarks. It must be stressed that this exchange of color neutral quark - antiquark pairs does not only dominate at great separations where confinement only allows the exchange of color neutral objects but also at relatively short distances. One may thus understand the nuclear force as a relativistic generalization of the covalent strong force via which the nucleons finally exchange quarks (the more details see [9, 10, 16]).

3.4. The Concepts of Quantum Chromodynamics.

Quantum chromodynamics, familiarly called QCD, is the modern theory of the strong interaction (see, e.g. [11, 16]). Historically its roots are in nuclear physics and the description of ordinary matter - understanding what protons and neutrons are and how they interact. QCD is renormalizeable quantum field theory of the strong interaction. Its fundamental constituents are spin 1/2 Fermi fields called quarks carry fractional electric charge and non - abelian spin gauge fields called gluons which interact with the quarks as well as among themselves. QCD is the realization that simple principle of a local gauge group SU (3) and the formal existence of fermions called quarks transforming as the fundamental representation of this group essentially specifies the complete theory. The main idea of QCD is to make the SU (3) color symmetry a local, rather than just a global symmetry [123]. As is well known, to implement this local SU (3) symmetry, one must introduce a compensating vector gauge field [124] $A^a_\mu(x)$, $a = 1, 2, \ldots 8$ which transforms as an adjoint representation of SU (3). The octet of gauge fields are called gluons (they do not carry flavor).

Thus, the theory that describes strong interaction in the Standard Model [125] is called QCD. Although this is not tested to the same extent or precision as QED, it is nevertheless in impressive agreement with large body of experimental data and is not contradicted by any known experiment. QCD is similar QED in that both describe interactions that are mediated by massless spin 1 bosons coupling to conserved charges. Theories of this type are called gauge theories because they have a characteristic symmetry called gauge invariance*)

---

*) In the gauge principle we use [126]

$\vec{E} = \vec{\nabla}\phi - \frac{\partial \vec{A}}{\partial t}, \qquad \vec{B} = \vec{\nabla} \times \vec{A}$ (1')

defined by $\phi(\vec{r}, t)$ and $\vec{A}(\vec{r}, t)$ are the scalar and vector potentials. In particular, one easily shows that substititing

$\phi \rightarrow \phi' = \phi + \frac{\partial f}{\partial t}, \qquad \vec{A} \rightarrow \vec{A'} = \vec{A} - \vec{\nabla} f$ (2')

in (1') leaves the electric and magnetic fields unchanged, when $f(\vec{r}, t)$ is an arbitrary scalar function. The replacement of $(\phi, \vec{A})$ by $(\phi', \vec{A}')$ in accordance with (2') is called a gauge transformation, and a theory whose physical predictions are unaltered by such a transformation is said to be gauge - invariant. Because observable quantities depend only on the fields $\vec{E}$ and $\vec{B}$, and not on the particular choice of potentials used to describe them, it is fundamental requirement that any theory formulated in terms of these potentials should be gauge - invariant.

As is well known the gauge invariance plays a fundamental role in theoretical treatments of QED and QCD, where it can be used to infer the detailed forms of the interactions. Here we shall adopt a more phenomenological approach. The spin 1 bosons are called gauge bosons. In QED they are photons, and in QCD they are called gluons. Gluons have zero electric charge, like photons, but couple to the color charges that rather than to the electric charge. This leads immediately to the so - called flavor independence of strong interactions: i.e. the different quark flavors a = u, d, s, c, b and t must have identical strong interactions, because they exist in the same three color states r, g, b with the same possible values of the color charges. This has its most striking consequences for u and d quarks, which have almost equal masses, where it leads to the phenomenon of isospin symmetry [14].

A second property of strong interactions that follows from the above picture without detailed argument is that the forces between the quarks must be long range, because the gluons have zero mass. This does not imply that the forces between hadrons are also long, because hadrons have zero color charges overall. The forces between the colorless hadrons are the residues of the forces between their quark constituents, and cancel when the hadrons are far apart*).

---

*) The main question are: How long - range electromagnetic quarks interaction inside hadrons reduces on the borders of hadrons to short - range nucleons strong interaction.

We have noted that QED and QCD both describe interactions, albeit of very different strengths, which are mediated by massless spin 1 bosons that couple to conserved charges. However, there is a crucial difference between them which profoundly affects the character of the resulting forces. It is that while the photons that couple to the electric charge are themselves neutral, gluons have nonzero values of the color charges to which

they couple. This is illustrated in Fig. 16,whlch shows a particular example of a quark - quark interaction by gluon exchange, where the gluon is represented, as early, by a 'corkscrew' line to distinguish it from a photon.

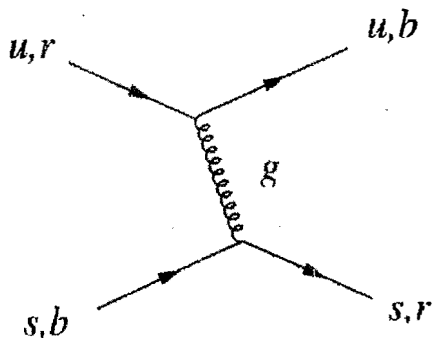

Fig. 16 Example of quark - quark scattering by gluon exchange. In this diagram the quark flavor u or s unchanged on gluon emission, but the color state can change, as shown.

In this picture, the color states of the two quarks are interchanged, and the gluon has the color quantum numbers

$$I_3^C = I_3^C(r) - I_3^C(b) = \frac{1}{2} \qquad (87)$$

and

$$Y^C = Y^C(r) - Y^C(b) = 1, \qquad (88)$$

which follow from applying color conservation at, for example, the lower vertex and using the values for the quark color states r, b listed in Table 4.

Table 4. Values of color isospin charge I_3^C and color hypercharge Y^C for the color states of quarks and antiquarks.

Quarks			Antiquarks		
	I_3^C	Y^C		$3I_3^C$	Y^C
r	1/2	1/3	$\bar{r}$	-1/2	-1/3
g	-1/2	1/3	$\bar{g}$	1/2	-1/3
b	0	-2/3	$\bar{b}$	0	2/3

Just as quarks exist in three different color states, gluons can exist in eight different color states, which is determined by symmetry [11, 124], and the I_3^C, Y^C values correspond to just one of them [15]. Further, we note that is gluons couple to particles with nonzero color charges, and if gluons themselves also have nonzero charges, then by implication gluons couple to other gluons. The two types of self - coupling that occur in QCD are illustrated in Fig. 17. The first is a gluon exchange process analogous to Fig. 17 for quark - quark scattering, while the second involves a zero - range 'contact' interaction (Fig. 17^b). The gluon - gluon interaction of Fig. 17 have no analogue in QED, and it can be shown that they lead to properties of the strong interaction that differ markedly

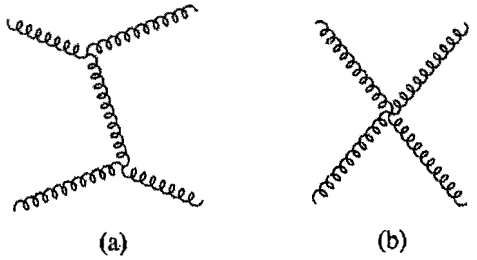

Fig. 17. The two lowest - order contribution to gluon - gluon scattering in QCD.

from those of the electromagnetic interaction. These properties are color confinement and asymptotic freedom. Color confinement is the requirement that observed states have zero color charges. This was discussed early, where, for example, it was shown that all quark bound states (hadrons) must have integral electric charges. It also implies that gluons, like quarks, cannot be observed as isolated free particles, because they have

nonzero values of the color charges. Bound states of two or more gluons with zero color charges overall can be formed in principle, due to the strong interaction between gluons themselves. such states are called glueballs and will be briefly discussed below.

Asymptotic freedom means that the interaction get weaker at short distances, and at distances less than about 0.1 fm the lowest - order diagrams dominate. At these distances quark - quark scattering, for example, is given approximately by one - gluon exchange diagrams like Fig. 17. However, as the distance between the quarks increases, the interaction gets stronger and many high - order diagrams become important. In this strong interaction regime the situation is very complicated, and it has not yet been possible to evaluate the theory precisely. We therefore have to rely an approximate results obtained by numerical simulations of the theory on very large computers, and the demonstration of confinement in QCD rests largely on such simulations. As will be shown below, another important consequence from asymptotic freedom is the fact that the strong coupling α_s is small enough, at sufficiently large momentum transfers, to allow application of perturbation theory in order to provide quantitative predictions of physical processes (see, also [102, 126]).

The above features are conveniently illustrated by considering the static potential between a heavy quark and its antiquark in a color singlet state. This is appropriate potential for a nonrelativistic discussion of charmonium and bottomium, and was determined empirically for the limited range $0.2 \leq r \leq 0.8$ fm [89]. Here we are concerned with the behavior predicted on the basis of QCD. At short distances $r \leq 0.1$ fm, the interaction is dominated by one - gluon exchange and we might expect a Coulomb - like potential analogous to that arising from one - photon exchange in QED. In fact it can be shown that the potential is given by

$$V(r) = -\frac{4}{3}\frac{\alpha_s}{r} \qquad (r \leq 0.1 \text{ fm}), \qquad (89)$$

where the strong coupling constant α_s is a measure of the strength of the interaction analogous to the fine structure constant α in QED. Because of asymptotic freedom, the strength of the interaction, and hence α_s, decreases with decreasing r, but for $r \leq 0.1$ fm this variation is slight and can in many application be neglected. At distances beyond 0.1 fm, however, the strength of the interaction increases more rapidly and one - gluon exchange no longer dominates. In this region, we are forced to rely on lattice gauge theory calculations of limited precision (see, also [4]). These are consistent with the empirical potential in Fig. 18 in the range where this is determined, and show that at large distances the potential rises approximately linearly

$$V(r) \approx \lambda r \qquad (r \geq 1 \text{ fm}), \qquad (90)$$

where the constant λ cannot be calculated precisely, but is of order 1 GeVfm^{-1}. This is

an example of confining potential in that it does not die away with increasing separation and the force between quark and antiquark cannot be neglected, even when they are very far apart.

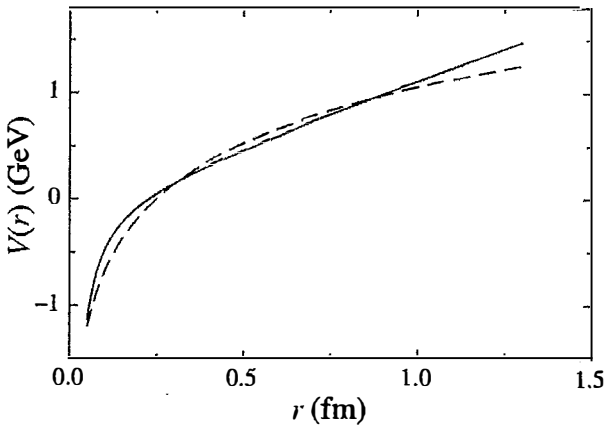

Fig. 18. Heavy quark - antiquark potentials obtained from fitting the energy levels of charmonium and bottomium. The solid line show the results of calculation used next relation $V(r) = -\frac{a}{r} + br$ (with a = 0.30 and b = 0.23 GeV^2) and dashed line obtained used the relation $V(r) = a\ln(br)$ (with a = 0.75 GeV and b = 0.80 GeV).

To conclude this part we should highlight that QCD, the gauge field theory of the strong interaction, has specific features, asymptotic freedom and confinement, which determine the behavior of quark and gluons in particle reaction at high and at low energy scales.

3.4.1. The strong coupling constant.

In this part of our review, we give more formal discussion of the strong coupling α_s in the perturbation domain. As is well - known the strong interaction, binding quarks and gluons inside hadrons, is the strongest of the four fundamental forces in Nature which we know today. In opposition to gravitational and electromagnetic forces, the strong force, as well as weak interaction, only acts at subatomic distances (see, however below). The strong force not only determine the binding of quarks and gluons inside hadrons, it also determines the cohesion of protons and neutrons inside atomic nuclei [14, 89]. Hadrons like protons and neutrons are responsible for more than 99 % of the mass of all visible matter in our

Universe, and those masses are mainly generated by the strong binding of quarks inside hadrons, rather than by the (generally small) masses of the quarks themselves. It is a common place in contemporary physics that the restriction of the strong force to subatomic distances is a consequences of two characteristic features: they are called "Confinement" and "Asymptotic Freedom". Confinement is a necessary requirement to explain the fact that no isolated quarks have ever been observed in any experiment, although symmetry arguments and scattering experiments in the 1960's established quarks [9, 84] with -1/3 or +2/3 of electrical charge units and a newly introduced quantum property called "colored charge", as the basic constituents of hadrons. Confinement determines that at large distances, or equivalent - at low momentum or energy transfer in elementary particle reactions. The strong force prevents the existence of free quarks: trying to separate two quarks from each other, for instance in high energy scattering reactions, apparently results in an increase of the force field's energy at large distances, such the new quarks are created out of the vacuum - the initial quarks "dress" up with other quarks to build hadrons. These hadrons exhibit no net color charge to the outside, such that they appear as elementary entities rather than the quarks themselveseww3.

The term "Asymptoti Freedom" is used to describe the behavior to describe of quarks at high energy or momentum transfer, or - equivalently - at small distances. Also this feature is based on experimental observations: in high energy scattering processes between leptons (e.g. electrons or neltrinos) with protons or neutrons, the dynamics reveal that scattering occurs at pointlike and massless constituents, the quarks, rather than at a homogeneous object with size of proton (neutron). Apparently, at sufficiently high momentum transfers, quarks behave like free of weakly bound particles. Also, quarks knocked out of a hadron, in a high energy scattering process, were never observed as free particles. this picture gives physical insight into the phenomenon of asymptotic freedom ("ultraviolet" UV regime) at high momentum transfer (at small distances) and to s strong coupling regime in the low momentum transfer regime ("infrared" IR regime) (large distanes). Sometimes the confinement, also called "infrared slavery" [127 - 130].

The coupling strength α_s is the basic free parameter of QCD, the theory of strong interaction [16]. QCD describes the interaction of quarks through the exchange of an octet of massles vector gauge bosons, the gluons, using similar concepts as known from QED. While QCD does not predict the actual size of α_s at a particular energy scale, its energy dependence is precisely determined. If the renormalized coupling $\alpha_s(\mu^2)$ can be fixed (i.e. measured) at a given scale μ^2, QCD definitely predicts the size of α_s at any other energy scale Q^2 through the renormalization group equation [63]

$$Q^2 \frac{\partial \alpha_s(Q^2)}{\partial Q^2} = \beta[\alpha_s(Q^2)]. \qquad (91)$$

The perturbative expansion of the β function, including higher order loop correction to the bare vertices of the theory, is calculated to complete 4 - loop approximation [126]:

$$\beta[\alpha_s(Q^2)] = -\beta_0\alpha_s^2(Q^2) - \beta_1\alpha_s^3(Q^2) - \beta_2\alpha_s^4(Q^2) - \beta_3\alpha_s^5(Q^2) + \acute{O}(\alpha_s^6), \quad (92)$$

Where

$$\beta_0 = \frac{33 - 2N_f}{12\pi},$$

$$\beta_1 = \frac{153 - 19N_f}{24\pi^2},$$

$$\beta_2 = \frac{77139 - 15099N_f + 325N_f^2}{3456\pi^3},$$

$$\beta_3 \approx \frac{29243 - 6946.3N_f + 405.089N_f^2 + 1.49931N_f^3}{256\pi^4}, \quad (93)$$

where N_f is the number of active quark flavors at the energy scale Q. The numerical constants in equation (93) are functions of the group constants $C_A = N$ and $C_F = (N^2 - 1)/2N$ for theories exhibiting SU(N) symmetry [55, 61]; for QCD and SU(3), $C_A = 3$ and $C_F = 4/3$ (for details see [4, 55].

A solution of equation (92) in 1 - loop approximation, i.e. neglecting β_1 and higher order terms, is

$$\alpha_s(Q^2) = \frac{\alpha_s(\mu^2)}{1 + \alpha_s(\mu^2)\beta_0 \ln\frac{Q^2}{\mu^2}}. \quad (94)$$

Apart from giving a relation between the values of α_s at two different energy scales Q^2 and μ^2, equation (94) also demonstrates the property of asymptotic freedom: if Q^2 becomes large and β_0 is positive , i.e, if $N_f < 17$, $\alpha_s(Q^2)$ will asymptotically decrease to zero. Likewise, equation (94) indicates that $\alpha_s(Q^2)$ grows to large values and, in this perturbatlve form actually diverges to infinity at small Q^2: for instance, with $\alpha_s(\mu^2 \equiv M_{Z_0}^2) = 0.12$ and for typical values of $N_f = 2 \ldots 5$, $\alpha_s(Q^2)$ exceeds unity for $Q^2 < \acute{O}(100\ \text{MeV} \ldots . 1\ \text{GeV})$ Clearly, this is the region where perturbative expansions in α_s are not meaningful anymore, and we may regardenergy scales below the order of 1 GeV as the nonperturbative region where confinement sets in, and where equations (93) and (94)

cannot be applied.

Including β_1 and higher order terms, similar but more complicated relations for $\alpha_s(Q^2)$, as a function of $\alpha_s(\mu^2)$ and of $\ln\frac{Q^2}{\mu^2}$ as in equation (94) emerge. They can solved numerically, such that for a given value of $\alpha_s(\mu^2)$, choosing a suitable reference scale like the mass of the Z_0 bozon, $\mu = M_{Z_0}$, $\alpha_s(Q^2)$ can be accurately determined at any energy scale $Q^2 \geq 1$ GeV^2.

If we set

$$\Lambda^2 = \frac{\mu^2}{e^{1/(\beta_0 \alpha_s(\mu^2))}},$$

a dimensional parameter Λ is introduced such that equation (94) transforms into

$$\alpha_s(Q^2) = \frac{1}{\beta_0 \ln (Q^2/\Lambda^2)}. \qquad (95)$$

Hence, the Λ parameter is technically identical to the energy scale Q where $\alpha_s(Q^2)$ diverges to infinity $\alpha_s(Q^2) \rightarrow \infty$ for $Q^2 \rightarrow \Lambda^2$. Further we give a numerical example [126] $\Lambda \approx 0.1$ GeV for $\alpha_s\left(M_{Z_0} \cong 91.2 \text{ GeV}\right) = 0.12$ and $N_f = 5$.

In complete 4 - loop approximation and using the Λ - parametrization, the running coupling is thus given by [126, 128] by

$$\alpha_s(Q^2) = \frac{1}{\beta_0 L} - \frac{1}{\beta_0^3 L^2}\beta_1 \ln L +$$

$$\frac{1}{\beta_0^3 L^3}\left(\frac{\beta_1^2}{\beta_0^2}\left[\ln^2 L - \ln L - 1\right] + \frac{\beta_2}{\beta_0}\right) +$$

$$\frac{1}{\beta_0^4 L^4}\left[\frac{\beta_1^3}{\beta_0^3}\left(-\ln^3 L + \frac{5}{2}\ln^2 L + 2\ln L - \frac{1}{2}\right) - 3\frac{\beta_1 \beta_2}{\beta_0^2}\ln L + \frac{\beta_3}{2\beta_0}\right] \qquad (96)$$

where $L = Q^2/\Lambda^2_{\overline{MS}}$. The first line of equation (118) includes 1 - and the 2 - loop coefficients, the second line of the 3 - loop and the third line is the 4 - loop correction respectively.

Measured values of $\alpha_s(\mu)$ [127 - 130], obtained from a variety of different processes are shown in Fig. 19, where the curves show the predicted behavior corresponding to the 'best - fit' value [129]

$$\alpha_s (M_z) = 0.118 \pm 0.002 \qquad (97)$$

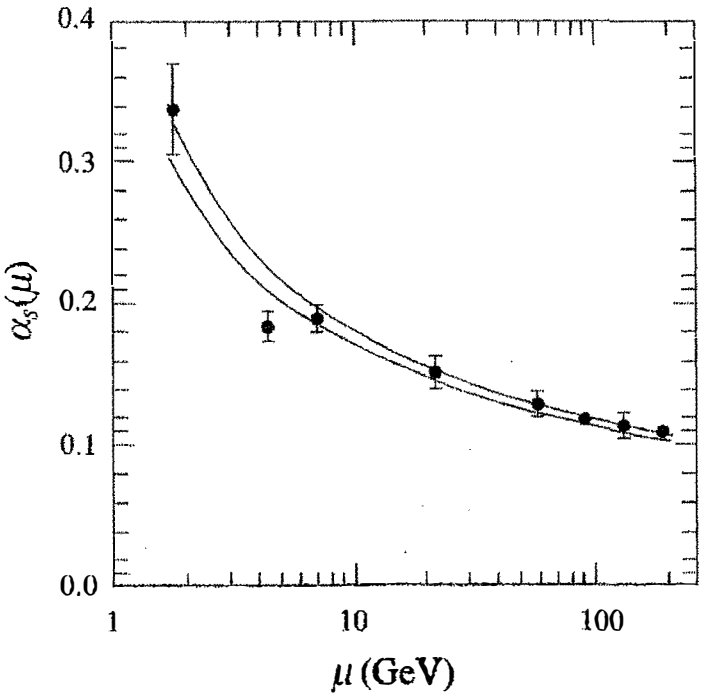

Fig. 19. Values of the running coupling constant α_s obtained in different measurements.

at the reference value $\mu_0 = M_z$ (see, also [128]). The decrease in $\alpha_s(\mu)$ as μ increases, corresponding to shorter distances, is clearly seen, and because of this variation, $\alpha_s(\mu)$ is often referred to as the running coupling constant*) (see, also [127 - 130]).

With QCD and the electroweak theory in hand, what remains to be understood? If both theories are correct, can they also be complete? Many observation are explained only in part, if at all, by the separate theories of the strong and the electroweak interactions. Some of them seem to invite a further unification of the strong, weak and electromagnetic interactions [131]. Among the hints of deeper patterns is the striking resemblance of quarks and leptons. Particles in both groups are structureless at current experimental resolution. Quarks possess color charges, whereas leptons do not, but both carry a half unit of spin and take part in electromagnetic and weak interactions. Moreover, the electroweak theory

itself suggest a relation between quarks and leptons. Unless each of the three lepton families (the electron and its neutrino, for example - see above) can be linked with the corresponding family of quarks (the u and d quarks, in their three colors) the electroweak theory will be beset with mathematical inconsistencies.

---

*)In this regard, it is necessary to add interesting results of a non - accelerator study of the strong interaction in LiD crystals. The measured dependence of the strong interaction constant on the distance between nucleons in the deuterium nucleus [15] showed that it changes from zero (LiH crystals, the hydrogen nucleus does not have a strong interaction) to maximum value in LiD crystals (the deuterium nucleus has a strong interaction). From experimental value of the isotopic shift (0.103 eV) in the paper [132] we have obtained a residual strong coupling constant equal to 2.4680.

What is known about the fundamental forces also points to a unification. All three can be described by gauge theories, which are similar in their mathematical structure. Moreover, the strengths of the three forces appear likely to converge at very short distances, a phenomenon that would be apparent only at extremely large energies Fig. 20. We have seen that the electromagnetic charge grows strong at short distances, whereas the strong, or color, charge becomes increasingly feeble. Might all the interactions become comparable at some gigantic energy?

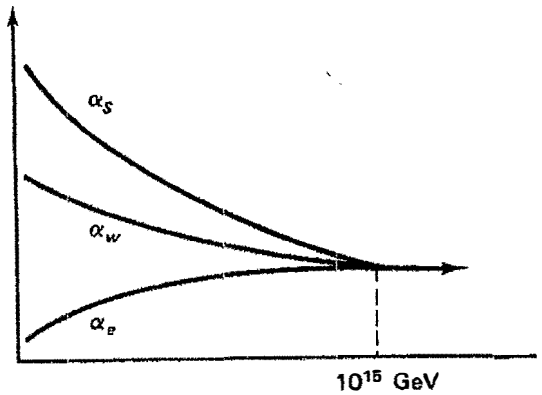

Fig. 20. Evolution of the convergence of coupling constants (α_e - electromagnetic; α_w - weak interaction and α_s - strong interaction) on extremely high energies, which are equivalent to very small scales of distance ($\approx 10^{-29}$ cm) is expected in unified theories (scheme).

If the interactions are fundamentally the same, the distinction between quarks, which respond to the strong force, and leptons, which do not, begins to dissolve. In the simplest example of a unified theory, put forward by authors of the paper [133], each matched set of quarks and leptons gives rise to an extended family containing all the various states of charge and spin of each of the particles. In mathematical consistency of the proposed organization of matter is impressive. Moreover, regularities in the scheme require that electric charge be apportioned among elementary particles in multiples of exactly 1/3, thereby accounting for the electrical neutrality of stable matter. The atom is neutral only because when quarks are grouped in threes, as they are in the nucleus, their individual charges combine to give a charge that is a precise integer, equal and opposite to the charge of an integral number of electrons. If quarks were unrelated to leptons, the precise relation of their electric charges could only be a remarkable coincidence.

In such a unification only one gauge theory is required to describe all the interactions of matter. In a gauge theory each particle in a set can be transformed into other particle. Transformation of quarks into other quarks and of leptons into other leptons, mediated by gluons and intermediate bosons, are familiar. A unified theory suggests that quarks can change into leptons and vice versa. As in any gauge theory, such an interaction would be mediated by a force particle: a postulated X or Y boson. Like other gauge theories, the unified theory describes the variation over distance of interaction strengths. According to the simplest of the unified theories, the separate strong and electroweak interactions converge and become a single interaction at a distance of $\approx 10^{-29}$ centimeter, corresponding to an energy of $\approx 3 \cdot 10^{16}$ Gev (see Fig. 20). Such an energy is far higher than may ever be attained in an accelerates, but certain consequences of unification might be apparent even in the low world we inhabit (see, also [134]). The supposition that transformations can cross the boundary between quarks and leptons implies that matter, much of whose mass consists of quarks, can decay. If, for example, the two u quarks in a proton were to approach each other closer than 10^{-29} centimeter, they might combine to form an X boson, which would disintegrate into positron and a d quarks. The antiquark would then combine with the one remaining quark of the proton, a d quark, to form a neutral pion, which itself would quickly decay into two photons. In the course of the process much of the proton's mass would be converted into energy.

The observation of proton decay would lend considerable support to a unified theory. It would also have interesting cosmological consequences. The Universe contains far more matter than it does antimatter. Since matter and antimatter are equivalent in almost every respect, it is appealing to speculate that the Universe was formed with equal amounts of both. If the number of baryons - three - quark particles as the proton and the neutron, which constitute the bulk of ordinary matter - can change, as the decay of the proton would imply, then the current excess of matter need tot represent the initial state of the Universe. Originally matter and antimatter may indeed have been in equal quantities, but during the first instants after the big bang, while the Universe remained in a state of extremely high energy, processes that alter baryon number may have upset the balance. A number

experiments have been mounted to search for proton decay. The large unification energy implies that the mean lifetime of the proton must be extraordinary long - 10^{30} years or more. To have a reasonable chance of observing a single decay it is necessary to monitor an extremely large number of protons; a key feature of proton - decay experiments has therefore been large scale. The most ambitious experiment mounted to date is an instrumented tank of purified water 21 meters on a side in the Morton salt mine near Cleveland. During almost three years of monitoring none of the water's more than 10^{33}protons has been observed to decay, suggesting that the proton's lifetime is even longer than the simplest unified theory predicts. Income rival theories, however, the lifetime of the proton is considerably longer, and there are other theories in which proton's decay in ways that would be difficult to detect in existing experiments. Furthermore, results from other experiments hint that proton can indeed decay.

Concluding this part we note that although the SM free of inconsistence, it is incomplete; one left hungry for further explanation [135 - 137]. The model does not account for the pattern of quark and lepton masses [138] or for the fact that although weak transitions usually observe family lines, they occasionally cross them. The family pattern itself remains to be explained. Why should there be three sets of quarks and leptons?

The history of elementary particle physics lends support to the idea that properties not calculable in the SM, such as mass spectrum of quarks and leptons, can be understood by going to a deeper level of structure in which many of particles of the SM are composite [6]. According Greenberg [139] the next candidates for compositeness are the dirons. The relatively large number (six) of flavors of quarks and leptons and their easy arrangement into generations is a superficial hint that they may be composite. If dirons, that is quarks and leptons, are composed of preons, there is an energy (denote by Λ) around which dirons are dissociated into preons; that is Λ/c^2 is the mass scale of compositeness. The radius of a composite diron is of order $\hbar c/\Lambda$. If the currently known dirons are the ground states of a composite system, we can expect many excited partners of the dirons at energies of the order Λ. According the results of the paper [139] Λ is greater than about 1 TeV.

As we know in the SM, the quark and lepton masses are proportional to the quark and lepton Higgs couplings. This origin of mass is likely to carry over to preon models. Then quark and lepton masses would be associated with the composite vertex functions connecting the Higgs particles and the quarks and leptons. Previous experience has been that mass spectra are calculable in terms of a deeper level of structure: The Bohr model of atom, the shell model of nuclei and the quark model of hadrons have all been highly successful in this regard. These examples lend strong support to the hope that a preon model of quarks and leptons will determine the mass spectrum of quarks and leptons (the more details see [140]).

4. Experimental manifestation of Quantum Chromodynamics.

All the below non - acceleratory experimental results were obtained on compounds

distinguished one neutron in the nucleus. Here, the new degree of freedom is the mass of the isotope. LiH and LiD crystals have the largest mass isotope effect. Natural diamond ^{12}C and synthetic ^{13}C also differ in a single neutron. This also applies to graphene.

Isotopic substitution only affects the wavefunction of phonons; therefore, the energy values of electron levels in the Schrödinger equation ought to have remained the same. This, however, is not so, since isotopic substitution modifies not only the phonon spectrum, but also the constant of electron-phonon interaction (see above). It is for this reason that the energy values of purely electron transition in molecules of hydride and deuteride are found to be different [141]. This effect is even more prominent when we are dealing with a solid [142]. Intercomparison of absorption spectra for thin films of LiH and LiD at room temperature revealed that the longwave maximum (as we know now, the exciton peak [143] moves 64.5 meV towards the shorter wavelengths when H is replaced with D. For obvious reasons this fundamental result could not then receive consistent and comprehensive interpretation, which does not be little its importance even today. As will be shown below, this effect becomes even more pronounced at low temperatures (see, also [144]).

The mirror reflection spectra of mixed and pure LiD crystals cleaved in superfluid liquid helium are presented in Fig. 21. For comparison, on the same diagram we have also plotted the reflection spectrum of LiH crystals with clean surface. All spectra have been measured with the same apparatus under the same conditions.

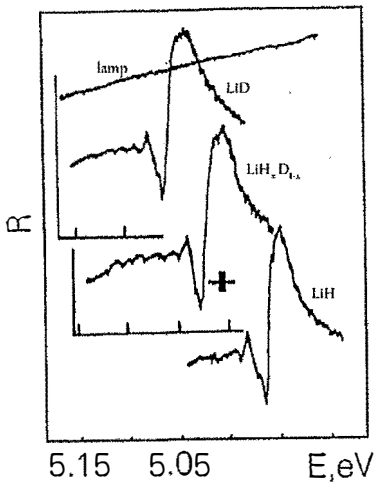

Fig. 21. Mirror reflection spectra in indicated crystals at 2 K cleaved in superfluid helium. Light source without crystals, curve is lamp.

As the deuterium concentration increases, the long-wave maximum broadens and shifts

towards the shorter wavelengths. As can clearly be seen in Fig. 21, all spectra exhibit a similar long-wave structure. This circumstance allows us to attribute this structure to the excitation of the ground (ls) and the first excited (2s) exciton states. The energy values of exciton maxima for pure and mixed crystals at 2 K are presented in Table 5. The binding energies of excitons E_b, calculated by the hydrogen-like formula, and the energies of interband transitions E_g are also given in Table 5.

Table 5. Values of the energy of maxima (in meV) in exciton reflection spectra of pure and mixed crystals at 2K, and energies of exciton binding E_b, band-to-band transitions E_g (after [43]).

Energy, meV	LiH	$LiH_{0.82}D_{0.18}$	$LiH_{0.40}D_{0.60}$	LiD	^6LiH (78K)
E_{1s}	4950	4967	5003	5043	4939
E_{2s}	4982	5001	5039	5082	4970
E_b	42	45	48	52	41
E_g	4992	5012	5051	5095	4980

The ionization energy, found from the temperature quenching of the peak of reflection spectrum of the 2s state in LiD is 12 meV. This value agrees fairly well with the value of ΔE_{2s} calculated by the hydrogen-like formula. Moreover, $E_b = 52$ meV for LiD agrees well with the energy of activation for thermal quenching of free-exciton luminescence in these crystals [43].

Going back to Fig. 21, it is hard to miss the growth of Δ_{12}, [145], which in the hydrogen-like model causes an increase of the exciton Rydberg with the replacement of isotopes (see below Fig. 22). When hydrogen is completely replaced with deuterium, the exciton Rydberg (in the Wannier-Mott model) increases by 20% from 40 to 50 meV, whereas E_g exhibits a 2% increase, and at $2 \div 4.2$ K is $\Delta E_g = 103$ meV.

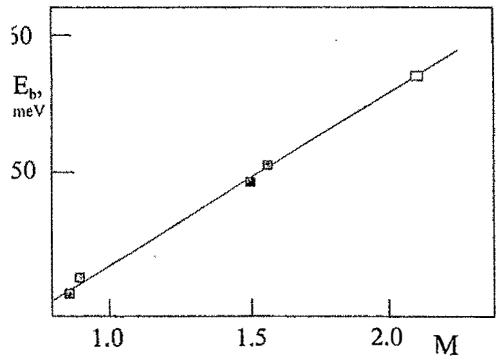

Fig. 22. Binding energy of Wannier - Mott excitons as function of reduced mass of ions based on values of reduced mass of ions for ^{6}LiH, ^{7}LiH, ^{6}LiD, ^{7}LiD and LiT (after [145]).

This quantity depends on the temperature, and at room temperature is 73 meV, which agrees well enough with ΔE_g = 64.5 meV as found in the paper of Kapustinsky et al. The single-mode nature of exciton reflection spectra of mixed crystals LiH_xD_{1-x} agrees qualitatively with the results obtained with the virtual crystal model (see e.g. Elliott et al. [146]; Onodera and Toyozawa [147]), being at the same time its extreme realization, since the difference between ionization potentials ($\Delta\zeta$) for this compound is zero. According to the virtual crystal model, $\Delta\zeta = 0$ implies that $\Delta E_g = 0$, which is in contradiction with the experimental results for LiH_xD_{1-x} crystals. As was shown above [43, 69} the change in E_g caused by isotopic substitution has been observed for many broad-gap and narrow-gap semiconductor compounds.

All of these results are documented in Table 5, where the variation of E_g, E_b, are shown at the isotope effect. We should highlighted here that the most prominent isotope effect is observed in LiH crystals, where the dependence of $E_b = f(C_H)$ is also observed and investigated. To end this section, let us note that E_g decreases by 97 cm^{-1} when ^{7}Li is replaced with ^{6}Li (see Table 21 in [69]). It was in the original work (Plekhanov et al. [143]) where the exciton binding energy E_b was found to depend on the isotopic composition that this change in E_b was attributed to the exciton-phonon interaction (originally with LO phonons). The preferential interaction of excitons with LO phonons in LiH (LID) crystals was later repeatedly demonstrated in the luminescence spectra [148] and resonant Raman light scattering [149], which consist of a phononless line (in the former case) and its LO repetitions.

At present time we know that the main consequences of interaction of electron and hole interaction in excitons with polarization vibrations are the static screening of the lattice charges (introducing ε_0) and the change in the effective masses of the particles. Both these effects of electron-(hole)- phonon interaction can easily be taken into account, and lead to a change in the exciton Rydberg E_b. These corrections do not destroy the hydrogen-like structure of the exciton spectrum. At the same time, the non-coulombic corrections to the

electron-hole Hamiltonian modify the hydrogen-like structure - removing, for example, degeneration of levels with respect to orbital and magnetic quantum numbers (see e.g. [150] and references therein). The very fact, however, that the problem of renormalization of energy spectra of Wannier - Mott excitons does not admit an exact solution even in the limiting cases, often gives rise to a situation in which there is no agreement between the results obtained by different authors. Starting with the classical works of Haken [34], all papers may be divided into two broad classes depending on how they take deal with the Coulomb interaction: between 'bare' electrons and holes, or between electrons and holes in the polaron state. In other words, first the interaction of band electrons and holes with LO optical phonons is taken into account, and then of the Coulomb interaction between electrons and holes clad in the 'polarization coats' is considered. As will be shown below, the study of exciton-phonon interaction in crystals with isotopic effect not only provides entirely new information, but also allows us to reconstruct experimentally the values of Frohlich and Coulomb interaction constants. From Fig. 22 we see that when hydrogen is completely replaced with deuterium, the binding energy of the exciton exhibits a 20% increase from 42 to 52 meV [144]. It is easy to see that in the model of virtual crystal the binding energy of the exciton in LiT crystals [69] must be equal to 57 meV (see Fig. 22). Hence it follows that in the linear approximation the isotopic dependence of binding energy of Wannier - Mott excitons may be expressed as

$$E_b = E_b(0)(1+\gamma). \quad (98)$$

where $E_b(0)$ is the purely coulombic binding energy of the exciton (in the frozen lattice), which in our case is equal to 31.5 meV, and the angular coefficient is $\beta = 12.18$ meV/M, where M is the reduced mass of ions of lithium and hydrogen (deuterium, tritium) ions; $\gamma = \beta M / E_b(0)$ (see also [69]). From the standard equation for the Coulomb binding energy of the exciton

$$E_b = \frac{e^4 \mu}{\hbar^2 \varepsilon_\infty^2} \quad (99)$$

we get the dimensionless constant of Coulomb interaction:

$$\eta^2 = \frac{E_b(0)}{\hbar\omega_{LO}} = 0.47. \quad (100)$$

Comparing the value of $\eta^2 = 0.47$ and the constant of Fröhlich exciton-phonon interaction $g^2 = 0.33$ [59] we see that they are close enough. This implies that both the Fröhlich and the Coulomb interactions between electrons (holes) and LO phonons in exciton must be treated with equal attention.

Under the continuous optical excitation a stationary population in the exciton states can be created. Due to the free motion in the crystal and the interaction with the crystal lattice the gas of free excitons is spread over some region of kinetic energy [36]. However, usually only the lowest $n = 1S$ (ground state) exciton is populated (Fig. 4) at low temperatures [151]. The photoluminescence emission of free excitons can take place either in resonance with the exciton absorption line (a so - called zero-phonon luminescence) or can be shifted in energy due to the simultaneous creation of phonon (phonon - assisted luminescence). In the resonant excitons emission only excitons with small wavevectors of the order of the photon wavevector $\vec{K} \simeq 0$ can participate. Phonon - assisted luminescence of free excitons in polar compounds is mainly due to the creation of longitudinal optical (LO) phonons [151,

36]. Since the energy of LO phonons has a weak dependence on wavevector $\vec{q}$ (see, e.g. [152], the spectrum of emitted photons is simply related to the initial distribution of exciton energy. Fig. 23 shows the free excitons photoluminescence in LiH and LiD crystals at 2 K with photoexcitation above the intrinsic absorption edge [151].

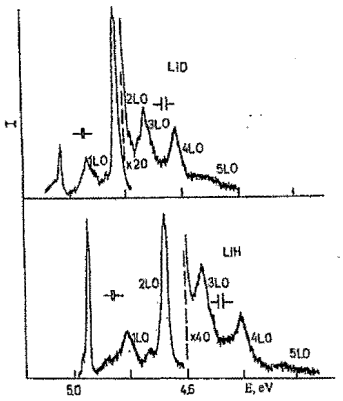

Fig. 23. Free exciton emission spectra at 2 K in LiH and LiD crystals cleaved in superfluid helium.

The free exciton photoluminescence spectrum of LiH crystals cleaved in superfluid liquid helium consists of the narrow zero - phonon line and its wider phonon replicas corresponding to the radiative annihilation of excitons accompanied by excitation from one to five LO phonons. The zero - phonon emission line is almost in resonance with the reflection line in the exciton ground state ($E_{n=1S}$ = 4.950 eV for LiH crystals at 2 K [151, 43]), which is due of the direct electron transition X_1 - X_4 of the first Brillouin zone [52]. Phonons replicas form an equidistant series to the red from resonance exciton emission line. The difference in energies of these replicas, as early [145] is 140 meV which is close to the energy of LO phonons in the center of the Brillouin zone obtained in [154, 155]. The photoluminescence spectrum of a LiD crystals with a pure surface shown also in Fig. 23 is similar in many respects to the free excitons luminescence spectrum of LiH crystals. However, there are some differences. These differences are related with the next manifestations:

1. The short - wavelength shift as whole of the free excitons photoluminescence spectrum of LiD crystals on 103 meV relatively the spectrum of LiH crystals.

2. In the case of LiD crystals the energy difference between lines in the spectrum is on average 104 meV corresponding to the energy of the LO phonons in the Γ - point of the Brillouin zone [43, 151, 153, 154].

Firstly the zero-phonon emission line of free excitons in LiD crystals shifts to the short -

wavelength side on 103 meV. These results directly show the violation of the strong conclusion (see, e.g. [5, 16]) that the strong force does not act on leptons. The second difference concludes in less value of the LO phonon energy, which is equal to 104 meV. When light is excited by photons in a region of fundamental absorption in mixed LiH_xD_{1-x} crystals at low temperature, line luminescence is observed (Fig. 24), like in the pure LiH and LiD crystals. As before [145], the luminescence spectrum of crystals cleaved in superfluid liquid hellum consists of the relatively zero - phonon line and its wide LO replicas. For the sake of convenience, and without scarfing generality, Fig. 24 shows the lines of two replicas. Usually up to five LO repetitions are observed in the luminescence spectrum as described in detail in [43]. In Fig. 24 we see immediately that the structure of all three spectra is the same. The difference is in the distance between the observed lines, as well as in the energy at which the luminescence spectrum begins, and in the half - width of the lines.

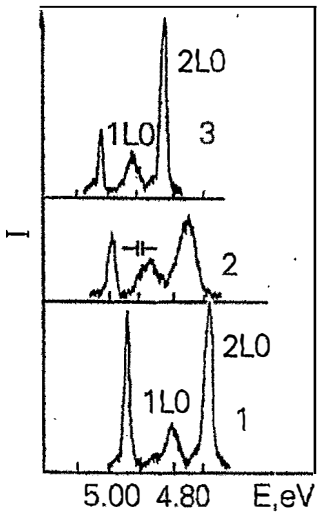

Fig. 24. Photoluminescence spectra of free excltons in LiH (1), LiH_xD_{1-x} (2) and LiD (3) crystals cleaved in superfluid helium at 2 K. Spectrometer resolution is shown.

The simplest approximation, in which crystals of mixed isotopic composition are treated as crystals of identical atoms having the average isotopic mass, is referred to as virtual crystal approximation (VCA) [156]. Going beyond the VCA, in isotopically mixed crystals one would expect local fluctuations in local isotopic composition within some effective volume, such as that an exciton. As follows from Fig. 21, excltons in LiH_xD_{1-x} crystals

display a unimodal character, which facilitates the interpretation of their concentration dependence. As will be shown in the discussion the concentration dependence of the power of strong nuclear interaction, i.e. dependence on the neutron concentration.

Because of the low intensity of scattered light, and thanks to the high resolution of modern spectroscopic instruments, the development of high sensitive techniques of detection of weak optical signals (photon counting mode, optical multichannel analyzers, optical linear arrays and the specialized systems [157]), the light scattering method has become one of the most common technique for the research.

In the last five decades, inelastic light scattering spectroscopy has become one of the most powerful and widely used optical method for obtaining quantitative information about the interaction of light with matter. For example, it has been used to investigate resonant Ramans cattering (RRS) in crystals. For a displacement of the excitation like frequency toward long wavelength by an amount compared to the exciton resonance, e.g. $E_i \langle E_{n=1s}$ (where $E_{n=1s}$ is the energy of the exciton ground state) intense light scattering is observed [154]. The spectrum of this scattering is shown in Fig. 25. As in the luminescence, the process of energy relaxation take place, mainly with emission of LO phonons. This is shown by the character of the structure in the scattering spectrum. Indeed, as for the case of the excitation well within the exciton zone (see Fig.4), the energy difference between the peaks in the scattered spectrum equals the energy of the LO phonon in the Γ - point of Brillouin zone [153 - 155].

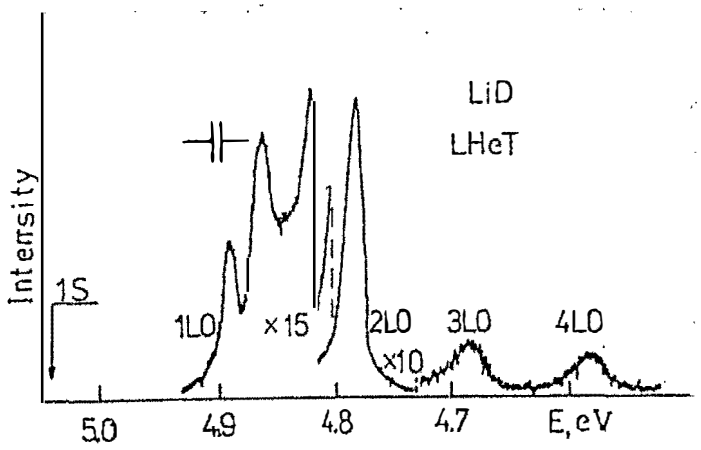

Fig. 25. Resonant Raman scattering spectrum of a LiD crystals cleaved in liquid helium at the excitation E = 4.992 eV at 4.2K. The arrow 1s indicates the energy position of the ground exciton states.

. The relatively large half - width of the scattered peaks should be noted [149]. Additional investigations have shown that their half - width are always larger than that of the excitation line [43]. In addition to the LO(Γ) lines the RRS spectrum contains two more bands the maxima of which are displaced by twice the energy of the TO(Γ) and LO(X) phonons from the exciting line (for LiH $\hbar\omega_{TO(\Gamma)}$ = 76 meV and $\hbar\omega_{LO(X)}$ = 117 meV [43,]. More precise measurement of the dependence of the second - order Raman spectra for LiH [158] and LiD on the excitation energy (below $E_{n=1s}$) is shown in Fig. 26. The presence of the second - order TO(Γ) phonons in the RRS spectrum may be explained by a relatively strong scattering deformation mechanism in these crystals, where, however the main mechanism as was seen from Figs. 24 and 25, is Fröhlich mechanism of intraband scattering [158].The longwavelength displacement of the excitation line frequency relatively exciton resonance a monotonic decrease the intensity of RRS spectrum as whole more than 60 fold in both LiH and LiD crystals (see, also Fig. 26).

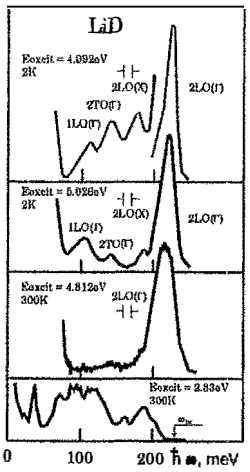

Fig. 26. The dependence of the shape and maximum frequency of the 2LO(Γ) Raman line on the excitation energy of LiD crystals.

As was indicated above another very interesting example is carbon. Carbon, one of the most elements in nature, still gives a lot surprises. It is found in many different forms - allotropes - from zero dimensional fullerene, one dimensional carbon nanotubes, two

dimensional graphene and graphite, to three dimensional diamond - and the properties of the various carbon allotropes can vary widely [62, 63,65]. Fullerenes are essentially hollow carbon shells of various sizes. the most well - known of these is a 60 - carbon unit called buckminster fullerene or C_{60} (more details see below). For instance, diamond is the hardest material, while graphite is one of the softest; diamond is transparent to the visible part of spectrum, while graphite is opaque; diamond is an electrical insulator, while graphite and graphene are a conductors. Very important is that all these different properties originate from the same carbon atoms, simply with different arrangements of the atomic structure. Below we describe the new phenomena of the carbon - isotope effect in diamond as well as graphene. Crystals ^{12}C and ^{13}C diamond differ only one neutron.

Due to the indirect gap of E_g = 5.47 ± 0.005 eV (295 K), at K = 0.76 X, diamond has intrinsic phonon - assisted free exciton luminescence lines (see, e.g. [68, 69]). The change of the indirect gap of diamond between pure ^{12}C and ^{13}C crystals has been determined by Collins et al. [159]. The luminescence spectra of the natural (^{12}C) and synthetic (^{13}C) diamond at electron excitation were investigated by Collins et al. [159], Ruf et al. [160], Watanabe et al. [161]. Fig. 27 compares the free exciton luminescence for a natural diamond with that for a synthetic diamond.

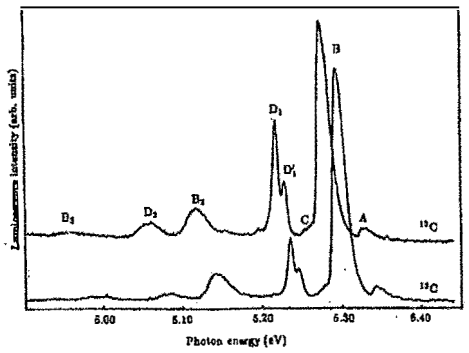

Fig. 27. Spectra measured at 77K phonon - assisted free cathodoluminescence feature (A, B and C) and the phonon assisted bound - exciton feature (D) from natural semiconducting ^{12}C diamond and a ^{13}C synthetic diamond (after [159]).

The peaks labeled A, B and C are due, respectively, to the recombination of a free exciton with the emission of transverse - acoustic, transverse - optic and longitudinal - optic phonons having wavevector ± k_{min} and quanta (in ^{12}C [43, 111].

$\hbar\omega_{TA} = 87 \pm 2$; $\hbar\omega_{TO} = 141 \pm 2$; $\hbar\omega_{LO} = 163 \pm 1$ meV. (101)

Features B_2 and B_3 are further free exciton processes involving the above TO phonon with one and two zone - center optic phonons respectively. As we can see from Fig. 27 the isotope shift of the free exciton luminescence spectrum of ^{13}C diamond is equal 16.5 ± 2.5 meV [69]. The more detailed and quantitative investigation of $E_g \sim f(x)$, where x is the isotope concentration was done by Ruf et all. [160] (Fig. 28) and Watanabe et all. [161] (Fig. 29) where five samples of diamond with different concentrations x were studied.

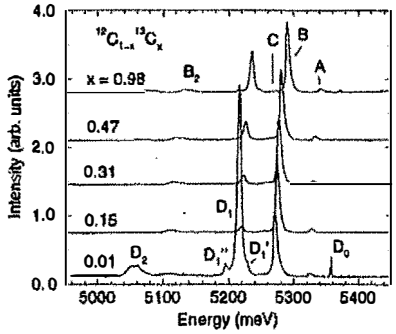

Fig. 12. Cathodoluminescence spectra of isotopically modified diamond at 36 K. Intrinsic phonon - assisted recombination peaks are labeled in the top spectrum, those from boron - bound excitons in that at the bottom. The spectra are normalized to the intensity of the B peak and vertically offset for clarity (after [160]).

Watanabe et al. have concluded that the maximum change of the band gap due to substitution of ^{12}C by ^{13}C is $\Delta E_g = 15.4$ meV.

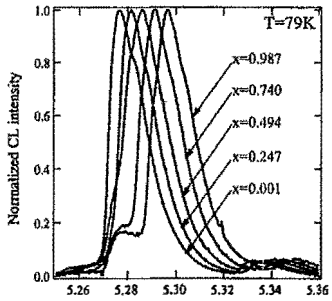

Fig. 29. Luminescence spectra of free excitons in homoepitaxial diamond films grown from mixture of methane in hydrogen by means of a microwave plasma - assisted CVD. The spectra illustrate the effects of isotope composition $^{12}C_{1-x}^{13}C_x$ (x = 0.001; 0.247; 0.494; 0.740; and 0.987) mixed in the CVD gas phase. All spectra are normalized to the same height (after [161]) .

This value is in good agreement with the estimate of 16.5 ± 2.5 meV by Collins et all. [159] using a zero - point renormalization obtained from a fit of the experimental temperature dependence of the band gap (see, also [68]).

It is clear that the lattice - dynamic properties of a crystal are directly affected by the atomic mass. To a first approximation, phonon behave like harmonic oscillators with frequencies [162]

$$\omega \propto m^{-1/2}. \qquad (102)$$

Crystals containing various isotope sare usually described within virtual crystal approximation (VCA) [162] where m in Eq. (102) is replaced by the average atomic mass

$$\overline{m} = \sum_i c_i m_i. \qquad (103)$$

It is obtained from the sum over the isotopes masses m_i and concentration c_i. In spite of VCA simplicity, the model describes the general feature of the lattice dynamics of mixed alkali - halide crystal sufficiently well (for details see [162]). Isotopes are ideal for lattice - dynamltlc investigations of crystals. One can make use of the unique isotopic properties by

varying the isotopic composition. Isotope substitution helps to disentangle the individual contributions of anharmonic and disorder - induced effects and to clarity the origin of phonon broadening mechanisms. Due to the fact that substitution of the isotopic mass in semiconducting crystals a small variation of E_g [81], perturbation theory is applicable (excluding LiH crystals [43]).

Raman spectroscopy is a powerful means to gain experimental access to phonons and their interaction and scattering mechanisms. All studies presented in this paragraph are restricted to stable, i.e. non - radioactive isotopes. About 300 stable and 1000 radioactive isotopes are known today. Some elements are isotopically pure (for example, Co), while others may contain numerous isotopic modifications (foe example, Sn has 10 stable isotopes with atomic masses ranging from 112 to 124, while Xe has 23 isotopes, 9 of which are stable (see, Table 1 in [68]) [163].

In this part, the modern understanding of first - order Raman slight scattering spectra in isotopically mixed elementary and compound (CuCl, GaN, GaAs, GaP) semiconductors having a zinc blende structure is described. It is well - known that materials having a diamond structure (C, Si Ge, α - Sn) are characterized by the triply degenerate phonon states in the Γ - point of the Brillouin zone ($\vec{k} = 0$) (see, e.g. [85]). Isotope effect in light scattering spectra in Ge crystals was first investigated by Agekyan et al. [164]. A more detailed study of Raman light scattering spectra in isotopically mixed Ge crystals has been performed by Cardona and coworkers [70]. Watanabe et all. have concluded that the maximum change of the band gap due to substitution of ^{12}C by ^{13}C is $\Delta E_g = 15.4$ meV. This value per one neutron and on seven neutrons we get $15.4 \times 7 \simeq 108$ meV. This value is very close to the observed one (103 meV) in LiD crystals.

The cubic modifications of crystalline carbon, diamond, is characterized by a tetrahedral coordination underlying its structure dictated by sp^3 bonding between the nearest neighbor atoms. Diamond has two atoms per primitive (Bravais) cell. The strong covalent bonding and the light mass of the constituent atoms result in a large frequency (see, Eq. (102)) for zone center, Raman active, triply degenerate F_2 mode [152]. Its crystalline perfection and transparency [165] make diamond ideally suited for inelastic light scattering. First Raman study of the dependence the frequencies of phonons on the isotopic composition was conducted on diamond by Chrenko [167] in 1988. Several publications on diamond by other groups followed later [88, 90, 91, 92]. Most clear results was obtained by Hanzawa et al. [166] (see Fig. 30).

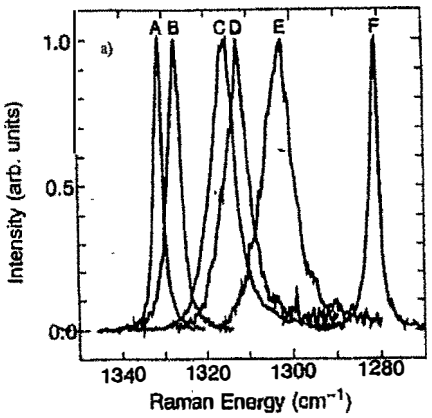

Fig. 30. First - order Raman scattering in isotopically mixed diamond crystals $^{12}C_x^{13}C_{1-x}$. The peaks A, B, C, D, E and F correspond to x = 0.989; 0.90; 0.60; 0.50; 0.30 and 0.001{after [166]).

First - order Raman light scattering spectrum in diamond crystals also includes one line with maximum $\omega_{LTO}(\Gamma)$ = 1332.5 cm^{-1} [170]. In Fig. 14 the first - order scattering spectrum in diamond crystals with different isotope concentrations is shown [166]. As was shown in [170], the maximum and width of the first - order scattering line in isotopically - mixed diamond crystals are nonlinearly dependent on the concentration of isotopes x. The maximum shift of this line is 52.3 cm^{-1}, corresponding to the two limiting values of x = 0 and x = 1. The effect of the isotopic ^{12}C to ^{13}C ratio on the first - and second - order Raman scattering of light in the diamond has been investigated in [172]. As ^{13}C content is increased from the natural ratio ($^{12}C/^{13}C$ = (1 - x)/x, where x = 0.011 to the almost pure ^{13}C (x = 0.987) the whole spectrum has shifted towards longer wavelength (Fig. 15) in good agreement with the expected $M^{-0.5}$ frequency dependence on the reduced mass M. For an approximately equal mix of the two isotopes, the authors reported that the feature seen in the above two - phonon spectra were either broadened or unresolved.

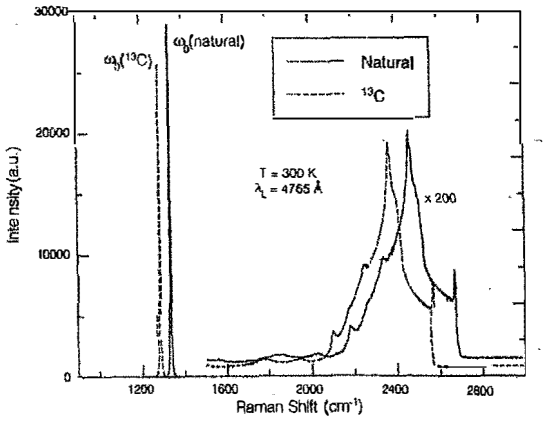

Fig. 31. The Raman spectra of natural and a ^{13}C diamond. The spectra show the dominant first - order Raman - active F_{2g} line and the significantly weaker quasi - continuous multiphonon features (after [171]).

The analogous picture was obtained on the isotope dependence of Raman spectra in silicon [172]. Fig. 16 shows the measured frequencies of the first - order Raman active modes in silicon for six different isotopic composition.

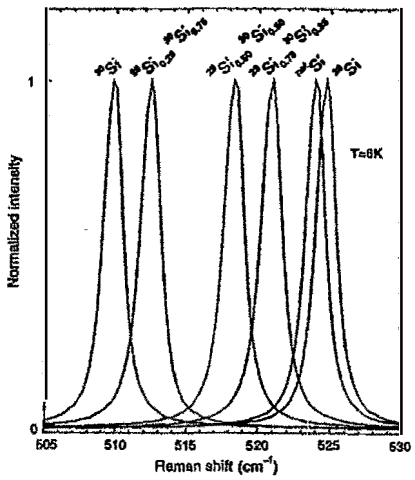

Fig. 32. Typical low temperature Raman spectra of silicon with various isotopic composition (after [172]).

As was shown above, in two - dimensional graphene, carbon atoms are periodically arranged in an infinite honeycomb lattice (see Fig. 6). Such an atomic structure is defined by two types of bonds within the sp^2 hybridization [60, 78]. Elastic and inelastic light scattering are powerful tools for investigating graphene [173 - 178]. Raman spectroscopy allows monitoring of doping, defects, disorder, chemical and isotope [68, 69] modifications, as well as edges and uniaxial strain. All sp^2 - bonded carbons show common features in their Raman spectra, the so - called G and D peaks (see, e.g. Fig. 8 in [179]), around 1580 and 1360 cm^{-1} (see, e.g. [174, 175]). The G peak (see, also below Fig. 34) corresponds to the E_{2g} phonon at the Brillouin zone center (Γ - point). The D peak is due to the breathing modes of six - atom rings and requires a defect for its activation. It comes from TO phonons around the Brillouin zone K point and it is activated by an intravalley scattering process 174]. The 2D peak is the second order of the D peak. This is a single peak in monolayer graphene, whereas it splits into four bands in bilayer graphene, reflecting the evolution of the band structure [7, 22]. The Raman spectrum of graphene also shows significantly less intensive defect - activated peaks such as the D' peak , which lies at ~ 1620 cm^{-1}. This is activated by an intravalley process i.e. connecting two points belonging to the same cone around K (see, Fig. 2) in [175]). The second order of the D' peak is called 2D' peak. Since 2D and 2D' peaks originate from a Raman scattering process where momentum conservation is obtained by the participation of two phonons with opposite wave vector ($\vec{q}$ and $-\vec{q}$), they do not require the presence of defects. Thus, they are always visible in the Raman spectrum (see cited papers [173 - 178] and references therein).

Graphene is one unique material which shows properties not fond in other materials. One of these unique features of graphene is the influence of long range strains on the electronic properties. The possibility of tuning the dynamics of carriers as well as phonons by appropriately designed strain patterns opens the way for novel applications of graphene, not possible with any other materials (see, e.g. [183] and references therein). At present time we have several reports, which have examined graphene properties under unlaxial deformation [178, 183, 184, 185].

Strain can be very efficiently studied by Raman spectroscopy since this modifies the crystal phonon frequency, depending on the anharmonicity of the interatomic potentials of the atoms. Raman spectra of strained graphene show significant redshifts of 2D and G band (see Table 6) because of the elongated of the carbon - carbon bonds.

Table 6. Red shift of the G and 2D bands in the Raman spectra in graphene monolayers under unlaxial tensile stress.

Ref.	Shift of G (G^+ and G^-) band cm^{-1}/%	Shift of 2D band cm^{-1}/%	E_g, meV
15	14.2	27.8	300
25	5.6; 12.5	21	
27	10.8; 31.7	64	
26	theory		≃ 500

The authors of the paper [184] have proposed that by applying uniaxial strain on graphene, tunable band - gap at K - point can be realized. First principle calculations predicted a band - gap opening of ≃ 300 meV for graphene under 1% uniaxial tensile strain (Fig. 33). Thus, the strained graphene provides an alternative way to experimentally tune the band - gap of graphene, which would be more efficient and more contollable than other methods (see, above) that are used to open band - gap in graphene.

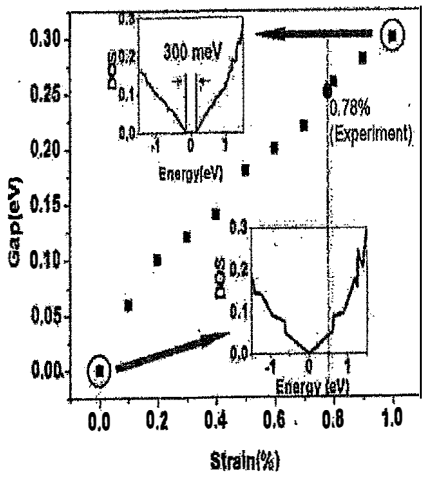

Fig. 33. The band - gap of strained graphene with the increase of uniaxial tensile strain on graphene. The magnitude of gap is determined by the gap opening of density of states. The insert show the calculated density of states of unstrained and 1% tensile strained graphene. The dash line and solid dot indicate the calculated bandgap of graphene under the highest strain (0.78 %) [18].

The method of the isotope renormalization of the energy of elementary excitations in solid very often used in last five decades and well described in the scientific literature (see, for example reviews [68, 69]). At now there is a large list of the paper devoted to

investigation of the isotope - mixed graphene [60, 177, 186 - 190]. Chen at al. [176] have reported the first experimental study of the isotope effect on the thermal properties of graphene. The thermal conductivity K, of isotopically pure ^{12}C (0.01 of ^{13}C) graphene determined was higher than 4000 W/mK (approximately two times more than it in diamond [80, 181]) at the measured temperature $T_m \sim 320K$, and more than a factor of two higher than the value of K in a graphene sheets composed of a 50% - 50% mixture of ^{12}C and ^{13}C. Raman spectroscopy transferred to the 285 nm SiO_2/Si wafer was performed under 532 nm laser excitation [176]. The G peak and 2D band positions in Raman spectra of graphene with 0.01%, 1.1% , 50% and 99.2% ^{13}C - isotope are presented in Fig. 34.

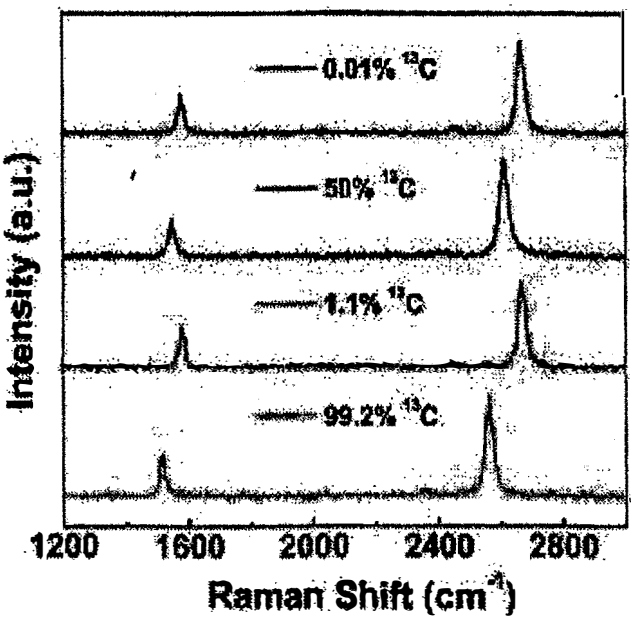

Fig. 34. Raman spectra of graphene with different isotope concentration at room temperature [176].

Isotope shift of the G and 2D bands in the Raman spectra depicted on the Fig.35 [191].

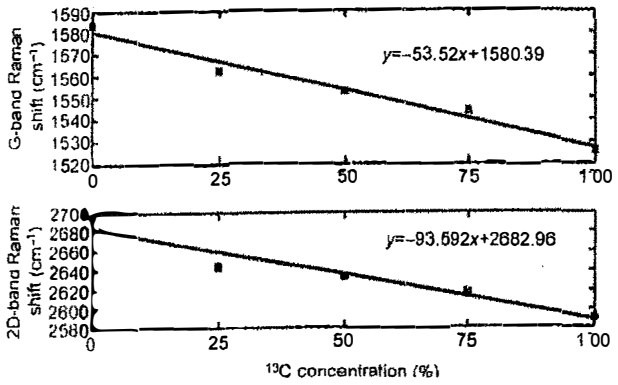

Fig. 35. Peak position of G and 2D bands in Raman spectra as a function of the concentration of ^{13}C [191].

As in the case of isotope - mixed diamond [68, 69] the Brillouin - zone - center optical - phonon frequency ω varies with the atomic mass M as $\omega \sim M^{-1/2}$ making the Raman shift for ^{13}C approximately $(12/13)^{-1/2}$ times smaller than that for ^{12}C. The experimental difference between the lowest 99.2% ^{13}C and the highest 0.01% ^{13}C peak is $\sim$ 64 cm^{-1} which is according [176] in agreement with the theory, and attests for the high quality of isotopically modified graphene. By the way we should indicate that in the Raman spectra in diamond (with sp^3 - bond) analogous shift of first - order line in Raman spectrum is equal 52.3 cm^{-1} [170], which is consistent with the isotope mass ratio. Substituting a light isotope (^{12}C, H) with a heavy one increases the interband transition energy in the case $^{12}C_x^{13}C_{1-x}$ on 14.7 meV and LiH_xD_{1-x} on 103 meV [150]. Taking into account a more soft bond (sp^2 - bond instead sp^3 - bond in diamond) isotope - induced band - gap opening in graphene of some hundreds meV (up to E_g of Si) was predicted in paper [60]. Such estimation of the value of isotopical band - gap opening in graphene agrees with not only the results of paper [170] but with very small value $C_{44} = 0.5 \cdot 10^{10}$ dyn/cm^2. Such small value indicates on the strong electron - photon interaction - main reason renormalization of electron excitation energy (for the details, see, e.g. [69]). Very close to isotopically renormalization of electronic excitation energy is the hydrogenation of graphene [60, 179]. In last mechanism there is observable band - gap opening in graphene. We should add that use deuteriun instead of hydrogen we may increase the value of E_g [69]. Thus, isotope substitution will be very useful method for renormalization of the band - gap in graphene - future semiconducting material. Moreover, this method allows to control not only of the strong nuclear interaction (quantum chromodynamics) but taking it into account at the renormalization of the electromagnetic interaction (quantum electrodynamics) [111]. Adding ^{13}C makes magnetic materials isotope out of graphene.

Discussion.

Traditionally nuclear - electron interaction (in our case neutron - electron interaction) taking into account the solving Schrödinger equation using Born - Oppenheimer (adiabatic) approximation [192]. Below we consider the essence of the Born - Oppenheimer approximation of the nuclear - electron interaction on the molecule example.. The Schrödinger equation for the molecule

$$\hat{H}\Psi(\vec{r}, \vec{R}) = E\Psi(\vec{r}, \vec{R}) \qquad (104)$$

here $\Psi(\vec{r}, \vec{R})$ is an eigenfunction and E the corresponding eigenvalue, $\hat{H}$ the Hamiltonian operator of molecule and $\vec{r}$ is electron and $\vec{R}$ is nuclear distance. The simplest approximate method for solving the Schrödinger equation (104) uses, as indicated above, the so - called Born - Oppenheime approximation [192]. This approximation is used that the nuclei are much heavier than an electron and, consequently, move very slowly in comparison with the electronic motion.

If the nucleus to be fixed in some configuration for this particular $\vec{R}$ (distance between nuclei) we get the next differential equation

$$-\frac{\hbar^2}{2m}\sum_i \Delta_i^2\Psi(\vec{r}, \vec{R}) - \frac{\hbar^2}{2}\sum_\alpha \frac{\Delta_\alpha}{M_\alpha}\Psi(\vec{r}, \vec{R}) + V(\vec{r}, \vec{R})\Psi(\vec{r}, \vec{R}) = E\Psi(\vec{r}, \vec{R}), \quad (105)$$

where Δ is Laplasian [100], m and M electron and nucleus mass, index i for electrons and α is index for nuclei.

Further we put

$$\Psi(\vec{r}, \vec{R}) = \chi(\vec{r}, \vec{R})\varphi(\vec{R}) \qquad (106)$$

here $\varphi(\vec{R})$ is the nuclear wavefunction, which depends on nuclear distance $\vec{R}$ and on electronic state.

After substitution (106) in (105) we have

$$-\frac{\hbar^2}{2m}\varphi(\vec{R})\sum_i \Delta_i\chi(\vec{r}, \vec{R}) - \frac{\hbar^2}{2}\sum_\alpha \frac{\Delta_\alpha}{M_\alpha}\chi(\vec{r}, \vec{R})\varphi(\vec{R}) + V(\vec{r}, \vec{R})\chi(\vec{r}, \vec{R})\varphi(\vec{R}) = E\,\chi(\vec{r}, \vec{R})\varphi(\vec{R}). \quad (107)$$

Further we neglect the next members in (107)

$$\hat{L}\Psi(\vec{r}, \vec{R}) = -\frac{\hbar^2}{2}\sum_{\alpha}\frac{1}{M_\alpha}[\varphi(\vec{R})\Delta_\alpha\chi(\vec{r}, \vec{R}) + 2\nabla_\alpha\varphi(\vec{R})\nabla_\alpha\chi(\vec{r}, \vec{R})]. \qquad (108)$$

Operator $\hat{L}$ is call the non - adiabatic operator, which describe the nuclear - electron interaction. after the last oeration the equation (108) splits on two equations:

$$-\frac{\hbar^2}{2m}\sum_{i}\Delta_i\chi(\vec{r}, \vec{R}) + V(\vec{r}, \vec{R})\chi(\vec{r}, \vec{R}) = E_l(\vec{R})\chi(\vec{r}, \vec{R}); \qquad (109)$$

and

$$-\frac{\hbar^2}{2}\sum_{\alpha}\frac{\Delta_\alpha}{M_\alpha}\varphi(\vec{R}) + E_l(\vec{R})\varphi(\vec{R}) = W\varphi(\vec{R}). \qquad (110)$$

Where $E_l(\vec{R})$ is electronic energy and W is the nuclear energy. Every equation have the view of the Schrödinger equation. The first equation (109) describes the electron stationary state in adiabatic approximation. Equation (110) is an equation for a wavefunction of the nuclei alone. Note, please that Equation (109) contains the nuclear charges through the Coulomb potential, but is doesn't include any reference to nuclear mass. Thus $E_l(\vec{R})$, the eigenvalue (energy) of the electronic Schrödinger equation (109) is the same for all isotopes, and consequently, is isotopically independent. The independent $E_l(\vec{R})$ on isotopic substitution is the essence of the Born - Oppenheimer approximation. However, we must repeat, that the Born - Oppenheimer approximation [192] is the standard anzatz to the description of the interaction between electrons and nuclei in solids (see, e.g. [193]). Moreover, comparison the non - accelerator experimental results on the luminescence (reflection) and light scattering [111] in the crystals which differ by a term of one neutron only is allowed to the next conclusions;

1. At the adding one neutron (using LiD crystals instead LiH ones) is involved the increase exciton energy on 103 meV.

2. At the addition one neutron the energy of LO phonons is decreased on the 36 meV that is direct seen from luminescence and scattering spectra [58].

3. In the isotope effect, the energy of acoustic phonons does not depend on the replacement of H by D [69], which is proved by the identical structure of the light scattering spectra [111]. Along with this, a small change in the energy of optical (LO) phonons (36 meV) observed in the luminescence and light scattering spectra indicates a non - electron -

phonon renormalization mechanism of the energy of zero - phonon emission line of free excitons in LiD crystals. The same results have been jbtained for diamond.

The X - ray diffraction investigations show that the LiH_xD_{1-x} mixed crystals [196] form a continuos row of the solid solution and testify themselves like a virtual crystal with a variable lattice constant (and exciton radius, respectively) that obeys Vegard's law (see Fig. 36).

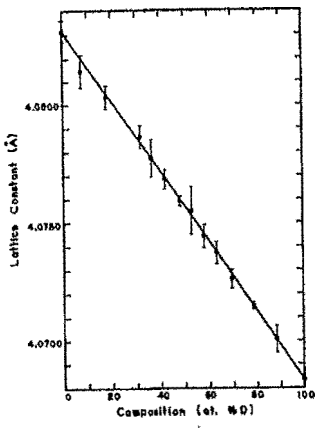

Fig. 36. Lattice constant in the ^{7}Li(H,D) crystals plotted against the isotopic composition [16].

The measurements of the low temperature of reflection [111] and luminescence spectra of the whole series of mixed crystals is permitted to obtain the dependence of the interband transition (the long - range force dependence of strong nuclear interaction on the distance between nucleons in deuterium nucleus) energy on the deuterium concentration (see below Fig. 37). Taking into account that the concentration of the isotopes is vary directly the lattice constant (see Fig. 36) we are plotting the dependence of the power of the force strong interaction on the distance between nucleons depicted on Fig. 37 This dependence has a nonlinear character (compzre to Fig. 14). As can be seen from Fig. 37, VCA method (the straight dashed line) cannot describe observed experimental results.

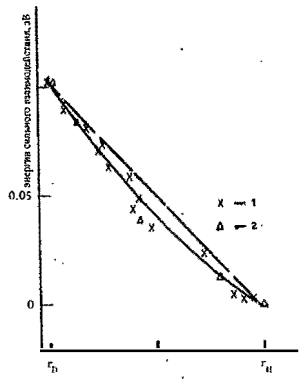

Fig. 37. The long – range part of the force of strong nuclear interaction dependence on the distance between nucleons in deuterium nucleus. The straight dashed line is the linear dependence of the force dependence F_s in the virtual model. The solid line corresponds to calculation using the polynom of second degree $F_s = f(r_d)$. Points derived from the reflection spectra indicated by crosses, and those from luminescence spectra by triangles.

Traditionally nuclear - electron interaction (in our case neutron - electron interaction) taking into account the solving of Schrödinger equation using a model of Born - Oppenheimer (adiabatic) approximation [20, 192]. Since electrons are much faster and lighter than the nuclei by a factor nearly 2000 the electron charge can quickly rearrange itself in response to the slower motion of the nuclei, and this is the essence of the Born - Oppenheimer approximation. This approximation results the omission of certain small terms which result from the transformation(see above equation 108). As was shown above the eigenvalue (energy) of the electronic Schrödinger equation depends on the nuclear charges through the Coulomb potential, but it doesn't include any references to nuclear mass and it is the same for the different isotopes [195]. The independent of the potential energy (the eigenvalue of the Schrödinger equation) is the essence adiabatic approximation. However, we must repeat, that the Born - Oppenheimer approximation [20] is the standard anzatz to the description of the interaction between electrons and nuclei in solids [193]. Now we should take into account a small contribution to isotopic shift through reduced electron mass $\mu = ((m_e M_{Nucl})/(m_e + M_{Nucl}))$ so far as M_{Nucl} is different for the hydrogen and deuterium nucleus. In this case the contribution equals $\Delta E \simeq 6$ meV. Contribution to isotope shift of the zero - phonon line in luminescence spectra of LiD crystals as well as Lamb shift and specific Coulomb potential approximately equal 1, and 1 meV, respectively. This values is less then isotope shift in our experiments on the two order and more. These all last results force us to search for new models and mechanisms of nuclear (neutron) - electron interaction including the results of subatomic physics, e.g. hadron - lepton interaction.

Out of four known interactions, three are described by SM - the electromagnetic, weak and strong ones. The first two of them have a common electroweak gauge interaction behind them. The symmetry of this interaction $SU(2)_L \times U(1)_Y$ manifests itself at energies higher than ~ 200 GeV. At lower energies, this symmetry is broken down to $U(1)_{EM} \neq U(1)_Y$ (the electroweak symmetry breaking): in SM this breaking is related to the vacuum expectation value of a scalar field [12]. The strong interaction in SM is described by the QCD, a theory with the gauge group $SU(3)_C$. The effective coupling constant of this theory grows when the energy decreased [16]. As a result, particles which feel this interaction cannot exist as free states and appear only in the form of bound states called hadrons (see, also [5]). Most of modern methods of quantum field theory work at small values of coupling constant, α_s, [127 - 130], that is, for QCD, at high energies. Quarks and leptons, the so - called SM matter fields, are described by fermionic fields. Quarks take part in strong interactions and compose observable bound state hadrons. Both quarks and leptons participate in the electroweak interaction. The matter fields constitute three generation: particles from different generation Interact identically but have different masses (see, e.g. [5]). For the case of neutrino, Yukawa [18] interactions are forbidden as well, so neutrinos are strictly massless in SM (see, however [194]). The gauge bosons, which are carriers of interactions, are massless for unbroken gauge groups $U(1)_{EM}$ (electromagnetism - photons) and $SU(3)_C$ (QCD - gluons), masses of $W^{\pm}$ and Z^0 bosons are determined by the mechanism of electroweak symmetry breaking. It should noted that the forces between the quarks must be long - range, because the gluons have zero mass. This does not imply that forces between hadrons are also long range, because hadrons have zero color charges overall. The forces between the colorless hadrons are the residues of the forces between their quark constituents, and cancel when the hadrons are far apart.

Returning to our non - accelerator experimental results, we should underline that in this paper we measure the strong coupling strength in crystals which differ by term of one neutron from each other. When we add one neutron in the hydrogen nucleus, we artificial activation of the strong Interaction. As far as the gravitation, electromagnetic and weak interactions are the same in both kind crystals (LiH and LiD), it only changes the strong interaction. Therefore a logical conclusion is made that the renormalization of the energy of electromagnetic excitations (isotopic shift equals 0.103 eV) is carried out by strong nuclear interaction. The short - range character of the strong interaction of nucleons does not possess direct mechanism of the elementary excitation (electrons, excitons, phonons) energy renormalization, which was observed in our low temperature experiments. Second reason that the interpretation of our experimental results is very difficult task because they are first demonstration of the violation of the strong conclusion in nuclear and particles physics that the strong nuclear force does not act on the colorless leptons (see, e.g. [5, 16]). Moreover we have some contradictions taking into account that the forces between quarks must be long - range, because the gluons have zero mass. But as was mentioned above, the short range when forces between the colorless hadrons are the residues of the forces between their quark constituents, and cancel when the distance between hadrons is more than nuclear size [15]. We can see that the nuclear size transforms long - range interaction in the short - range strong one. It is very old question which up to present time

has not any theoretical explanation.

In spite of above discussion, at present time we can distinguish the following mechanisms of the isotopic shift zero phonon line:

1. Long - range electric field of the neutron's quarks. This mechanism owing to the confinement quarks is limited by the boundary of the neutron.

2. The possible new structure of the quarks and leptons - so - called preons [15, 197 - 202].

3. The most likely mechanism of the neutron - lepton interaction is connected to the magnetic - like strong field of neutron 's quarks. Taking into account anomalous magnetic moment of the neuron in the paper [132] was obtained the value of strong coupling constant α_s = 2.4680 [195]. Quite large value in comparison with the accelerator technique value $\alpha_s(M_Z)$ = 0.1198 [127]. The large value α_s is thus justified to think that residual strong forces acting beyond nucleon could exist. a possible interpretation is to assume that in addition to the 8 gluons predicted by QCD $SU(3)_c$ group there is a ninth gluon color singlet [5]

$$g_9 = \frac{1}{\sqrt{3}} (r\bar{r} + g\bar{g} + b\bar{b}) \qquad (111)$$

This massless photon - like gluon may be strongly interacts between nucleons (neutrons) and leptons (electrons) (see, also [5, 16]. Returning to Fig. 37 we can note that our measurements permit to obtain value of strong coupling constant from α_s = 2.4680 (pure LiD crystals) to α_s = 0 (pure LiH crystals). Moreover, in Fig. 38 we show the dependence of α_s on neutron's number in different substances. We can see as early in the case of pure LiD crystals we have non - of α_s on the neutron's number in different substances.

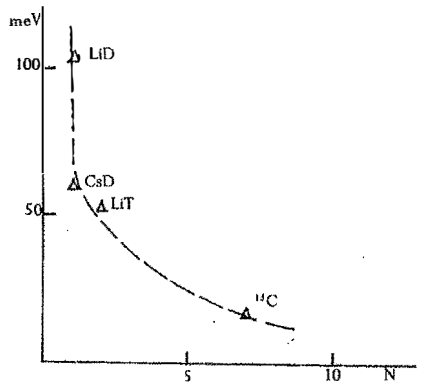

Fig. 38. The dependence of the strong force on the number of neutrons in different substances.

Thus, the tentative interpretation of describing non - accelerator experimental results does not find consisted explanation at the change of strong interaction leaving to another mystery of SM. We should remind that intrinsic contradiction of Standard Model is already well - known. Really, the Lagrangian of QCD (theory of the strong interaction) has the next form (see, e.g. [35]):

$$L = i\sum_{q} \overline{\Psi}^{a}_{q}(\nabla_{\mu}\gamma_{\mu} + im_{q})\Psi^{a}_{q} - \frac{1}{4}G^{n}_{\mu\nu}G^{n}_{\mu\nu}, \quad (112)$$

where

$$\nabla_{\mu} = \partial_{\mu} - ig\frac{\lambda^{n}}{2}A^{n}_{\mu},$$

$$G^{n}_{\mu\nu} = \partial_{\mu}A^{n}_{\mu} - \partial_{n}A^{n}_{\mu} + gf^{nml}A^{n}_{\mu}A^{l}_{\nu}. \quad (113)$$

Ψ^{a}_{q} and A^{n}_{μ} are quark and gluon fields, a=1,2,3,...8 are color indices , λ^{n} and f^{nml} are Gell - Mann matrices and f symbols, m_{q} - are bare (current) masses, q = u, d, s, c, ... different quarks. It is common place [5, 16] that the Lagrangian (112) contains the members which

describe both free motion and interaction between quarks and gluons, which is defined by the strength couple g. Spacing of which it is necessary to remark that although the Lagrangian (112) possesses rather attractive peculiarities (see, also [5, 16]), its eigenstates are the quarks and the gluons which are not observed in free states [83, 203]. The observed hadrons in the experiment don't eigenstates in QCD. It is obvious to expect that the modern theory of QCD should finally overcome these difficulties.

The next step our discussion is devoted to the neutron - electron binding energy. From our non - accelerator experimental results is followed that this value equals 0.106 eV on LiH_xD_{1-x} and 0.107 eV on the diamond. In electrostatic model, it is shown [204] the neutron - electron binding energy is less than analogous proton with an electron (13,6 eV) by approximately 128 times. Hence it follows that the theoretical value of the binding energy of a neutron with an electron is 106, 7 meV. Our experimental value of a neutron - electron binding energy is in excellent agreement with theoretical value.

The remarkable properties of the graphene promise unheard of applications, especially in the semiconductor state. Especially graphene nanostructures are promising candidates for future nanoelectronics and solid - state quantum information technology. As was shown above, in the vicinity of K - points (Fig. 8), the low - energy electron/hole dispersion relation is proportional to momentum, rather than its square (see, e.g. [80, 205]). This is analogous to the energy dispersion relation of massless relativistic electrons, so the electrons/holes of graphene are described as Dirac fermions having no mass. In a simple neighbor model graphene is a semimetal with zero - overlap between valence and conduction bands. In order to make graphene a real technology, a special issue must be solved: creating an energy gap at K - points in the Brillouin zone (see, Fig. 5).

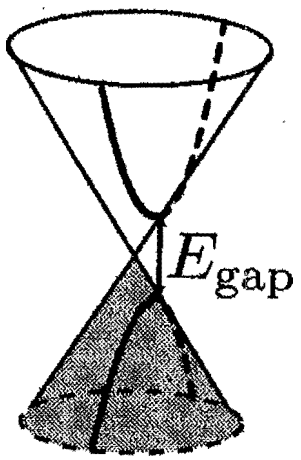

Fig. 39. The energy dispersion of semimetal (solid line) and semiconductor (dashed line).

Different attempts have been made by researches, such as patterning graphene into nanoribbon, forming graphene quantum dots, making use of multilayer graphene sheet and applying an external electric field (see, e.g [80, 205]. It was shown that the uniaxial strain can open a band - gap in a metallic carbon nanotubes as well as carbon nanoribbon . As an example Fig. 40 shows the dependence of the energy of interband transition on the width of the graphene nanoribbons. The observed dependence is well described by the following expression $E_g = \alpha^*/ (W - W^*)$, where $\alpha^* = 0.38$ eV/nm, and $W^* = 16$ nm accounts for inactive edges [206]. This formula gives value of E_g equal to several eV, if W is reduced to a size , for example, ^{13}C, but it is impossible. The isotopic transformation of graphene, a semimetal into emiconductor deserves special attention [207, 208] This means of the cones dispersion pattern $E(\vec{k})$ at the K point of the Brillouin zone of graphene reformes into the usual parabolic dispersion of band structure pattern (see Fig. 39).

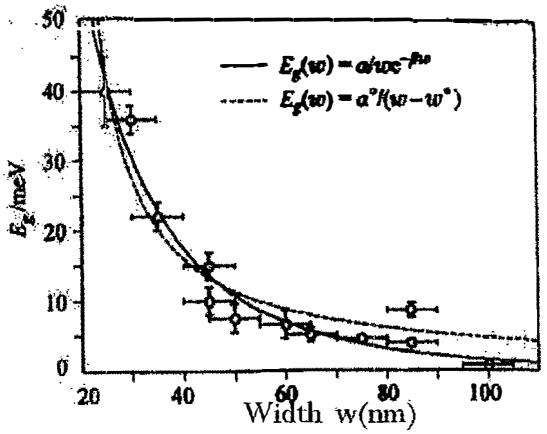

Fig. 40. The dependence of E_g as a function of width of the graphene nanoribbons (after [206]).

According to the results of Ref. 207 this method can be used to obtain E_g of several hundred meV. Since value of E_g depends on the concentration of ^{13}C in graphene, this mechanism is easily realized either chemically or technologically. With the opening E_g of massless fermions (leptons = electrons) acquire mass. Estimates of different ways of opening E_g in graphene give the following equality: $E_g = 2m$ [208]. When $E_g = 1$ eV [207] leptons acquire a mass equal 0.5 eV - the value is not large, but finite. One of the mechanisms of acquire mass in elementary particle physics is considered in the paper [209]. This paper predicts that both quarks and gluons acquire running mass distribution in QCD, which are large at infrared momenta. The current quark of perturbative QCD evolves into a constituent quark as its momentum becomes smaller. The constituent quark mass arises from a cloud of low - momentum gluons attaching then selves to the current quark. This is DCSB: an essentially nonperturbative effect that generates a quark mass from nothing; namely it occurs even in the chiral limit. DCSB namely the generation of mass from nothing is a theoretically established nonperturbative feature of QCD. The solution of a gap equation shows that gluons are cannibals: they are particle species whose members become massive by eating each other (the details see [207 - 210]).

5. Conclusion.

The artificial activation of the strong nuclear interaction by adding one (two or more) neutrons in atomic nuclei leads it to the direct observation of the strong interaction in low - temperature optical spectra of solids. This conclusion opens new avenue in the investigation of the constant of strong nuclear interaction in the wide value range by means the condensed matter alike traditional methods. The observation of an isotopic shift (0.103 eV) of the zero-phonon line of free excitons in the luminescence spectra of LiH (without strong interaction in the hydrogen nucleus) and LiD (with strong interaction in the deuterium nucleus) crystals was the first and direct evidence of the long-range interaction of the Yukawa potential. Indeed, in both crystals, the lithium ions, the proton and the electron are the same and, therefore, the gravitational, electromagnetic and weak interactions are the same, and the addition of a neutron, according to Yukawa, a strong interaction appears, the influence of which manifests itself in the isotopic shift. These experimental results demonstrate the neutron-electron binding energy (0.106 eV) which is in excellent agreement with the theoretical Breit estimate of 0.1067 eV Experimental observation of the renormalization of the elementary excitation energy of solids by the strong nuclear interaction stimulates its count in the process of description of the elementary excitations dynamics in quantum electrodynamics. Present review continuous to develop between nuclear and condensed matter physics.

References.

1. E.E. Boos, The SMEET formalism: the basis for finding deviations from the Standard Model, Phys. - Usp (Moscow) **65** (2022) 653 - 676.

2. B.L. Ioffe, The origin of mass and experiments on high - energy particle accelerators, ibid, **49** (2006)1077 - 1078.

3. V.F. Weisskopf, Physics in Twentieth Century: Selected Essays (MIT press, Cambridge, 1972)

4. R.M. Santilli, The physics of new clean energies and fuels according to hadronic mechanics, J. New Energy 1 (1998) **5** - 314; a quantative isotopic representation of the deuteron magnetic moment, Proceed. Int. Symp., Dubna Deuteron - 93, 1994, p.p. **117** - 126; Sudhar S. Dhondge, Studies three - body model of the deuteron according to hadronic mechanics, Amer. J. Mod. Phys. **5** (2016) 46 - 55.

5. G. Griffiths, Introduction to Elementary Particles (Wiley - VCH, Weinheim, 2008).

6. S. Weinberg, The Discovery of Subatomic Particles (Penguin Books, New York, 1993).

7. D.I. Iwanenko, Interactions of neutrons and protons, Nature **133** (1934) 981 - 982 .

8. W. Heisenberg, Structure of atomic nuclei, Zs. Physik **77** (1932) 1 - 9.

9. E. Segre, Nuclei and Particles (W.A. Benjamin, Inc. , Reading, MA, 1977).

10. E.M. Henley, A. Garcia, Subatomic Physics (World Scientific Publishing Co., Singapore, 2007).

11 F.E. Close, An Introduction to Quarks and Partons (Academic Press, london, NewYork, 1979).

12. F.I. Yndurain, The Theory of Quark and Gluon Interactions (Springer, Berlin, 2013).

13. V.G. Plekhanov, Isotopes in Condensed Matter (Springer, Heidelberg, 2013).

14. W.N. Cottingham, D.A. Greenwood, An Introduction to the Standard Model of Particle Physics (Cambridge University Press, Cambridge, 2007).

15. V.G. Plekhanov, Hadron - Lepton Interaction (LAMBERT Academic Publishing, Saarbrucken, Germany, 2021).

16. D.H. Perkins, Introduction to High Energy Physics (Cambridge Ubiversity Press, Cambridge, 2006).

17. F. Iachello and P. Isacker, The Interacting Boson - Fermion Model (Cambridge University Press, Cambridge, 1991).

18. Y. Yukawa, On the interaction of elementary particles, Proc. Phys. Math. Soc. Jap. **17** (1935) 48 - 57.

19. W.A. Harrison, Solid State Theory (McGraw - Hill Book Company, New York - London, 1970).

20. M. Born, H. Kun, Dynamical Theory of Crystal Lattices (Clarendon Press, Oxford, 1954).

21. L.D. Landau, E.M Lifshitz, Quantum Physics (Batteworth - Heinman, Oxford, 1988).

22. J.I. Frenkel, On the transformation light into heat in solids, I, Phys. Rev.**37** (1931) 17 - 44); On the transformation light into heat in solids, II, **37** (1931 1276 - 1294.

23. R. Peierls, Zur theorie der Absorptionsspektren fester Körper, Annalen Phys. **31** (1932) 905 - 942.

24. J.K. Slater and W.H. Shockley, Optical absorption by alkali halides, Phys. Rev. **50** (1936) 705 - 719.

25. G.H. Wannier, Structure of electronic excitation levels in insulating crysals, Phys. Rev. **52** (1937) 191 - 197.

26. N. F. Mott and M. J. Littleton, Conduction in polar crystals. I. Electrolytic conduction in solid salts, Trans. Faraday Soc. **34** (1938) 485 - 499; Conduction in polar crystals. II. The conduction band and ultra-violet absorption of alkali-halide crystals, Trans. Faraday Soc. **34** (1938) 500 - 505; R. W. Gurney and N. F. Mott, Conduction in polar crystals. III. On the colour centres in alkali-halide crystals, Trans. Faraday Soc. **34** (1938) 506 - 511

27. A.S. Davydov, Theory of Molecular Excitons (Science, Moscow, 1968) (in Russian).

28. V.M. Agranovich, Theory of Excitons (Science, Moscow, 1976) (in Russian).

29. V.M. Agranovich and V.L. Ginzburg, Crystallooptic and the Theory of Excitons (Science, Moscow, 1979) (in Russian).

30. E.F. Gross, Selected Papers (Science, Leningrad,1976) (in Russian).

31. V.F. Agekyan, Spectroscopic properties of semiconductor crystals with direct forbidden energy gap, Phys. Stat. Solidi (a) **43 (1977)** 11 – 42.

32. S. Permogorov, Hot excitons in semiconductors , Phys. Stat. Solidi (b) **68** (1975) 9–42.

33. S.I. Pekar, Crystal Optics and Additional Light Waves (Benjamin Cummings, Menlo Park, CA, 1983).

34. H. Haken, Quantum Field Theory of Solids (North-Holland, Amsterdam, 1976).

35. H. Haug and S.W. Koch, Quantum Theory of Optical and Electronic Properties of Semiconductors (World Scientific, London, 1993).

36. R.S. Knox, Theory of Excitons (Academic Press, New York - London,1963).

37. R.M. Martin, Electronic Structure - Basic Theory and Practical Methods (Cambridge University Press, Cambridge, 2004).

38. J.I. Pankove, Optical Processes in Semiconductors (Prentice - Hall, Inc., Englewood Cliffs, New Jersey, 1971).

39. V.G. Plekhanov, Application of Isotopic Effect in Solids (Springer, Heidelberg - Berlin, 2004).

40. G. Arfken, Mathematical Methods (Academic Press, New York - London, 1968).

41. A. Baldareshi, N.O. Lipari, Energy levels of direct excitons in semiconductors with degenerate bands, Phys. Rev. **B3** (1971) 439 - 451.

42. Excitons, E.I. Rashba and M.D. Sturge (eds.) (North - Holland, Amsterdam, 1982).

43. V.G. Plekhanov, Giant Isotope Effect in Solids (Stefan University Press, La Jolla, 2004).

44. N.F. Mott, R.V. Gurney, Electron Processes in Ionic Crystals (Clarendon Press, Oxford, 1948).

45. J. Slater, The Self - Consistent Field for Molecules and Solids (McGraw - Hill, New

York, 1975).

46. W.B. Fowler, Influence of electronic polarization on the optical properties of insulators, Phys. Rev. **151** (1966) 657 - 667.

47. D.H. Ewing, F. Seitz, On the electronic constitution of crystals: LiF and LiH, Phys. Rev. **50** (1936) 760 - 777.

48. F. Perrot, Bulk properties of lithium hydride up to 100 Mbar, Phys. Stat. Sol. (b) **77** (1976) 517 - 525.

49. G.S. Zavt, K. Kalder et al., Electron excitation and luminescence LiH single crystals, Fiz. Tverd. Tela (St. Petersburg) **18** (1976) 2724 - 2730 (in Russian).

50. N.I. Kulikov, Electron structure, state equation and phase transitions insulator - metal in hydride lithium, ibid, **20** (1978) 2027 - 2035 (in Russian).

51. G. Grosso, G.P. Parravichini, Hartree - Fock energy bands by the orthogonalized - plane - wave method: lithium hydride results, Phys Rev. **B20** (1979) 2366 - 2372 .

52. S. Baroni, G.P.Parravichini, G. Pezzica, Quasiparticle band structure of lithium hydride, Phys. Rev. **B32** (1985) 4077 - 4087.

53. A.B. Kunz, D.J. Mikish, Electronic structure of LiH and NaH, ibid, **B11** (1975) 1700 - 1704.

54. J. Hama, N. Kawakami, Pressure induced insulator - metal transition in solid LiiH, Phys. Lett. **A126** (1988) 348 - 352.

55. T.A. Betenekova, I.N. Shabanova, F.F. Gavrilov, The structure of valence band in lithium hydride, Fiz. Tverd. Tela **20** (1978) 2470 - 2477 (in Russian).

56. K. Ichikawa, N. Susuki, K. Tsutsumi, Photoelectron spectroscopic study of LiH, J.Phys. Soc. Japan **50** (1981)3650 - 3654.

57. R.A. Kink, M.F. Kink, T.A. Soovik, Reflection spectra of lithium hydride crystals in 4 - 25 eV at 5K, Nuclear Instruments and Methods in Physics Research, **A261** (1987) 138 - 140.

58. V.G. Plekhanov, Isotopic and disorder effects in a large exciton spectroscopy, Physics - Uspekhi **40** (1997) 553 - 579.

59. V.G. Plekhanov, V.I. Altukhov, Determination of exciton and exciton - phonon interaction parameters via resonant secondary emission of insulators, Sov. Phys. Solid State **23** (1981)439 - 447 .

60. V.G. Plekhanov, Nuclear technology of the creation of quantum dots in graphene, Sci. Transaction of SHI, Tallinn, 2011, p.p. 66 -71 (in Russian).

61. V.G. Plekhanov, Manifestation of the strong nuclear interaction in the isotope - induced band - gap opening of graphene, in, Horizons in World Physics, Vol. 281 (Nova Science Publishers, Inc., New York, 2013), p.p. 197 - 202.

62. V.G. Plekhanov, Inroduction to Isotopic Materials Science (Springer, Heidelberg, 2018).

63. J.E. Field, The Properties of Natural and Synthetic Diamond (Academic Press, New York, 1992).

64. V.C. Vavilov, A.A. Gippius, E.A. Konorova, Electron and optical processes in diamond (Moscow, Science, 1985) (in Russian).

65. R.P. Mildren, Intrinsic optical properties of diamond, in: Optical Engineering of

Diamond, R.P. Mildren and J.R. Ratenau (eds.) (Wiley - VCH Verlag GmbH, 2013).

66. J.R. Chelikowsky and S.G. Louie, First - principles linear combination of atomic orbitals method for the cohesive and structural properties of solids: Application to diamond, Phys. Rev. B**29**, 3470 - 3482 (1984).

67. M.S. Hybertsen and S.G. Louie, Electron correlation in semiconductors and insulators: Band gaps and quasiparticle energies, Phys. Rev. B **34** (1986) 5390 - 5413.

68. P.Y. Yu, M. Cardona, Fundamentals of Semiconductors, (Berlin - Heidelberg, Springer, 1996).

69. V.G. Plekhanov, Elementary excitations in isotope - mixed crystals, Phys. Rep. **410** (2005) 1 - 235.

70. M. Cardona and M.L.W. Thewalt, Isotope effect on optical spectra of semiconductor, Rev. Mod. Phys. **77** (2005)1173 - 1224.

71. K.S. Novoselov, A.K. Geim, S.V. Morozov, et al., Two dimensional gas of massless Dirac fermions in graphene, Nature **438** (2005) 197 - 200.

72. P.R. Wallace, The band theory of graphite, Phys. Rev. **71** (1947) 622 - 629.

73. A. Jorio, G. Dresselhaus, M.S. Dresselhaus (eds.) Carbon nanotubes, Topics Applied Physics 111 (Springer, Heidelberg, 2008).

74. J.C. Charlier, P.C. Eklund, A.C. Ferarl, Electron and phonon properties of graphene, in, A. Jorio, G. Dresselhaus, M.S. Dresselhaus (eds.) Carbon nanotubes, Topics Applied Physics 111 (Springer, Heidelberg, 2008).

75. V.G. Plekhanov, Isotope Effect - Macroscopic Manifestation of the Strong Interaction (LAMBERT, Academic Publishing, Saarbrücken, 2017) (in Russian).

76. Zh.H. Ni, T. Yu, Y.H. Lu, et al., Uniaxlal strain on graphene: Raman spectroscopy study and band - gap opening, ACS Nano, **3** (2009) 483 - 492.

77. K.S. Novoselov, A.K. Geim, S.V. Morozov, et al., Electric field in anomally thin carbon films, Science **306** (2004)666 - 670.

78. W.A. Harrison, Electronic Structure and the Properties of Solids (W.H. Freeman and Company, San Francisco, 1980).

79. T. Ando, in Nano - Physics and Bio - Electronics: A New Odyssey, Chap 1 (Elsevier, Amsterdam, 2002).

80. A.H. Castro Neto, F. Guinea, M.N. Peres et al., The electronic properties of graphene, Rev. Mod. Phys. **81** 109 - 162.

81. A. Grünels, C.A. Attaccallte, A. Rubio et al., Angle - resolved photoemission study of the graphite intercalation compound KC_8: A key to graphene, Phys. Rev. B**80**, 075431 - 9 (2009).

82. M. Lazzeri, C. Attaccalite, I. Wirtz et al., Impact of the electron - electron correlation on phonon dispersion: Failure of LDA and GGA DFT functionals in graphene and graphite, Phys. Rev. B**78** (2008) 081406 - 4.

83. D. Vretenar and W. Weise, Exploring the nucleus in the context of low - energy QCD, Lecture Notes Phys. **641** (2004)65 - 117.

84. I.M. Dremin, A.B. Kaidalov, Quantum chromodynamics and the phenomenology of strong interaction, Phys - Uspekhi **49** (2006) 263 - 273.

85. E. Segre, Nuclei and Particles: An introduction to Nuclear and Subnuclear Physics,

Second Ed. (Addison Wesley Publishing Co., New York, 1977).

86. V.B. Berestesky, E.M. Lifshitz and L.P. Pitaevsky, Relativistic Quantum Theory (Pergamon Press, New York, 1967).

87. G.A. Miller, A.K. Oper, E.J. Stephenson, Charge symmetry and QCD, Annual Rev. of Nuclear and Particle Science, **56** (2006) 253 - 294.

88. K.S. Krane, Introductory Nuclear Physics (Wiley & Sons, New York - Chichester, 1998).

89. B. Povh, K. Rith, C. Scholz, F. Zetsche, Particles and Nuclei (Springer - Verlag, Berlin - Heidelberg, 2006).

90. G.A. Miller, Charge density of neutron and proton, Phys. Rev. Lett. **99** (2007) 112001 - 4.

91. V.G. Plekhanov, Hadron - Lepton Strong Interaction (Service for Science and Education , UK, 2021) e - print.

92. Ju. M. Shirokov, N. P. Judin, Nuclear Physics (Science, Moscow, 1980) (in Russian).

93. A.R. Edmonds, Angular Momentum in Quantum Mechanics (Princeton University Press, New Jersey, 1957).

94. S.D. Bass, The Spin Structure of the Proton (World Scientific, Singapore, 2007).

95. C.A. Aidala, S.D. Bass, D. Hasch et al., The spin structure of the nucleon, Rev. Mod. Phys. **85** (2013) 655 - 691.

96. J.J. Kelly, Nucleon charge and magnetization densities from Sachs form factors, Phys. Rev. C**66** (2002) 065203 - 065206.

97. A. Martin, History and spin statistics, ArXiv/hep - ph/0209068 (2002).

98. R.P. Feynman, QED - The Strange Theory of Light and Matter (Princeton University Press, Princeton, 1983).

99. J.D. Bjorken, S.D. Drell, Relativistic Quantum fields (McGraw - Hill, New York, 1965).

100. See, e.g. A. Korn, M. Korn, Mathematical Hanbook, McGraw Hill Book Co., New York - London, 1968.

101. P.C. Davies, Particle do not exist, in Quantum Theory of Gravity, ed. by S.M. Christensen (Adam Hilger, Bristol, 1984).

102. F. Halzen, A.D. Martin, Quarks and Leptons (J. Wiley & Sons, New York, Chichester, 1984).

103. Y. Nagashima, Elementary Particle Physics (Vol. 2. Foundation of the Standard Model and Experiments) (Verlag, Wiley - VCH, Weinheim, Chichester, 2013).

104. W. Greiner, J. Reinhart, Quantum Electrodynamics, 3rd Ed.(Springer, Berlin - New York, 2003).

105. M. Tanabashi et al., The Review of Particle Properties, Phys. Rev. D**98** (2018) 030001 - 93.

106. J.P. Elliott and P.G. Dawber, Symmetry in Physics (MacMillan Press LtD, 1979).

107. H. Leutwyler, The mass of two lightest quarks, Mod. Phys. Lett. A **28** (2013) 136014 - 11.

108. H. Leutwyler, On the history of the strong interaction, ibid, A **29** (2013) 143023 - 16.

109. M. Gell - Mann, Y. Neeman, The Eightfold Way (Benjamin, Reading, Mass., 1964).

110. Q. Ho - Kim, X - Y Pham, Elementary Particles Intoruction (Springer, Berlin, 1998).

111. V.G. Plekhanov, Comparative study of isotope and chemical effects on the exciton states in LiH crystals, Prog. in Sol. State Chem., **29** (2001) 71 - 177.

112. V.G. Plekhanov, Modern View of the Origin of Isotope Effect (LAP, LAMBERT Academic Publishing, Saarbrücken, Germany, 2018).

113. A. Faessler, Interaction between two baryons and the six quark model, Prog. Part. Nucl. Phys. **20** (1988) 151 -173.

114. P.A. Guichon, J.R. Stone, A.W. Thomas, Quark - meson coupling (QMC) model for finite nuclei, nuclear matter and beyond, ibid, **100**, 262 - 297.

115. A. Faessler, F. Fernandez, G. Lűbeek, The nucleon - nucleon interaction and the role of the [42] orbital six - quark - symmetry, Nucl. Phys. **A402** (1982) 555 - 568.

116. U. Straub, Z - Y. Zhang, K. Bräer et. al., Hyperon - nucleon interaction in the quark cluster model, ibid **A483** (1988) 686 - 710.

117. J.J. Aubert, G. Bassompierre, K.H. Becks et. al., The ratio of the nucleon structure functions F2N for iron and deuterium, Phys Lett., **23** (1983) 275 - 278.

118. O. Hen, G.A. Miller, E. Piasetzky et. al., Nucleon - nucleon correlation, short - lived excitations, and the quarks, Rev. Mod. Phys. **89** (2017) 045002 - 63.

119. V.G. Plekhanov, Macroscopic manifestation of the strong nuclear interaction in the optical spectra of solids, in, Proc. ISINN - 25, Dubna, Russia, 2018, p.p. 49 - 56.

120. V.G. Plekhanov, Isotope effect is the paradigm of a non - accelerator study of the residual nuclear srong interaction, Edelweiss Chem. Sci. J. **3** (2020) 8 - 14.

121. see e.g. M.A. Eliashevich, Atomic and Molecular Spectroscopy (Fizmatgiz, Moscow, 1962) (in Russian).

122. M. Rosina, B. Povh, Contribution of the covalent and van der Waals force to the nuclear binding, Nucl. Phys. **A572** (1994) 48 - 56.

123. H. Fritzsch and M. Gell - Mann, Current algebra: quarks and what else? in, Proc. XVI Int Conf. High energy physics, Chicago, 1972, vol. 2, p. 135 - 156.

124. R. Utiyama, Invariant Theoretical Interpretation of Interaction, Phys. Rev. **101** (1956) 1597 - 1608.

125. P. Langancker, Structure of the Standard Model, ArXiv/ hep - ph/ 0304186 (2003).

126. G.M. Prosperi, M. Raciti, and C. Simolo, On the running coupling constant in QCD, Prog. Part. Nucl. Phys. **58** (2007) 387 - 438.

127. A. Deur, S.J. Brodsky and G.F. Toramond, The QCD running coupling, Progress in Particle and Nuclear Physics **90** (2016)1 - 74.

128. S. Bethke, World summary of α_s (2012), Eur. Phys. J. C**64** (2012) 689 - 695.

129 G. Altarelli, The QCD running coupling and its measurements, in, Proc. Corfu Summer Institute and Workshops on Elementary Particle Physics and Gravity, ArXiv: hep - ph/1303.6065 (2013).

130. G. Altarelli, Collider Physics within the Standard Model: a Primer, ArXiv: hep - ph/ 1303. 2842.

131. C.D. Froggatt, The origin of mass, Surveys High Energ. Phys. **18** (2003)77 - 99.

132. V.G. Plekhanov and J. Buitrago, Evidence of residual strong interaction of nuclear - atomic level shift in LiH - LiD crystals, Prog. Phys. **15** (2019) 68 - 71.

133. H. Georgi, S.L. Glashow, Unity of all elementary - particle forces, Phys. Rev. Lett. **33** (1974) 438 - 441.

134. B.L. loffe, QCD at low energy, Prog. Part. Nucl. Phys. **56** (2006) 232 - 277.

135. S.F. Novaes, Standard Model: An Introduction, ArXiv/ hep - ph/ 0001383 (2000).

136. S. Weinberg, The making of the Standard Model, ArXiv/ hep - ph/ 0401010 (2004).

137. C.D. Frogatt, H.B. Nielsen, Trying to understand the Standard Model, ArXiv/ 0308144 (2003).

138. V.G. Plekhanov, Non - accelerator stude of the strong interaction dependence on the distance between nucleons, Hadronic J. **46** (2023) 143 - 156.

139. O.W. Greenberg, A new level of structure, Phys. Today **38** (1985) 22 - 30.

140. M. Arghirescu, The Cold Genesis of Matter and Fields (Science Publishing Group, New York, 2015).

141. G. Herzberg, Molecular Spectra and Molecular Structure of Diatomic Molecules (Van Nostrand, New York, 1945).

142. A.F. Kapustinsky, L.M. Shamovsky and K.S. Bayushkina, Thermochemistry of isotopes, Acta Physicochem (USSR) **7** (1937) 799 - 811.

143. V.G. Plekhanov, T.A. Betenekova and V.A. Pustovarov, Excitons and some peculiarities of exciton -phonon interaction, Sov. Phys. Sōid State **18** (1976) 1422 - 1425.

144. A.A. Klochikhin and V.G. Plekhanov, Isotope effect on the Wannier - Mott exciton level, Sov. Phys. Solid State **22 (1980)** 342 - 345.

145. V.G. Plekhanov, Wannier - Mott excitons in isotope - disordered crystals, Reports Prog. Phys. **61** (1998) 1045 - 1097.

146. R.J. Elliott, J. Krumhansl, P. Leath, The theory and properties of randomly disordered crystals and related physical systems, Rev. Mod. Phys. **46** (1974) 465 - 543.

147. Y. Onodera, Y. Toyozawa, Persistence and amalgamation types in the electronic structure of the crystals, J. Phys. Soc. Japan **24** (1968) 341 - 355.

148. V.G. Plekhanov, A.V. Emel'yanenko, A.U. Grinfelds, Excitonic structure of NaI and LiH crystals cleaved in liquid helium, Phys. Lett. A**101** (1984) 291 - 293.

149. V.G. Plekhanov and A.I. Altukhov, Light scattering in LiH crystals with LO phonon emission, J. Raman Spectr. **16** (1985) 358 - 365.

150. V.G. Plekhanov, Isotope Effects in Solid State Physics, in: R.K. Willardson, E. Weber (Eds.) Semiconductor and Semimetals, Vol. 68 (Academic Press New York, 2001).

151. V.G. Plekhanov, Exciton spectroscopy of isotopic crystals, Opt. Spectrosc. (St. - Petersburg) **79** (1995) 715 - 734.

152. H. Bilz, W. Kress, Phonon Dispersion Relation in Insulators (Springer - Verlag, Berlin - Heidelberg, 1979).

153. J.L. Verble, J.L. Warren, J.L. Yarnel, Lattice dynamics of lithium hydride, Phys. Rev. **160** (1968) 980 - 989.

154. V.G. Plekhanov, A.A. O'Konnel - Bronin, Resonant Raman scattering in the wide - gap insulators of LiH and LiD, JETP Lett. (Moscow) **27** (1978) 413 - 416.

155. H. Dammak, E. Antoshchenkova, M. Hayoum and F. Finocchi, Isotope effects in lithium hydride and lithium deuteride crystals by molecular dynamics simulations, J. Phys.: Condens. Matter **24** (2012) 435402 - 6.

156. I. Nordheim, Zur Elektonentheorie der Metalle Ann. Phys. (Leipzig) **401** (1931) 641 - 678.

157. R.K. Chang, M.B. Long, Optical multichannel registration, in M. Cardona, G. Gűntherodt (eds.) Light Scattering in Solids, Vol. 2 (Springer, Berlin, 1982) pp 238 - 276.

158. V.G. Plekhanov, Isotope effects in lattice dynamics, Phys. - Uspekhi **46** (2003) 689 - 711.

159. A.T. Collins, S.C. Lawson, G. Davies and H. Kanda, Indirect Energy gap of ^{13}C, Phys. Rev. Lett. **65** (1990) 891 - 893.

160. T. Ruf, M. Cardona, P. Pavone et al., Cathodoluminescence investigation of isotope effect in diamond, Solid State Commun. **105** (1998) 311 - 316.

161. H. Watanabe, T. Koretsune, S. Nakashina et al., Isotope composition dependence of the band - gap energy in diamond, Phys. Rev. B**88** (2013) 205420 -5.

162. D.W. Taylor, Phonon response theory and the Infrared and Raman measurements, in: R.J. Elliott, I.P. Ipatova (eds.), Optical Properties of Mixed Crystals (Elsevier Sci. Pub. B.V., Amsterdam, 1988).

163. C.M. Lederer, V.S. Shirley, Tables of Isotopes (Wiley, New york, 1978).

164. V.F. Agekyan, V.M. Asnin, A.M. Kryukov et al., Isotope effect in germanium, Fiz. Tverd. Tela (St. - Petersburg) **31** (1989)101 - 104 (in Russian).

165. C.D. Klark, P.J. Dean and P.V. Harris, Intrinsic edge absorption in diamond, Proc. Roy. Soc. **277** (1964) 312 - 329.

166. H. Hanzawa, N. Umemura and Y. Nisida et al., Direct efects of nitrogen impuriries, and ^{13}C isotope composition on the Raman spectrum in synthetic Ib diamond Phys. Rev. B**54** (1996) 3793 - 3799.

168. R.M. Chrenko, ^{13}C - doped diamond: Raman spectra, J. Appl. Phys. **63** (1988) 5873 - 5875.

169. J. Spitzer, P. Etchegoin and M. Cardona et al., Isotopic - disorder induced Raman scattering in diamond, Solid State Commun. **88** (1992) 509 - 514.

170. K.C. Hass, M.A. Tamor and T.R. Anthony et al., Lattice dynamics and Raman spectra of isotopically mixed diamond, Phys. Rev. B**45** (1992) 7171 - 7182.

171. A.K. Ramdas and S. Rodriguez, Lattice vibrations and electronic excitation in Isotoplcally controlled diamonds, phys. stat. sol. (b) **215** (1999) 71 - 80.

172. F. Widule, T. Ruf, M. Konuma et al., Isotope effects in elemental semiconductors: a Raman study of silicon, Solid State Commun. **118** (2001) 1 - 23.

173. S. Prawer and R.J. Nemanich, Raman spectroscopy of diamond and doped diamond, Phil. Transac. R. Soc. (London) **362** (2004) 2537 - 2565.

174. M.S. Dresselhaus, G. Dresselhaus and M. Hofman, Raman spectroscopy as a probe of graphene and carbon nanotubes, ibid, **366** (2008) 231 - 236.

175. C. Casiraghl, A. Hartschuh, H. Qian et al., Raman spectroscopy of graphene edges, Nano Lett. **9** (2009) 1433 - 1441.

176. Sh. Chen, Q. Wu, C. Mishra et al., Thermal properties of isotopically engineered graphene, Nature Mater. **11** (2012) 203 - 207; ArXiv:cond - mat/1112.5752 (2011).

177. A. Ferrari, Raman spectroscopy of graphene and graphite: Disorder, electron -

phonon coupling, doping and nonadiabatlc effects, Solid State Commun. **143** (2007) 47 - 57.

178. M. Huang, H. Yan, C. Chen et al., Raman spectroscopy of graphene under uniaxlal stress: phonon softening and determination of crystallographic orientation, Proc. Natl. Acad. Sci. USA **106** (2009) 7304 - 7315.

179. J. C. Charlier, P.C. Eklund, A.C. Ferrari, Electron and phonon properties of graphene:their relationship with carbon nanotubes, in [180] p.p.673 - 709.

180. A. Jorio, G. Dresselhaus, M.S. Dresselhaus (eds.), Carbon Nanotubes, Topics Appl. Physics **111** (Springer, Heidelberg, 2008).

181. V.G. Plekhanov, Renormalzation of the band - gap by isotope in graphene, Nano Techn. & Nano Sci. J. **3** (2020) 121 - 130.

182. V.G. Plekhanov, Necessary additions, Phys - Uspekhi **62** (2019) 947 - 948.

183. M. Farjam and H. Rafii - Tabar, Comment on " Band structure engineering of graphene by strain: First - principles calculations", Phys. Rev B**80** (2009) 167401 - 3.

184. Zh.H. Ni, T. Yu, Y.H. Lu, et al., Uniaxlal strain on graphene: Raman spectroscopy study and band - gap opening, ACS Nano, **3** (2009) 483 - 492.

185. T.M. Mohiuddin, A. Lombarto, R.R. Nair et al., Uniaxial strain in graphene by Raman spectroscopy: G peak splitting, Grűneisen parameter and sample orientation, Phys. Rev. , B**79** (2009) 205433 - 8.

186. N. Vandecasteele, M. Lazzeri and F. Mauri, Boosting electronic transport in carbon nanotube, Phys. Rev. Lett. **102** (2009) 196801 - 4.

187. S.D. Costa, C. Fantini, A. Righi et al., Resonant Raman spectroscopy on enriched ^{13}C carbon nanotubes, Carbon **49** (20011) 4919 -4723.

188. J.F.Rodriguez - Nieva, R. Saito, S.D. Costa et al., Effect of ^{13}C doping on the optical phonon modes in graphene: Localization and Raman spectroscopy, Phys. Rev. B **85** (2012) 245406 - 8 .

189. S. Bernard, E. Whiteway, V. Yu et al., Probing the experimental phonon dispersion of graphene using ^{12}C and ^{13}C isotopes, ibid, B **86** (2012) 085409 - 5.

190. E. del Corro, M. Kolbac, C. Fantini et al., Isotopic $^{12}C/^{13}C$ effect on the resonant Raman spectrumof twiated bilayer graphene, ibid, B **88** (2013) 155436 - 5.

191. Z.C. Kun, L.Q. YU, T. Bo, et al., Isotope effect of the phonons mean free path in graphene by micro - Raman measurement, Science China, Phys., Mech. and Astro., **57** (2014) 1817 - 1821 .

192. M. Born and R. Oppenheimer, On the quantum theory of molecules, in, Quantum Chemistry (Classic Scientific Papers) (World Sci. Publ. Co, 2000).

193. R.M. Martin, Electronic Structure - Basic Theory and Practical Methods (Cambridge University Press, Cambridge, 2004).

194. J. Jaeckel, A. Ringwad, The low - energy frontier of particle physics, Annu. Rev. Nucl. Part. Sci. **60** (2010) 405 - 450.

195. V.G. Plekhanov, Measurements of the wide value range of strong interaction coupling constant, SSRG - IJAP **6** (2019) 32 - 37.

196. W.B. Zimmerman, Lattice constant dependence on isotopic composition in the $^{7}Li(H,D)$ system, Phys. Rev. B**5** (1972) 4704 - 7.

197. O.W. Greenberg, A new level of structure, Phys. Today, **38** (1985) 22 - 30.

198. B. Robson, The Generation model of particle physics, in, Particle Physics, E. Kennedy ed. (In Tech. Open Access Publisher, Rijeka, Croatia, 2012).

199. M. Aghlrescu, The Cold Genesis of Matter and Fields (Science Publishing Group, New York, 2015).

200. C.S. Kalman and I. D'Souza, Preons: Models of Leptons, Quarks and Gauge Bosons as Composite Particles (World Scientific, Singapore, 1992).

201. C.S. Kalman, Why quarks cannot be fundamental particles, Nuclear Phys. B: Proceedings Supplements **142** (2005) 235 - 237.

202. O. Consa, The Helicon: A new preon model, Prog. Phys. **14** (2019) 215 - 219.

203. V.G. Plekhanov, Direct observation of the strong nuclear interaction in the optical spectra of solids, Proceed. 3rd Conf. High Energy Phys. Rome, Italy, 2017, p.46.

204. G. Breit, Theory of isotope shift, Rev. Mod. Phys**30** (1958) 507 - 517.

205. V.G. Plekhanov, Paradigm of graphene and quantum information, Proceed. Int. Conf. Computer Claster, L'viv, Ukraina, 2013.

206. Ch. Stampfer, S. Fringe, J. Guttinger, Transport in graphene nanostructures, Front. Phys. **6** (2011) 271 - 293.

207. V.G. Plekhanov, Chapter 1 in, Understanding Quarks, N ova Science Publishers, Inc., New York, 2021, p.p. 1 - 92.

208. Ken - ichi Sasaki, Massive Dirac Fermions Signal in Raman Spectrum of Graphene, Phys. Rev. B**97** (2018)115413 - 6.

209. C.D. Roberts, Hadron physics and QCD: Just the basic facts, ArXiv: nucl - th/ 1501.06581.

210. C.D. Roberts, Empirical consequence of emergent mass, Symmetry **12** (2020) 1468 - 1506.

HADRONIC JOURNAL 46, 459 - 472 (2023)
DOI 10.29083/HJ.46.04.2023/SC459

LASER ASSIST SCATTERING IN LENNARD-JONES POTENTIAL

Narayan Babu Shrestha[1,4], Suresh Prasad Gupta[1], Yadhav Poudel[1], Kishori Yadav[1,4], Saddam Husain Dhobi[2,3,4], Jeevan Jyoti Nakarmi[1,4]
[1]Department of Physics, Patan Multiple Campus, Tribhuvan University, Patandhoka, Lalitpur, Nepal
[2]Central Department of Physics, Tribhuvan University, Kirtipur, Kathmandu, Nepal
[3]Nepal Academy of Science and Technology, Khumaltar, Lalitpur, Nepal
[4]Innovative Ghar Nepal, Lalitpur, Nepal
saddam@ran.edu.np

Received October 31, 2023
Revised November 6, 2023

Abstract

The aim of this study is to study the Differential Cross Sections (DCS) in the presence of a linear polarized laser field for Bessel functions of various orders, with oxygen molecules as the target within a Lennard-Jones potential framework. The developed model is theoretical in which different assumptions are used, born approximation, Bessel function, central approximation, etc. the developed model was computed for analysis using online MATLAB. The observation shows projected electron gain and loss energies in the presence of the oxygen molecules. A pronounced deep peak in the results suggests an alignment of incidence and final energies, potentially indicating new particle formation. Additionally, a minimum DCS point signifies an intense interaction and scattering between the incident electron and the target, suggesting the formation of particles smaller than both the target and the electron. Notably, the zero-order Bessel function exhibits a higher DCS than its higher-order counterparts, likely owing to distinct mathematical and physical properties. At a zero-radian scattering angle, the DCS achieves its minimum, highlighting a heightened probability of particle formation due to close alignment and collision between incident and scattered particles. This finding underscores the significance of this particular angle in understanding particle interactions. This study's revelations offer valuable implications for understanding energy exchange and particle formation processes in similar contexts. Further research in this area could delve into specific mechanisms underlying the observed phenomena, potentially leading to advancements in particle interaction dynamics. Moreover, these findings contribute to the broader understanding of the fundamental physics governing such interactions, with potential applications in various fields of science and engineering.

Keywords: Differential cross section, Bessel function, oxygen molecules, Lennard-Jones Potential, scattering angle

I. Introduction

The phenomenon of evaporation and condensation at the liquid/vapor interface is common yet poorly understood. To delve into these processes at the molecular level, extensive molecular dynamics simulations have been conducted on Lennard-Jones (LJ) fluids, comprising monomers, dimers, or trimers. These simulations revealed that when LJ monomers touch a vacuum, evaporation rates are notably high due to strong evaporative cooling and a density differential near the interface. However, when the structure is reduced to dimers, the evaporation rate significantly decreases. The study also involves measuring evaporation and condensation coefficients, as well as velocity distributions of evaporated molecules, comparing the results with a model based on kinetic theory of gases. The research underscores the importance of considering physical quantities and appropriate parameters for computational material production.

The LJ equation proves valuable in predicting material characteristics, facilitating interactions between pairs of neutral atoms and molecules. These interaction potential values can be theoretically calculated through quantum mechanics or confirmed through classical simulation, which can further be used to fine-tune experimental data. Overall, this approach allows for the anticipation of material properties through simulations tracking atom movements within a molecular dynamics framework. Lennard-Jones Potential (LJP) studies are crucial for analyzing the differential cross-section of shielding materials, especially due to the impact of atomic binding on radiation shielding. Materials with appropriate wavelength and bond length are considered ideal for shielding, as they effectively absorb and protect against various radiation hazards. Additionally, LJP plays a significant role in scattering, influencing the interaction of photons and atoms. This proves instrumental in studying energy, momentum, differential cross-section, and particle formation—a valuable method for comprehensive analysis [1-3].

The investigation of Lennard-Jones Potential (LJP) interactions among various atoms and molecules using a mathematical model and MATLAB. It explores the Lennard-Jones Potential direct correlation function (LJPDCF) for carbon-carbon, carbon-oxygen, oxygen-oxygen, water-water, silver-silver, gold-silver, gold-carbon, and silver-carbon interactions. The research unveils significant findings, such as a maximum LJP of -133.75 kcal/mole for silver-silver at 3.5 Å and a minimum potential of -2.08 kcal/mole for carbon-carbon at 3.8 Å. These insights have implications for molecular physics, computational chemistry, and molecular modeling applications [4]. The pivotal role of interatomic potentials in material physics models,

particularly those derived from first principles. These potentials underpin diverse phenomena like phase transitions, diffusion, and adsorption. Parameters are deduced from thermodynamic properties and crystal structures through simulations, aligning macroscopic properties with experimental data. Simplified pair interaction potentials, characterized by v(rij), offer crucial approximations. However, limitations arise from neglecting electron density redistribution. Despite this, they serve as vital starting points for more complex potential constructions. Yet, a research gap emerges: the evaluation of potentials in simulating real physical phenomena does not sufficiently consider the impact of electron density redistribution, warranting further exploration [5].

The Lennard-Jones potential quantifies the bond interaction energy between two atoms or molecules, contingent on their separation distance. Utilizing molecular dynamics simulations, this research determines material properties, focusing on melting points. Employing the LAMMPS program, the study normalizes potential parameters by comparing simulated and experimental melting points. The outcome is a Lennard-Jones potential parameter value that provides a concise description of material melting points, particularly for Fe, Pb, Ni, and Cr [6]. The potential is increasingly used to determine the intermolecular parameters for simple molecules (H2, O2, N2,CO, CH4), in which we add the inter-action terms in some cases potential iodide(KI) molecule [7].

$$U = 4\epsilon_{ij}\left[\left(\frac{\sigma_{ij}}{r_{ij}}\right)^{12} - \left(\frac{\sigma_{ij}}{r_{ij}}\right)^{6}\right] \quad (1)$$

r_{ij}=Internuclear separation, σ_{ij} =equilibrium distance and ϵ_{ij}=binding energy [8]. In 1897, J.J. Thompson's discovery of the electron revolutionized physics beyond classical principles. Rutherford's 1911 experiment, scattering alpha particles off foil, led to the nucleus's revelation and birthed the planetary atomic model. Bohr's 1912 hydrogen model, rooted in Coulomb force and angular momentum quantization, ushered in new physics laws. Compton's 1923 experiment confirmed photons' existence, supported by Bothe and Geiger's validation [9].

The study focuses on inelastic electron-H(2s) dispersion in a linearly polarized laser beam, characterized by high scattering energy and moderate field intensities. It examines angular distributions, resonance structures, and states transitions in both elastic and inelastic scattering. The research underscores the complexity of the mathematical treatment, given the involvement of a projectile, atomic target, and photon. Assumptions, like

rapid projectile electrons and moderate field intensities, simplify the analysis. The Gordon-Volkov wave function delineates the projectile electron-laser field relationship, while first-order time-dependent perturbation theories describe the laser field's effect on the hydrogen atom. The first Born approximation handles the interaction between the hydrogen atom and fast projectile electrons [10].

The impact of circularly polarized laser fields on electron scattering by hydrogen atoms. It scrutinizes how the laser's polarization influences hydrogen and subsequently affects differential scattering cross sections. Dispersed electrons with 100 eV kinetic energy allow for a first-order Born approximation treatment. Yadav et al. observed that, under fixed laser and electron conditions, the differential scattering cross-sectional area decreases with increasing scattering angle. The polarization of the laser field significantly influences the differential scattering cross section [11]. The elliptically polarized laser field to analyze electron scattering by hydrogen. It examines how laser field polarization influences hydrogen atoms and subsequently impacts differential scattering cross-sections. Utilizing the first Born assumption and the Volkov wave function, scattered electrons possess high kinetic energy (>3000 eV) under moderately intense laser beams. The differential scattering cross-section area expands with increased incident electron energy, while changes in polarizing angle have no effect. Laser power and incident energy in a linearly polarized field determine the differential scattering cross-section in elliptical polarization, particularly in the highly energetic zone [12].

Dhobi et al. investigate inelastic scattering, focusing on low laser fields (visible and UV). Their model predicts that the differential cross-section expands as the target absorbs energy. Upon energy emission, the cross-section initially drops, eventually reaching its maximum. Energy emission occurs at specific electron voltages. Moreover, the cross-section grows with increasing scattering angles [13]. The study of elliptically polarized laser field to investigate electron scattering by hydrogen. It explores how the laser's polarization impacts hydrogen and subsequently influences differential scattering cross-sections. Applying the first Born assumption and Volkov wave function, scattered electrons possess high kinetic energy (>3000 eV) under a moderately intense laser beam. The area of differential scattering cross-section expands with increasing incident electron energy, with polarizing angle changes having no effect. Differential scattering cross-sections in elliptical polarization at high energy levels are determined by laser power and incident energy in a linearly polarized field [14].

II. Research Gap

The research presented in the provided sources primarily focuses on various aspects of scattering experiments involving electrons and atoms in the presence of laser fields. While these studies investigate differential scattering cross-sections, the influence of laser polarization, and energy emission in scattering processes, none of them directly involve the application or utilization of the Lennard-Jones potential (LJP). The LJP is not discussed or employed in the context of these scattering experiments. The absence of LJP in these studies highlights a research gap in the understanding of how the LJP, a well-established potential energy model for describing interactions between atoms and molecules, might be relevant or applicable in laser-assisted electron-atom scattering experiments. Future research could explore the potential role of LJP in such scattering phenomena, investigating whether it can provide insights or improve the accuracy of theoretical models used to describe these interactions. Additionally, research could explore whether LJP-based models have any implications for predicting or interpreting experimental outcomes in this specific field of study.

The motivation for further research in this field stems from a notable research gap identified in the existing studies. While these studies explore complex electron-atom scattering processes in the presence of laser fields, they notably overlook the application of the well-established Lennard-Jones potential (LJP). This omission presents an intriguing opportunity for investigation, as the LJP has proven valuable in describing atom-molecule interactions. Understanding how LJP may influence or enhance the accuracy of models in laser-assisted electron-atom scattering experiments could lead to valuable insights and potentially improve our ability to predict and interpret experimental outcomes. Bridging this gap could contribute to a deeper comprehension of these intricate interactions and advance the field of optical research further.

III. Significant

The significance of this approach lies in its potential to bridge a critical research gap. While existing studies delve into intricate electron-atom scattering processes under laser fields, they overlook the applicability of the established Lennard-Jones potential (LJP). This omission opens an intriguing avenue for exploration, as LJP has shown promise in elucidating atom-molecule interactions. Understanding how LJP may impact or refine models in laser-assisted electron-atom scattering experiments could yield valuable insights, potentially enhancing our capacity to predict and interpret

experimental outcomes. This endeavor holds the promise of advancing our comprehension of these complex interactions, thus driving forward the field of optical research.

IV. Method and Materials

According to Bransden&Joachain, cross sections are "the ratio of the flux of the acting on a particle with regard to the target to the number of events of this kind per unit time and per unit scatterer." Cross sections can be regarded as transition probabilities per unit time (transition rate), per unit target scatterer, and per unit flux of the incident particles with regard to the target if the incident flux is set to unity. The quantum scattering theory's transition rate [15] is given by

$$w(i \rightarrow f) = \frac{2\pi}{\hbar} | T_{fi} |^2 \delta(E_f - E_i) \tag{2}$$

where $T_{fi}$is the transition matrix or T matrix, which is assumed to be integrated across energy with the density of final states in equation (2),

$$w(i \rightarrow f) = \frac{mk_f(2\pi)^3}{(2\pi)^2\hbar^3} |T_{fi}|^2 d\Omega \tag{3}$$

The scattering particle's mass and final wavenumber are given by dΩ. m and k_f, respectively. The wave functions then normalized to a delta function, according to equation (3). Divided by the incident flux equation in variables of wavenumber, equation (3) yields the differential cross section.

$$F_{incident} = \frac{p_i}{m(2\pi)^3} = \frac{\hbar k_i}{m(2\pi)^3} \tag{4}$$

On consideration of electron density unity in a volume of $(2\pi)^3$, the differential cross section is

$$\frac{d\sigma}{d\Omega} = \frac{k_f}{k_i}\left(\frac{m(2\pi)^3}{(2\pi)\hbar^2}\right)^2 | T_{fi} |^2 \tag{5}$$

The quantum free-free differential cross - sectional area can be determined if the T matrix for free-free transitions is discovered. We examine the connection between the S and the T matrices in order to determine the T matrix.

$$S_{fi} = \delta_{fi} - i2\pi\delta(E_f - E_i)\ T_{fi} \tag{6}$$

Now, S matrix for free-free scattering

$$S_{fi} = \delta_{fi} - \frac{i}{\hbar}\int \int_{-\infty}^{+\infty} \langle X_f(r,t')|V(r)|\Psi_i(r,t')\rangle dt' \tag{7}$$

where X (r, t) denotes the wave function for an electron connected to an external electromagnetic field and Ψ (r, t) denotes the wave function for an electron coupled to an external electromagnetic field while also being in the existence of a scattering potential V (r).

$$X(r,t) = 1\frac{1}{(2\pi)^{3/2}}\exp\left\{i\frac{\boldsymbol{p}}{\hbar}.\left(\boldsymbol{r} + \frac{e}{m}\int^{t}\boldsymbol{A}(t')dt'\right) - i\frac{E}{\hbar}t - i\frac{e^2}{2m\hbar}\int^{t}\boldsymbol{A}^2(t')dt'\right\} \tag{8}$$

Equation (8) is Volkov wave function, E is the free electron's kinetic energy. Keep in mind that the momentum operator's eigenvalue is $\hat{\boldsymbol{p}}$. The Volkov wave function's general form is given by equation (8) to continue to determine

$$X(r,t) = \frac{1}{(2\pi)^{\frac{3}{2}}}exp\left\{-\frac{i}{\hbar}\left(E + \frac{e^2a^2}{4m}\right)t + i\frac{\boldsymbol{p}}{\hbar}\cdot\left(\boldsymbol{r} + \frac{e\boldsymbol{a}}{m\omega}sin(\omega t)\right) - i\frac{e^2\boldsymbol{a}^2}{8m\hbar\omega}sin(2\omega t)\right\} \tag{9}$$

This equation explain the wave function of electrons in a laser field.The Kroll Watson Approximation (KWA), a common model for free-free processes, in this section. Since the electromagnetic field is treated conventionally yet quantum scattering theory is employed, the model is regarded as semiclassical. We use a similar reasoning as that presented by [16]. Going back to equation (7), we apply equation (9),

$$S_{fi} = \delta_{fi} - \frac{i}{\hbar}\int_{-\infty}^{+\infty}\langle X_f(r,t)|V(r)|\Psi_i(r,t)\rangle dt' \tag{10}$$

Using the first Born approximation, let's calculate the time integral by supposing that the scattered potential is low [17].

$$\frac{i}{\hbar}\int_{-\infty}^{+\infty}\langle X_f(r,t)|V(r)|X_i(r,t)\rangle dt'. \tag{11}$$

To determine, we assess the matrix element and integrate.

$$\int_{-\infty}^{+\infty}\langle X_f(r,t)|V\,(r)|X_i(r,t)\rangle dt' = \frac{1}{(2\pi)^3}\frac{i}{\hbar}\int_{-\infty}^{+\infty} e^{i(E_f-E_i)t'/\hbar}dt'$$

$$\times\int_{-\infty}^{+\infty} exp\,\{-i\frac{e}{m\hbar\omega}\boldsymbol{Q}\cdot\boldsymbol{a}sin(\omega t)\}\,dt'$$

$$\times\int V(\boldsymbol{r})e^{-i(\boldsymbol{Q}\,.\,r)/\hbar}d^3r' \tag{12}$$

When the momentum transfer formula $\boldsymbol{Q}=\boldsymbol{p_f}-\boldsymbol{p_i}$ was utilized. Lets use the Bessel function with expanding plane wave Jacobi-Anger Expansion. The scattering amplitude of the first born approximation [15],

$$f_{Born}{}^{(1)} = -\frac{m}{2\pi\hbar^2}\int V(r)e^{-iQ\cdot\frac{r}{\hbar}}d^3r \tag{13}$$

Using Bessel function and solving equation (12) we obtain,

$$\frac{i}{\hbar}\int_{-\infty}^{+\infty}\langle X_f(r,t)|V(r)|X_i(r,t)\rangle dt'$$

$$= -\frac{1}{(2\pi)^3}\frac{i}{\hbar}\frac{2\pi\hbar^2}{m}\sum_{n=-\infty}^{+\infty}J_n\left(-\frac{e}{m\hbar\omega}(\boldsymbol{Q}\,.\boldsymbol{a})\right)-\frac{me^2}{\hbar^2Q^2}\int_{-\infty}^{+\infty}e^{\frac{i\left(E_f-E_i+n\hbar\omega\right)}{\hbar}}dt'$$

$$= -2\pi\frac{1}{(2\pi)^3}\frac{i}{\hbar}\frac{2\pi\hbar^2}{m}\sum_{n=-\infty}^{+\infty}J_n\left(-\frac{e}{m\hbar\omega}(\boldsymbol{Q}\,.\boldsymbol{a})\right)\left(-\frac{me^2}{\hbar^2Q^2}\right)\delta\left((E_f-E_i\right.$$

$$\left.+\,n\hbar\omega)/\hbar\right) \tag{14}$$

Now, taking the Fourier transformation of equation (13), and considering first imigainary and real part and also applying central approximation in real and imaginary on solving we get

$$f_{Born}{}^{(1)} = -16\epsilon\pi\hbar\left[\frac{q^9\sigma^{11}}{907200}+\frac{q^3\sigma^5}{6}\right] \tag{15}$$

Now, the S matrix can be expressed from above for the n^{th} element.

$$S_{fi} = \delta_{fi} - i2\pi\delta(E_f - E_i + n\hbar\omega)\left[-\frac{1}{(2\pi)^3}\frac{2\pi\hbar^2}{m}J_n\left(-\frac{e}{m\hbar\omega}(\boldsymbol{Q}.\boldsymbol{a})\right)f_{Born}^1\right] \quad (16)$$

Comparing equation (6) with equation (16) and the value of $f_{Born}^1$from equation (15), and recognizing that the T_{fi} matrix interm of atomic unit is

$$T_{fi} = J_n\left(-\frac{e}{m\hbar\omega}(\boldsymbol{Q}.\boldsymbol{a})\right)\left(16\epsilon\pi\hbar\left[\frac{Q^9\sigma^{11}}{907200}+\frac{Q^3\sigma^5}{6}\right]\right) \quad (17)$$

We determine the differential cross - sectional area for LAFF scattering for n photons using the solution to equation (17) in equation (5) and in atomic unit:

$$\frac{d\sigma_{FF}^n}{d\Omega} = \frac{256k_f\pi^2\epsilon^2}{k_i}\left[\frac{Q^9\sigma^{11}}{907200}+\frac{Q^3\sigma^5}{6}\right]^2 J_n^2\left(-\frac{Qacos\theta}{\omega}\right) \quad (18)$$

Where J is Bessel function defined [18]. Taking first term of first order function to remove the complixcity we have, $J_0 = 1$ and hence, DCS for zero order Bessel function we get

$$\frac{d\sigma_{FF}^n}{d\Omega} = \frac{256k_f\pi^2\epsilon^2}{k_i}\left[\frac{Q^9\sigma^{11}}{907200}+\frac{Q^3\sigma^5}{6}\right]^2 \quad (19)$$

Similarly, for first order Bessel function and hence the DCS for first order Bessel function, we get,

$$\left(\frac{d\sigma}{d\Omega}\right)_{J_1} = \frac{256k_fQ^2a^2\pi^2\epsilon^2\cos^2\theta}{4\omega^2k_i}\left[\frac{Q^9\sigma^{11}}{907200}+\frac{Q^3\sigma^5}{6}\right]^2 \quad (20)$$

Similarly, for second order Bessel function and hence the DCS for second order Bessel function we get

$$\left(\frac{d\sigma}{d\Omega}\right)_{J_2} = \frac{256k_f\pi^2\epsilon^2Q^4a^4\cos^4\theta}{64k_i\omega^4}\left[\frac{Q^9\sigma^{11}}{907200}+\frac{Q^3\sigma^5}{6}\right]^2 \quad (21)$$

V. Results and Discussion

The study employs Equations (19), (20), and (21) to analyze the Differential Cross Sections (DCS) for Bessel functions of zero, first, and second orders. Computational results, generated using online MATLAB, are depicted in

Figure 1 and Figure 2. The investigation centers on oxygen molecules within a Lennard-Jones potential framework. The underlying computational data is drawn from a reference [19]. The experiment utilizes a He-Ne laser emitting 2 electron volts (2eV) and applies an electric field strength of 10^6 volts per centimeter (V/cm). This comprehensive approach seeks to elucidate the interaction dynamics of oxygen molecules under these specified conditions.

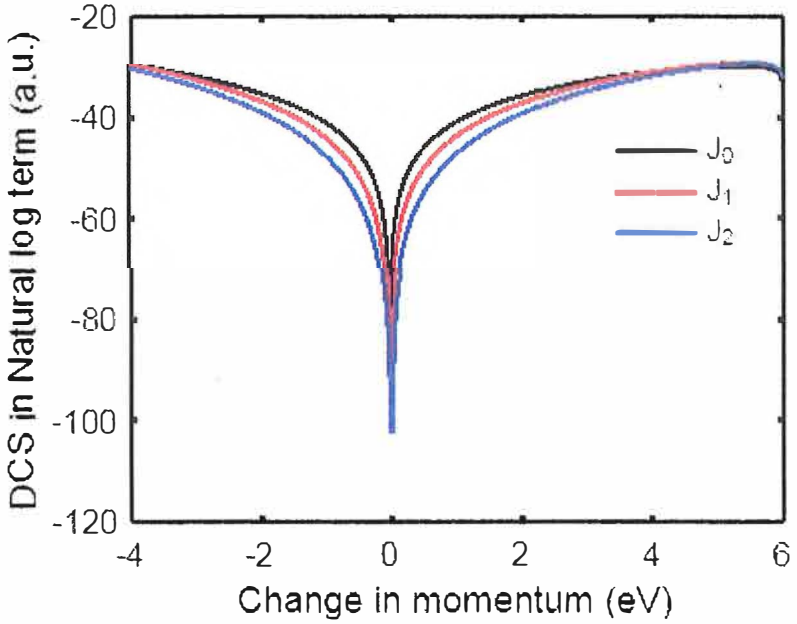

Figure 1: DCS vs Change in momentum

Figure 1 provides a comprehensive representation of the Differential Cross Section (DCS) nature in logarithmic terms, illustrating changes in momentum. In this context, it's crucial to note that negative values of change in momentum indicate that the final energy of the electron is lower than the incidence energy. This signifies electron energy loss due to interaction with the laser field in please of target. Conversely, positive values of momentum change suggest that the final energy of the electron is higher than the incidence energy, indicating an energy gain from the laser field in presence of target. The prominent deep peak in the graph is particularly significant. It indicates instances where the incidence energy matches the final energy, implying a potential for the formation of new particles. This phenomenon is crucial in understanding the transformative potential of these interactions. Moreover, the deep point also serves as a notable observation. It signifies a minimum value of the Differential Cross Section, indicating a high level of interaction between the incident electron and the target. This suggests that the incident electron experiences a significant level of scattering, potentially resulting in a deviation from its initial trajectory. Furthermore, the graph

reveals an intriguing trend: the DCS of the zero-order Bessel function surpasses that of the first and second-order Bessel functions. This observation suggests that the fundamental Bessel function mode exhibits a greater propensity for interaction compared to higher-order modes. This phenomenon could be attributed to the distinctive mathematical properties and physical characteristics associated with these different orders of Bessel functions.

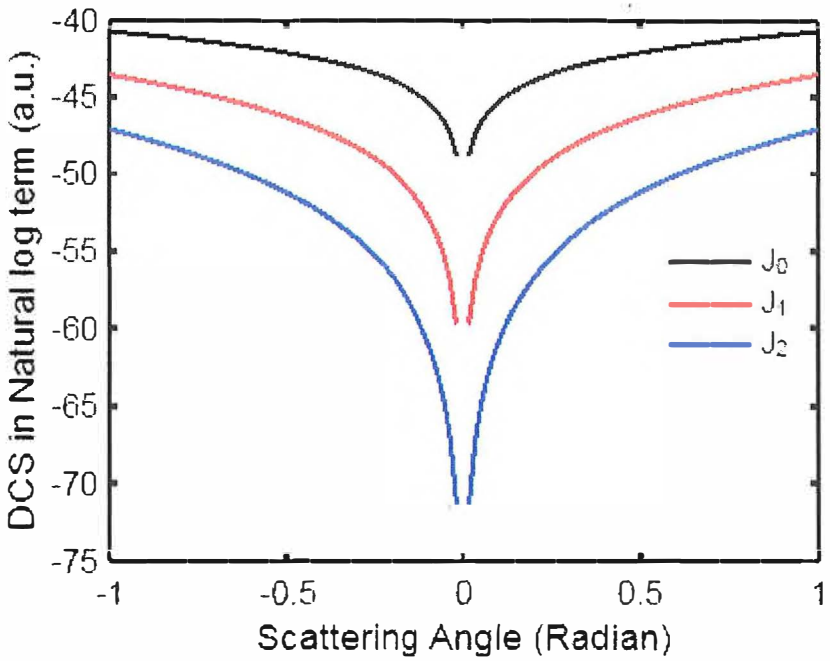

Figure 2: DCS with scattering angle

Figure 2 provides a detailed view of the DCS behavior in relation to scattering angle. Notably, at a scattering angle of zero radians, the DCS reaches its minimum value. This phenomenon can be attributed to a significant physical process occurring at this specific angle. The minimum DCS at zero radian scattering angle is indicative of a high likelihood of particle formation. This is due to the fact that at zero radians, the incident and scattered particles are effectively aligned, leading to a high probability of collision. This alignment results in a substantial change in the trajectory of the particles, leading to a greater chance of particle formation. Moreover, the DCS being at its lowest point signifies a particularly intense interaction between the incident particle and the target. In practical terms, this suggests that the incident particle experiences a substantial degree of scattering, meaning it deviates significantly from its original path. This high level of interaction is indicative

of the strong forces at play during this specific scattering event. The observed minimum in DCS at zero radian scattering angle points to a heightened potential for particle formation, underlining the significance of this specific scattering event. Additionally, the low DCS value indicates an intense interaction, with the incident particle being in close proximity to the target material.

VI. Conclusion

The study's findings provide valuable insights into particle interactions. Negative momentum changes indicate electron energy loss to the laser field, while positive changes imply energy gain. The occurrence of a deep peak suggests potential new particle formation, reflecting a high level of interaction with the target material. This results in significant scattering and trajectory alteration. Additionally, at a zero-radian scattering angle, the DCS reaches its minimum, indicating an elevated likelihood of collision and subsequent particle formation. This underscores the intensity of interaction at this specific angle, offering crucial understanding of the underlying physical processes.

VII. Acknowledgement

We acknowledge the Department of Physics, Patan Multiple Campus, Tribhuvan University, Patandhoka, Lalitpur, Nepal. Our gratitude extends to the Central Department of Physics, Tribhuvan University, Kirtipur, Kathmandu, Nepal. We appreciate the support of Nepal Academy of Science and Technology, Khumaltar, Lalitpur, Nepal. We thank Innovative Ghar Nepal, Lalitpur, Nepal.

References

[1] Dhobi, S. H., Rangrej, M. D. J., Patel, U., Shrestha, N. B., & Sharma, S. K. (2020a). Maximum Time and Distance needed for Pair Production inside Atom, Analytical and Theoretical. International Journal of Scientific Research in Physics and Applied Sciences, 8(1), 16-19.

[2] Dhobi, S. H. (2020b). Nature of Masses Formed During Pair Production Reaction. International Journal of Scientific Research in Journal of Physics and Chemistry of Materials, 7(4), 1-4.

[3] Dhobi, S. H., Das, S. K., Yadav, K. (2021). Klein Nishina Differential Equation for the Selection of Radiation Shielding Material (C, Al, Fe, and Zn) on the Basis of Attenuation and Cross sectional Area. European Journal of Applied Physics, 3(1), 30-34.

[4] Koirala, B., Dhobi, S. H., Subedi, P., Gurung, M., & Teemilsina, N. K. (2022). Study of Lennard-Jones Potential at 300K between Carbon, Silver, Gold and Oxygen Atom. International Journal of Scientific Research in Physics and Applied Sciences, 10(4), 8-14.

[5] Filippova, V. P., Kunavin, S. A., & Pugachev, M. S. (2015). Calculation of the Parameters of the Lennard-Jones Potential for Pairs of Identical Atoms Based on the Properties of Solid Substances. Inorganic Materials: Applied Research, 6(1), 1–4.

[6] Maghfiroh, C. Y., Arkundato, A., Misto, & Maulina, W. (2020). Parameters of Lennard-Jones Potential for Fe, Ni, Pb for ε, σ Parameters based on Melting Point Values Using the Molecular Dynamics Method of the Lammps Program. Journal of Physics: Conference Series, 1491, 012022. doi:10.1088/1742-6596/1491/1/012022

[8] Stephan, S., Thol, M., Vrabec, J., & Hasse, H. (2019). Thermophysical Properties of the Lennard-Jones Fluid: Database and Data Assessment. Journal of Chemical Information and Modeling, 59, 4248–4265. PMID: 31609113.

[7] Stephan, S., Staubach, J., & Hasse, H. (2020). Review and comparison of equations of state for the Lennard-Jones fluid. Fluid Phase Equilibria, 523, 112772.

[9] Bhatia, A. K. (2020). Scattering and Its Applications to Various Atomic Processes: Elastic Scattering, Resonances, Photoabsorption, Rydberg States, and Opacity of the Atmosphere of the Sun and Stellar Objects. Atoms, 8(4).

[10] Buica, G. (2015). Laser-assisted inelastic electron scattering by excited hydrogen atoms, XXIX International Conference on Photonic, Electronic, and Atomic Collisions (ICPEAC2015). Journal of Physics: Conference Series, 635, 092063. doi:10.1088/1742-6596/635/9/092063

[11] Yadav, K., Nakarmi, J. J., & Maharjan, S. (2017). Free Scattering Theory in Circularly Polarized Laser Field. Journal of Nepal Physical Society, 4(1), 78-87.

[12] Yadav, K., Gupta, S., & Nakarmi, J. (2020). Elliptically polarized laser assisted elastic electron-hydrogen atom collision and differential

scattering cross-section. Himalayan Physics, 9(1), 93–102. https://doi.org/10.3126/hp.v9i01.40205

[13] Dhobi, S. H., Yadav, K., Gupta, S. P., Nakarmi, J. J., & Koirala, B. (2022). Differential Cross-Section in the Presence of a Weak Laser Field for Inelastic Scattering. Ukrainian Journal of Physics, 67(4), 227-228.

[14] Yadav, K., Dhobi, S. H., Maharajan, S., Gupta, S. P., Karki, B., & Nakarmi, J. J. (2021). Elliptically Polarized Laser-Assisted Elastic Electron-Hydrogen Atom Collision in Coulomb Potential. Eurasian Physical Technical Journal, 18(4), 82-84.

[15] Sakurai, J. J., & Napolitano, J. (2011). Modern Quantum Mechanics. Addison, Wesley, San Francisco, CA.

[16] Kroll, N. M., & Watson, K. M. (1973). Charged-particle scattering in the presence of a strong electromagnetic wave. Physical Review A, 8, 804–809.

[17] Griffiths, D. J. (2004). Introduction to Quantum Mechanics. Pearson, 2nd.

[18] Mhtlab. (2022). http://www.mhtlab.uwaterloo.ca/courses/me755/web_chap4.pdf

[19] El Asri, S., Mouslih, S., Ouali, M., Taj, S., & Manaut, B. (2022). Laser-assisted scattering of a muon neutrino by an electron within the Electroweak theory. Retrieved from https://arxiv.org/pdf/2203.14955.pdf

INDEX
HADRONIC JOURNAL, VOLUME 46, 2023